DOE/NASA/0212-1
NASA CR-165543

CONCEPTUAL DESIGN AND COST ANALYSIS OF HYDRAULIC OUTPUT UNIT FOR 15kW FREE-PISTON STIRLING ENGINE

M. A. WHITE

UNIVERSITY OF WASHINGTON
JOINT CENTER FOR GRADUATE STUDY
AND
FLOW INDUSTRIES INC.

AUGUST 1982

PREPARED FOR
NATIONAL AERONAUTICS AND SPACE ADMINISTRATION
LEWIS RESEARCH CENTER
UNDER CONTRACT DEN3-212

FOR

U.S. DEPARTMENT OF ENERGY
DIVISION OF SOLAR THERMAL ENERGY SYSTEMS

DOE/NASA/0212-1
NASA CR-165543

CONCEPTUAL DESIGN AND COST ANALYSIS OF HYDRAULIC OUTPUT UNIT FOR 15kW FREE-PISTON STIRLING ENGINE

M. A. WHITE

UNIVERSITY OF WASHINGTON
JOINT CENTER FOR GRADUATE STUDY
AND
FLOW INDUSTRIES INC.

AUGUST 1982

PREPARED FOR
NATIONAL AERONAUTICS AND SPACE ADMINISTRATION
LEWIS RESEARCH CENTER
UNDER CONTRACT DEN3-212

FOR

U.S. DEPARTMENT OF ENERGY
DIVISION OF SOLAR THERMAL ENERGY SYSTEMS
WASHINGTON, D.C. 20545
UNDER INTERAGENCY AGREEMENT DE-AT04-81-AL-1628

1. Report No.	2. Government Accession No.	3. Recipient's Catalog No
NASA CR-165543		

4. Title and Subtitle	5. Report Date
Conceptual Design and Cost Analysis of Hydraulic Output Unit for 15 kW Free-Piston Stirling Engine	August 1982
	6. Performing Organization Code
7. Author(s)	8. Performing Organization Report No.
M. A. White	
	10. Work Unit No.
9. Performing Organization Name and Address	11. Contract or Grant No.
University of Washington Joint Center for Graduate Study 100 Sprout Road Richland, WA 99352 Flow Industries, Inc. 21414 68th Ave. S. Kent, WA 98031	DEN3-212
12. Sponsoring Agency Name and Address	13. Type of Report and Period Covered
National Aeronautics and Space Administration Lewis Research Center Cleveland, OH 44135	Contractor Final Report
	14. Sponsoring Agency Report No.
	DOE/NASA/0212-1

15. Supplementary Notes

Project Manager, Donald Alger, Stirling Engine Technology Section, NASA Lewis Research Center, Cleveland, Ohio

16. Abstract

A long-life hydraulic converter with unique features was conceptually designed to interface with a specified 15 kW(e) free-piston Stirling engine in a solar thermal dish application. Hydraulic fluid at 34.5 MPa (5000 psi) is produced to drive a conventional hydraulic motor and rotary alternator. Efficiency of the low-maintenance converter design was calculated at 93.5% for a counterbalanced version and 97.0% without the counterbalance feature. If the converter were coupled to a Stirling engine with design parameters more typical of high-technology Stirling engines, counterbalanced converter efficiency could be increased to 99.6%. Dynamic computer simulation studies were conducted to evaluate performance and system sensitivities. Production costs of the complete Stirling hydraulic/electric power system were evaluated at $6506 which compared with $8746 for an alternative Stirling engine/linear alternator system.

17. Key Words (Suggested by Author(s))	18. Distribution Statement
Stirling Engine Hydraulic Output Free Piston Solar Electric	Unclassified - unlimited STAR Category - 44 DOE Category - VC62B and VC62E

19. Security Classif (of this report)	20 Security Classif. (of this page)	21. No. of Pages	22. Price*
Unclassified	Unclassified	133	

* For sale by the National Technical Information Service, Springfield, Virginia 22161

FOREWORD

The work reported in this document was jointly pursued by the Joint Center for Graduate Study (JCGS) and Flow Industries, Incorporated. Work carried out at JCGS included that of M. A. White , who was responsible for overall coordination, S. G. Emigh, who worked in the area of overall mechanical design, J. E. Noble, who performed diaphragm design and analysis, and P. Riggle, who performed systems analysis. Work carried out at Flow Industries included that of A. Bennett, who executed the computer simulation studies, M. Hashish, who performed bellows flow loss analysis and clearance seal optimization, and J. Olsen, who coordinated the manufacturing cost analysis. The NASA project manager was D. L. Alger.

CONTENTS

1.0 SUMMARY

The primary objective of this contract was to develop a preliminary design for a long-life hydraulic converter capable of interfacing with the free-piston Stirling engine designed under NASA Contract DEN3-56, "Design of a 15-kW Free-Piston Stirling Engine-Linear Alternator for Dispersed Solar Electric Power Systems," NASA CR-159587. The engine/converter system interfaces directly with a heat receiver suspended at the focus of a parabolic dish solar collector. The hydraulic converter produces hydraulic flow at pressures suitable for operating a ground-based commercial hydraulic motor, which in turn drives a commercial rotary alternator to produce 15 kW of electric power output. A further objective was to assess the production costs of the hydraulic converter designed under this contract (coupled to the Contract DEN3-56 engine subsystem) at a production rate of 25,000 units per year. Production costs of two versions of the complete Contract DEN3-56 system design were also estimated and compared with costs of the Stirling hydraulic system.

The hydraulic converter design progressed through several iterative stages before arriving at the final layout design. Major efforts were required to successfully incorporate a counterbalance feature which avoids the necessity of isolating vibration induced by the 60 Hz oscillation with peak forces of ±24,180 N (5435 lbf). A unique new approach was developed in response to the problem of high hydraulic flow losses in the primary coupling fluid without compromising the very long-life low-maintenance characteristics of the hydraulic converter concept. This improves efficiency, virtually eliminates adverse pressure differences across primary metal bellows and enables extrapolation of the hydraulic converter technology to much higher power levels than would otherwise be practical.

Efficiency of the final layout design hydraulic converter was calculated at 93.5%, but this is increased to 97.0% by removing the counterbalance feature. A counterbalanced converter efficiency of 98.7% is also possible by coupling to an engine with a higher charge pressure more typical of high technology Stirling engines. For the converter coupled to an engine with the higher charge pressure and which also exhibits an average value of the Beale Number, the counterbalanced converter efficiency reaches an outstanding 99.6%. The reason for this wide variation in hydraulic converter efficiency is that the Contract DEN3-56 engine exhibits an exceptionally high stroke volume to power output ratio. This is ideally suited for coupling to a linear alternator, but imposes severe penalties on a hydraulic converter. Overall system efficiency is projected to be 35.0% for the nominal case and 36.3% in the non-counterbalanced version. This compares with 37.4% projected for the non-counterbalanced linear alternator system using SaCo magnets. An unspecified lower efficiency would result from using alternative magnetic materials which do not require large quantities of strategic cobalt. Substantially higher system efficiency is anticipated for a hydraulic converter coupled to an appropriately redesigned engine.

Extensive computer simulation studies were conducted using both a Coulomb load for the hydraulic converter and a viscous load for the linear alternator. Stability and stall problems were encountered with the engine dimensions and operating parameters as specified in NASA CR-159587. This problem was addressed by varying regenerator matrix porosity and utilizing alternative output control

means. Operating characteristics of the engine remain less than fully satisfactory, however, and it is recommended that a revised engine conceptual design phase be conducted to address these problems prior to implementing detail design and fabrication activities.

Production costs for both the linear alternator and hydraulic output systems were substantially higher than the linear alternator system costs given in the above-mentioned report NASA CR-159587. Approximately three years of inflation contributed to this difference. The primary difference, however, was the use of factory overhead on labor and machine tools for the present case, in addition to the prime costs as used in NASA CR-159587. The final cost figures cover eight alternate configurations. The most significant simple comparison is between single 15-kW systems rather than the option where four units are coordinated to reduce costs by using some common elements. The total system costs for the hydraulic system are $7,240 when the power train inertial loads are counterbalanced and $6,506 for the non-balanced version. The latter figure is more appropriate for comparing with the non-balanced linear alternator system. The total cost for the linear alternator system is $8,746 for the nominal version using SaCo magnets. The alternative system utilizing low cost magnets was costed at $7,896. The last figure has little real significance however, since substitution of any alternate magnets with a much lower coercive force would dictate a complete redesign of the linear alternator with undetermined impact on cost and performance. In all cases, the Stirling engine cost is $3,364.

The hydraulic system is concluded to be a very attractive alternative to the linear alternator system, offering some cost advantages and requiring less development of new technology. Maintenance-free lifetime of both systems should be much longer than for any kinematic Stirling engine, and elimination of costly mechanical linkages and dynamic seals also offer other significant advantages.

2.0 INTRODUCTION

Rapidly escalating energy costs underscore the desirability of developing more efficient energy conversion systems, particularly those which also include multifuel capability. Stirling engines satisfy the above criteria and appear to be particularly well-suited for use with point-focus distributed receiver solar thermal collectors. This point was underscored in a study (Reference 1) conducted by the Systems Analysis Branch of the Solar Energy Research Institute. Eleven solar thermal electric options were compared, based on technical, economic, social, and commercial criteria. Point-focus central receivers with Rankine power conversion and parabolic dish collectors with distributed Stirling engines were ranked significantly higher than the other nine alternatives.

Problems associated with the most highly developed kinematic Stirling engines include their high cost, heavy weight, severely limited operational life and dynamic seal problems (Reference 2). Free-piston Stirling engines offer outstanding potential for solving or reducing these problems, but they have not yet been brought to an advanced state of development except in very small sizes for use as an artificial heart power source (Reference 3). One promising approach was considered under NASA Contract DEN3-56 (Reference 4). In this concept, the seal problem is avoided by using an all-pneumatic free-piston power takeoff utilizing gas bearings. The high heater head cost is addressed by proposing a cast annular flow gas heater. The linear alternator, however, is in an early state of development and contains substantial quantities of costly cobalt, which is also a strategic material with an uncertain future supply. Alternate magnetic materials are feasible, but they impose significant size, weight, and performance penalties.

The purpose of the current contract is to evaluate a concept in which the Reference 4 linear alternator is replaced by a hydraulic converter. This converter utilizes an integral intensifier piston to pump hydraulic fluid from a low-pressure reservoir to a high-pressure accumulator. The pumped fluid pressures are suitable for operating a ground-based hydraulic motor which in turn drives a commercial rotary alternator to produce 15 kW of electric power output. The sliding seal problem is avoided by incorporating a flexing diaphragm or bellows interface to transmit the pressure pulses and volume changes from the Stirling engine to the hydraulic fluid. As with the linear alternator system, cyclic loads are carried by a pneumatic bounce chamber rather than the heavy bearings in a conventional kinematic engine.

The consequent elimination of crankshaft, bearings and connecting rods provides the potential for reducing size and weight of either free-piston system relative to a kinematic engine. Even more important for some applications, including the solar thermal case of primary concern in this study, is the potential for increased efficiency by greatly reducing the mechanical friction losses encountered with kinematic engines. A third major consideration for the free-piston systems is that elimination of the sliding seal should result in a much longer maintenance-free operating life than appears to be practical with kinematic engines (Reference 2).

The hydraulic converter of the Stirling hydraulic engine offers several demonstrated or potential advantages relative to the linear alternator as used in the free-piston Stirling engine system of Reference 4. These include the following:

- o Flexibility in selecting converter piston mass and stroke for optimum system performance.
- o Decoupling of engine speed from alternator speed through hydraulic accumulation to reduce frequency control problems.
- o Costly gas bearings and permanent magnets are eliminated.
- o Optional capability of counterbalancing power piston to eliminate its vibration.
- o Wide flexibility in design output pressure to optimally interface with hydraulic motor.
- o Ability to utilize pumped hydraulic fluid rather than auxiliary coolant loop for waste heat removal.
- o Bellows seal allows optimum choice of bounce chamber gas to almost entirely eliminate the substantial hysteresis losses normally encountered when using helium or hydrogen in the bounce chamber.

All sliding components in the hydraulic converter are lightly loaded and immersed in lubricating oil. Flexing elements can be reliably designed for virtually unlimited life by maintaining stress levels well below the endurance limit. In contrast, the lifetime and effectiveness of sliding seals are dependent on a variety of relatively uncertain empirical relationships and practical execution factors. All diaphragms and bellows in the hydraulic converter incorporate pressure balancing features so that only deflection stresses need be considered. Most of the basic features of the hydraulic converter design have been subjected to thorough performance documentation and life testing at the 5-watt output level under an NHLBI contract (Reference 3).

3.0 SYSTEM DESIGN AND AYALYSIS

The Stirling hydraulic solar electric power system concept will first be described in this section. Subsections which follow will discuss the conceptual design of the hydraulic converter, detailed loss calculations in the converter, computer simulation and engine analysis, and system cost studies.

A block diagram in Figure 1 illustrates the basic elements of the system. A parabolic collector (not shown) concentrates the solar input on the heat receiver which interfaces with the free-piston Stirling engine as described in Reference 4.

High-pressure output from the hydraulic converter, which is intimately coupled to the engine, is piped to a ground-based high pressure accumulator. A small accumulator adjacent to the converter is used to smooth flow and reduce losses in the delivery line. The high-pressure oil is used to operate a conventional hydraulic motor which in turn drives a standard rotary alternator to produce the desired electrical output. The low-pressure return flow from the hydraulic motor is collected in a ground-based low pressure accumulator from which it returns to the hydraulic converter. This return flow may be directed as illustrated through a ground-based cooling system and the engine heat exchanger to eliminate the need for an auxiliary cooling loop.

The same components shown in the block diagram are presented in a schematic fashion in Figure 2A. Relationships are as described for Figure 1 and key elements of the hydraulic converter are also identified. These include the power bellows which separates the engine working gas from the hydraulic converter working fluid. The power bellows end terminal is an integral part of the power piston which includes an intensifier piston section. The intensifier piston section, together with hydraulic check valves, provides the system output by pumping hydraulic fluid from the low pressure accumulator at 0.69 MPa (100 psi) to a high pressure accumulator at 34.5 MPa (5000 psi).

An alternate version of the system schematic is shown in Figure 2B. This includes most of the elements from Figure 2A but also illustrates detailed features of the final hydraulic converter design. The latter is fully described in Section 3.1.3, but the schematic functional characteristics of key features are briefly described here.

The power piston has the form of a cylinder with one end closed off and with a small central pumping piston or intensifier piston. The cylindrical portion connects the power bellows to the buffer bellows and separates the external hydraulic fluid from the internal buffer gas. A step on the central outside diameter of this sleeve provides a differential area which couples to two diametrically opposite counterbalance pistons. The dynamically optimum piston mass is distributed with 50% in the power piston and 25% in each counterbalance piston. This eliminates vibration and couples in the main power train.

The flat end of the power piston forms the power bellows end terminal and separates the engine working gas from the buffer gas. The pumping piston attached to the center of this end plate, in conjunction with the inlet and outlet check valves, produces the net engine/converter power output by pumping hydraulic fluid from the low pressure reservoir to the high pressure accumulator. The oil above the pumping piston is sealed from the buffer gas region by the

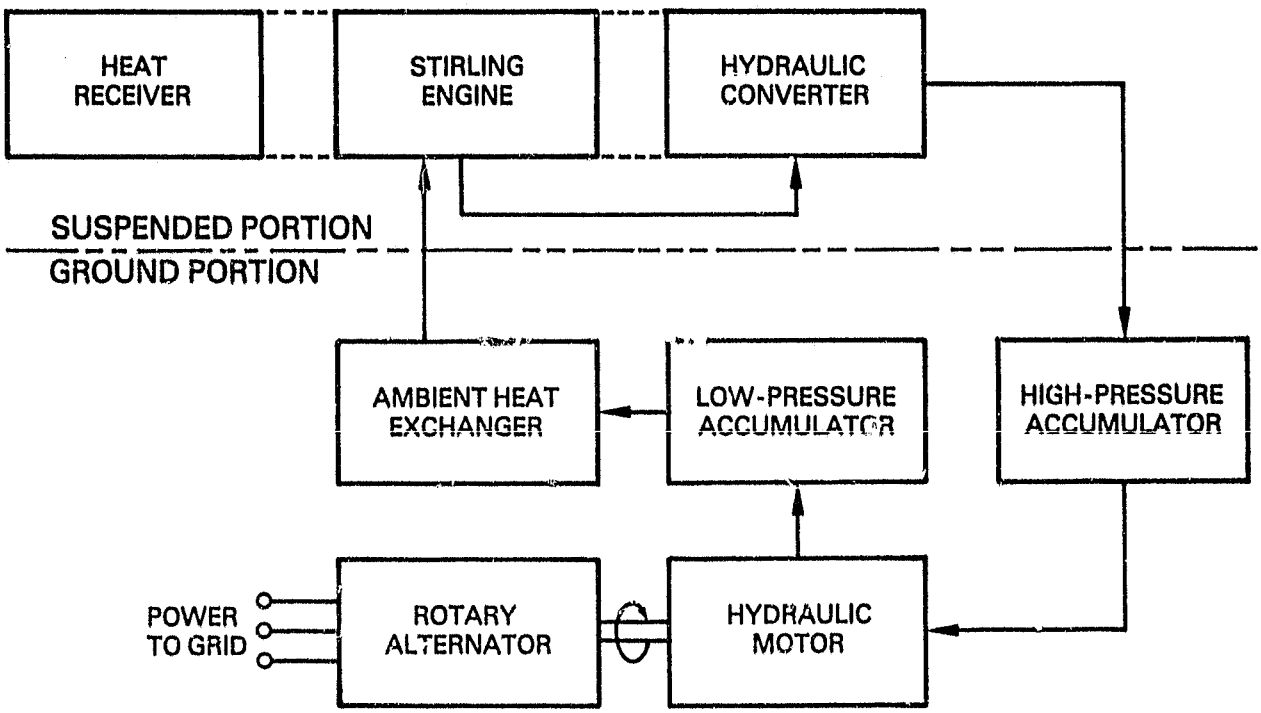

Figure 1. Block Diagram of Solar/Electric Power System.

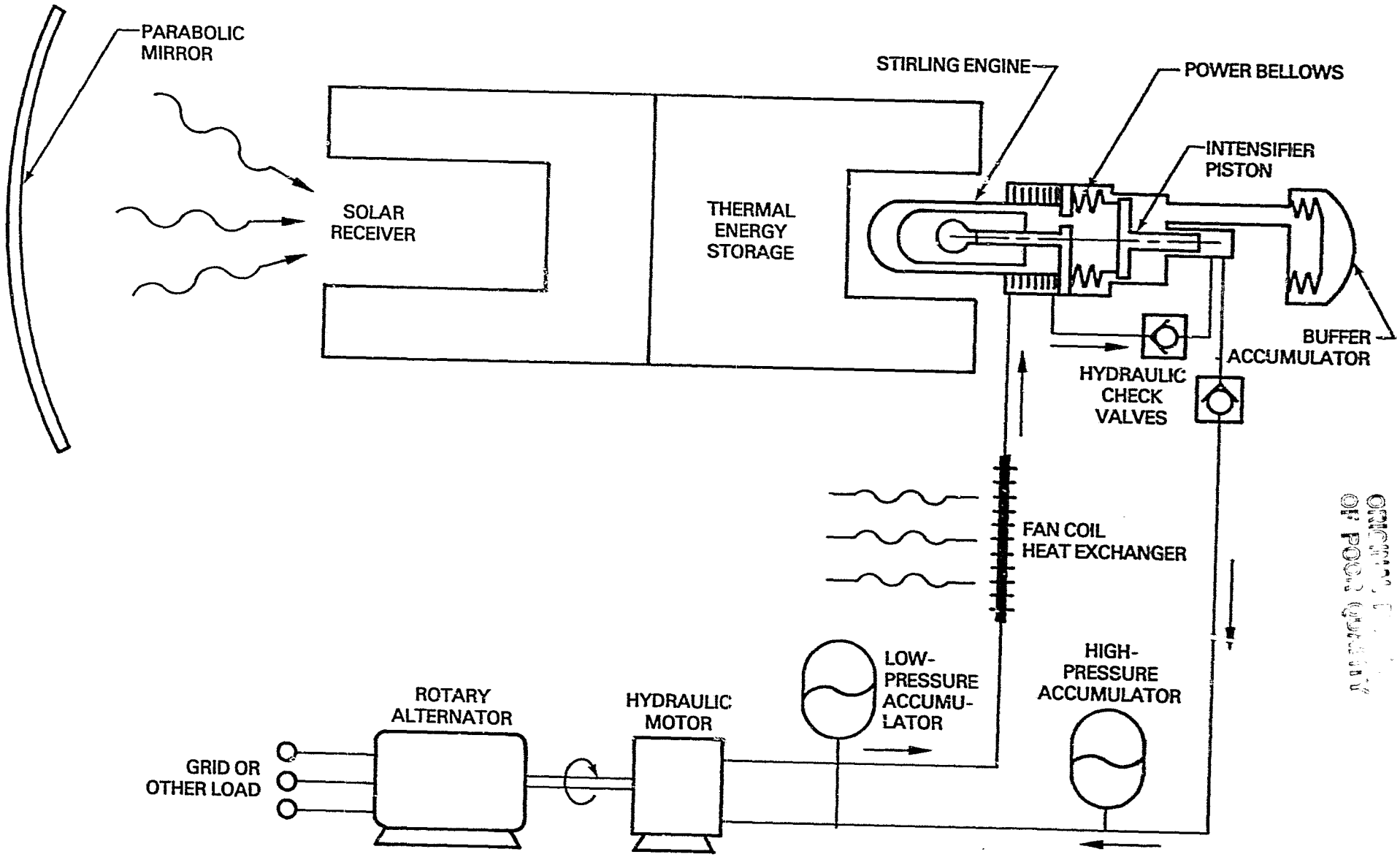

Figure 2A. Solar Electric System Schematic.

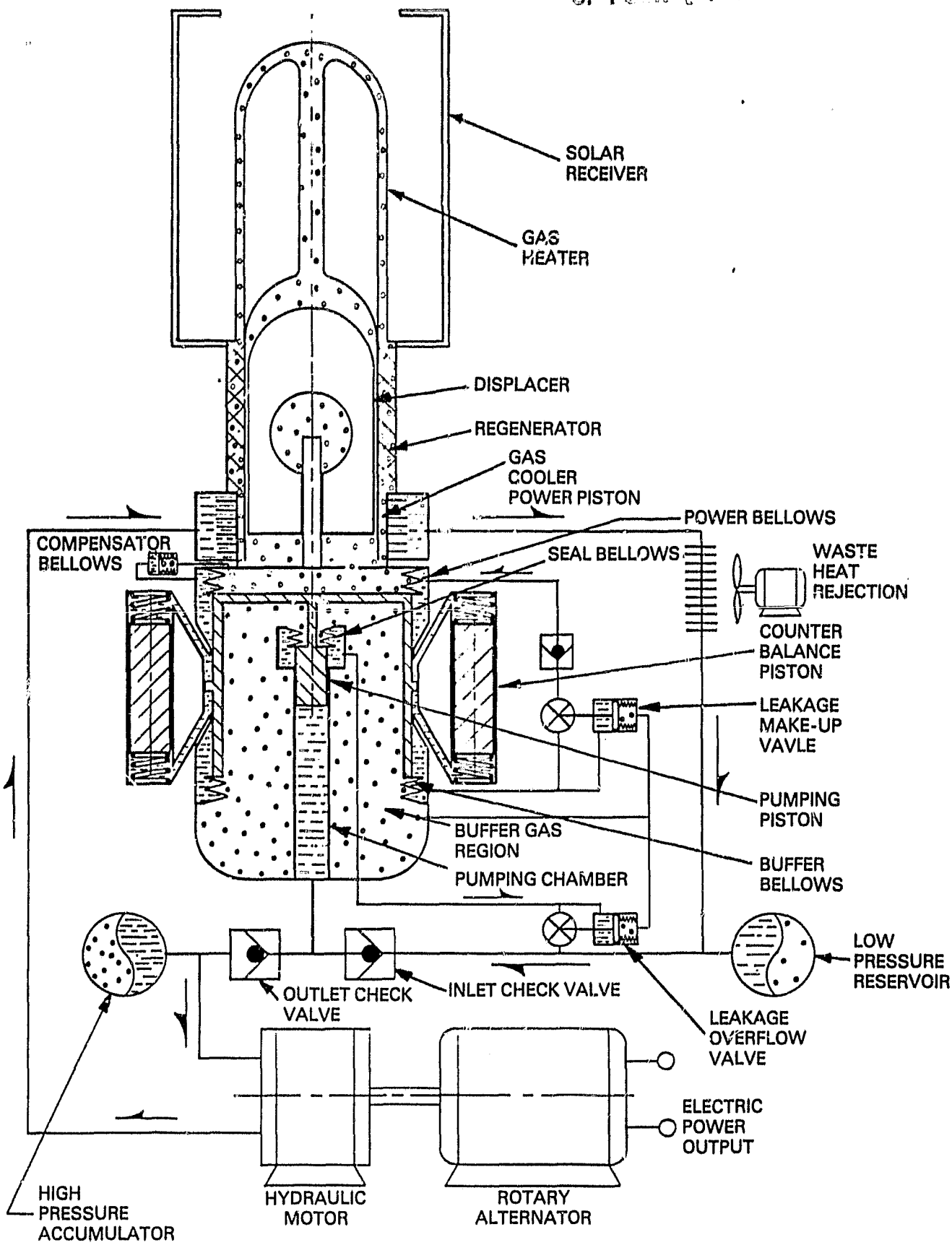

Figure 2B. Stirling Hydraulic System Schematic

seal bellows. The seal bellows is always pressure balanced by means of the hermetically sealed leakage overflow valve assembly which always references the oil pressure to buffer pressure. The high average pressure in the pumping chamber results in a net hydraulic leakage into the seal bellows oil region. This excess fluid moves the leakage overflow valve pilot and dumps the excess oil into the low pressure hydraulic line.

The hydraulic fluid in the counterbalance, buffer bellows and power bellows regions is fully independent from the hydraulic fluid in the main power train. The leakage makeup valve assembly acts in a similar fashion to the leakage overflow valve assembly. It pressure balances the buffer bellows and, in conjunction with a check valve, provides makeup flow from the buffer bellows hydraulic region back to the power bellows hydraulic region. As described in Section 3.1.1, this makeup flow is necessitated by the fact that the buffer pressure is slightly lower than average engine pressure, so a slow leakage occurs past the clearance seals. The final component in this hydraulic circuit is the compensator bellows which maintains a pressure balance across the power bellows.

The most innovative aspect of this design is an approach used to greatly reduce hydraulic flow power losses by eliminating most of the hydraulic fluid volume flow rate directly coupled to power piston displacement and velocity. Such flow produces negligible flow losses in very small Stirling hydraulic engines (Reference 3), but scales up to become a major problem in large engines. That was the motivating factor which led to the current configuration, described as a "dry inertia" concept in Section 3.1.2.

Several variables make a direct and simple statement about system efficiency impossible. The component efficiencies given in the stage-by-stage efficiency summary of Figure 3 were selected to provide the most reasonable comparison with the reported linear alternator system efficiency of 37.3% in Reference 4. In questionable areas, decided advantage was extended to the linear alternator system.

The first ambiguous area is engine efficiency. The Reference 4 value of 41.5% was used even though the results of Section 3.3.4 predict 42.2%. The dynamic analysis used here would predict a much lower engine efficiency for the linear alternator system which required a power piston approximately 50% heavier than optimum. Use of the optimum power piston mass for the hydraulic system would almost certainly boost hydraulic system efficiency above linear alternator system efficiency.

At least three efficiency numbers could be used for the hydraulic converter. The nominal hydraulic converter efficiency is 93.5%, but this includes a counterbalancing feature not included with the linear alternator. The same basic converter without counterbalancing has a conservatively calculated efficiency of 97.0%, which is used in Figure 3.3. A solid case is made in Section 3.3.3 below that the unusually large stroke volume of the Reference 4 engine (which is ideal for the needs of the linear alternator) presents a very punitive constraint on the hydraulic converter. If the converter were coupled to an engine of typical stroke volume, the efficiency of the counterbalanced version would jump to 99.6% as shown in Section 3.2.5. The coincident engine dead volume and Beale number improvements would also lead to substantial

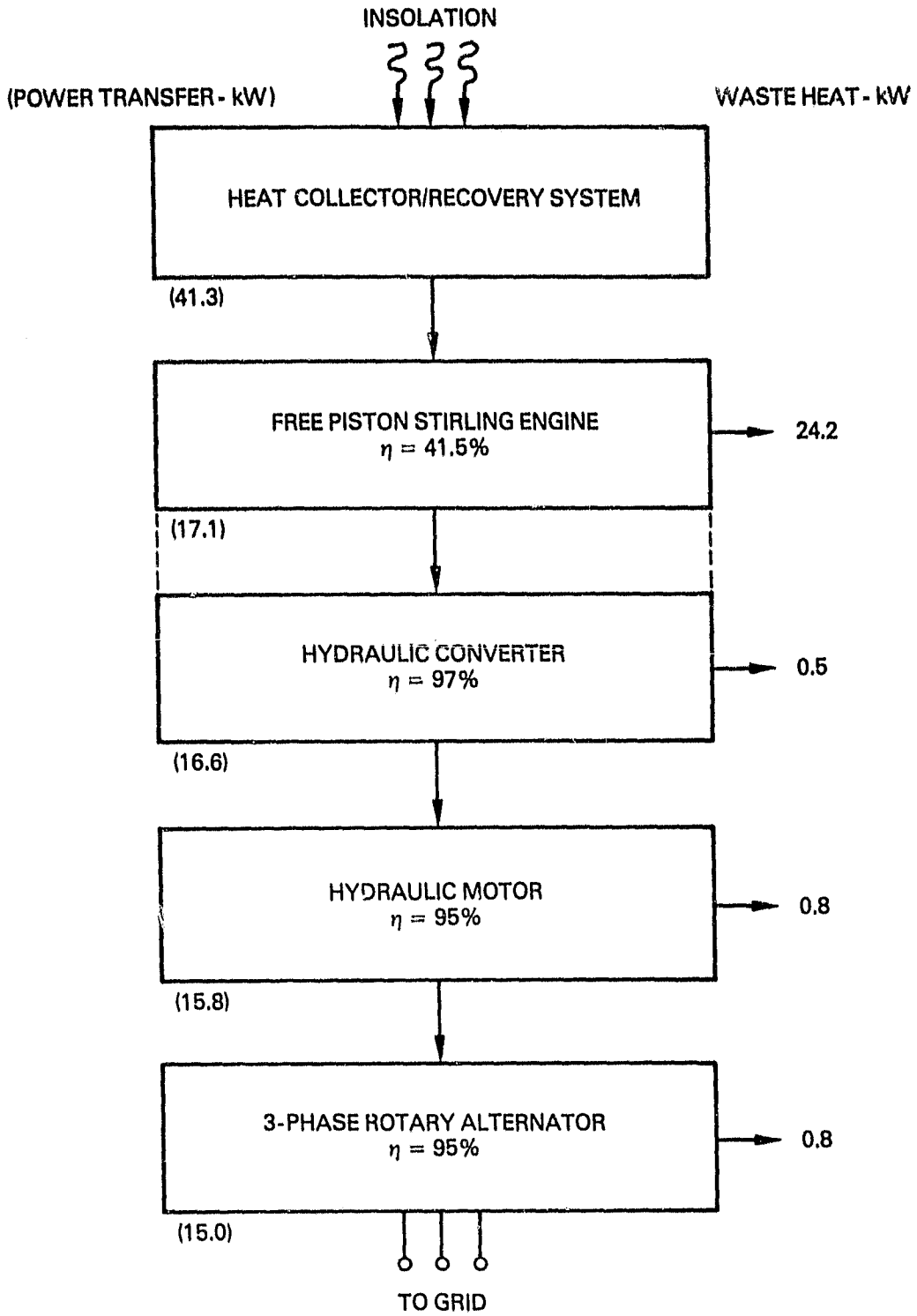

Figure 3. Stage-by-Stage Efficiency for Non-Counterbalanced System.

improvements in engine efficiency. These factors fully accounted for would give a decided efficiency advantage to a mature hydraulic system.

It should finally be noted that the linear alternator efficiency of 90% reported in Reference 4 was not extensively documented, but based on the best efficiency ever obtained with a linear alternator using large quantities of strategically valuable cobalt. Practical linear generator efficiencies may well be lower than this anticipated level.

In summary, both the Stirling engine/linear alternator and Stirling hydraulic/electric systems are represented only by preliminary conceptual designs at the present time. Both are very promising concepts with outstanding potential to be developed into a reasonable cost, high performance, very low maintenance alternative to conventional kinematic Stirling engines. On balance however, the facts presented throughout this report strongly suggest that in fully developed forms the hydraulic alternative would be superior in virtually every important aspect. Moreover, the development effort for the hydraulic system should be substantially lower since major off-the-shelf components would be utilized and the hydraulic converter is a fundamentally simple and technologically straightforward unit.

3.1 Hydraulic Converter Layout Design Development

The conceptual layout design progressed through several stages as improvements were made or problems were encountered and resolved. This section outlines the design development rationale and provides a detailed description of the final design configuration including internal fluid makeup systems.

3.1.1 Baseline Design

The baseline design concept used as a point of departure for the present contract effort was the design presented in the original proposal which led to the contract. The baseline design was revised significantly during the conceptual development. It still provides a good basis for understanding the work that followed and retains a viability for certain applications while illustrating some interesting features in its own right. A description of the baseline design is therefore included here as the first subsection under Layout Design Development.

A layout of the proposed baseline design for the 15-kW hydraulic Stirling engine is shown in Figure 4. The design of the hydraulic converter is based on established technology (Reference 3) and requires no technological breakthroughs to make it practical. All basic features of the Stirling engine design as presented in Reference 4 have been retained. These include a posted displacer supported by a cantilevered gas bearing, an investment cast annular heater head which interfaces with the solar heat receiver and integrates with an annular regenerator and a tubular gas cooler.

The hydraulic converter, which interfaces to the engine support plate, is relatively simple in design and concept. The helium working gas of the engine is separated from the hydraulic fluid in the converter by a low-dead-volume power bellows and an integral intensifier power piston which forms the power bellows end terminal. Most of the fluid displaced by the power piston is

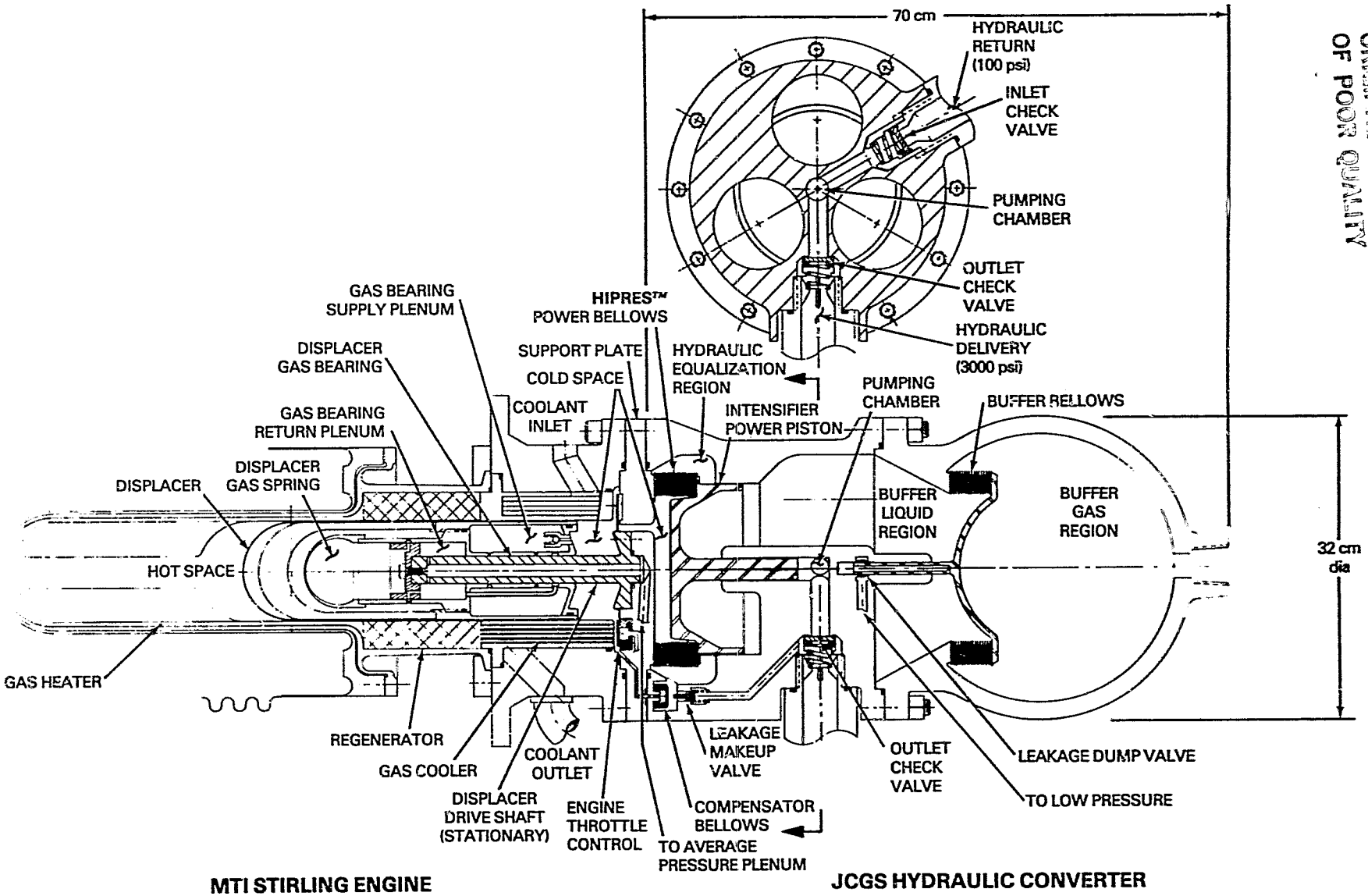

Figure 4. Baseline Design for 15- kW Hydraulic Stirling Engine.

shuttled through three large passageways in the converter housing to a buffer accumulator which has a similar bellows seal to the buffer gas reservoir which acts as a bounce chamber. The small end of the intensifier piston displaces hydraulic fluid in the pumping chamber from which it is pumped through the outlet valve to a high-pressure accumulator during the power stroke. Oil from a low-pressure reservoir flows into the pumping chamber through the inlet check valve on the return stroke.

The only portion of the converter baseline design which impacts engine hardware is the engine throttle control which is incorporated into the support plate. This device consists of a washer-shaped ring which is normally retracted into a position which makes it flush with the support plate surface. It can, however, be raised to the position shown by means of three equally spaced bellows which are fed by an external hydraulic actuator. This action serves to increase the total windage in the gas circuit through the heat exchangers by increasing flow resistance at the base of the gas cooler tubes. This reduces displacer amplitude and therefore engine power output. Very little throttling is required to effect a significant reduction in power output. This action is exactly analogous to the hydraulic drive line throttle control used in the artificial heart engines (Reference 3) where operation of the output control concept has been automated and experimentally shown to be energy conservative. Although this remains the most energy efficient means for achieving part load operation, computer simulation studies described in Section 3.3 showed that it was not well suited to operation with the specified engine design. This control approach has therefore been supplanted by a variable volume displacer gas spring for the present application. Windage control should be evaluated further if the recommended engine redesign task is implemented.

The effective inertial mass of the "free piston" consists of the intensifier piston, the buffer bellows end terminal plate, and the hydraulic fluid between them. The cross-sectional flow area in this region is maintained as nearly constant as practical to minimize the local flow losses. This also allows the contribution of fluid inertia to the effective piston mass to be more easily evaluated.

The diameter of the large end of the intensifier piston is machined so that its area is equal to the effective area of the power bellows. The compensator bellows accommodates any small volumetric change caused by a mismatch in the actual areas. It also assures that the instantaneous engine pressure will be transmitted to the outside of the power bellows to maintain an effective pressure equalization across the bellows convolutions.

The pumping chamber pressure is essentially equal to the high accumulator pressure or hydraulic delivery pressure of 34.5 MPa (5000 psi) during the power stroke and the hydraulic return pressure of 0.7 MPa (100 psi) during the return stroke. The average pumping chamber pressure is therefore about 17.6 MPa (2550 psi). The free converter piston (intensifier power piston) operates with dynamic cyclic stability, so the time averaged forces must balance. Since the specified average engine pressure of 5.8 MPa (844 psi) is lower than the average pumping chamber pressure, the average buffer pressure must be below the average engine pressure. The exact level is dependent on the actual intensifier and primary piston areas. For the final reference design, average buffer pressure is 5.7 MPa (828 psi).

As a consequence of the fact that the average buffer region pressure is less than the average engine pressure, there will be a slight net leakage of hydraulic fluid from the hydraulic equalization region around the power bellows to the buffer region. When this occurs, the compensator bellows described above serves a third function, namely to operate the leakage makeup valve which allows a small volume of high-pressure fluid to replenish the power bellows region. Similar makeup devices have routinely and successfully been used in artificial heart hydraulic Stirling engines (Reference 3) for years to maintain dynamic equilibrium in free pistons.

The average pressure in the pumping chamber is substantially higher than the average pressure in the buffer region. Consequently, there is a net leakage of fluid into the buffer region from the pumping chamber as well as from the power bellows region. In order to dispose of this small quantity of excess fluid, a dump path is provided from the buffer region to the low-pressure return line through the guide shaft attached to the buffer bellows end plate. This guide shaft uncovers the low-pressure port to function as a leakage dump valve when the buffer bellows reaches its desired limiting stroke away from the engine. The clearances are sized such that the normal leakage past the guide shaft when the low-pressure port is covered will be appreciably less than leakage into the buffer region.

3.1.2 Design Refinements and Alternative Approaches

o Counterbalance Approaches and Design Evolution

One of the first items considered under this contract was the unbalanced inertial force generated by the reciprocating power piston and associated inertia. This force is the product of the inertial mass and piston acceleration. If sinusoidal motion is assumed, the acceleration is proportional to the amplitude of oscillation and the square of the operating frequency. For the reference design case with an optimum inertial mass of 10 kg, stroke of 3.4 cm (for 17.8-cm piston diameter) and frequency of 60 Hz, the peak unbalanced force is 24,180 N (5435 lbf). This value is substantially below the 37,280 N (8380 lbf) developed by the Reference 4 linear alternator design. Absorption of these inertial forces at 60 Hz by the support structure, even with vibration isolation, remains a formidable challenge. The much smaller unbalanced displacer force of 8026 N (1804 lbf) still represents a significant problem. The recommended engine redesign effort would greatly reduce both piston and displacer inertial forces.

Taking action to balance the displacer inertial force is not within the ground rules of the present effort. Balancing of the converter piston, however, was deemed to be highly desirable in order to achieve a truly viable design. Several approaches were evaluated in which the power piston was decoupled from the power bellows and its mass was distributed equally between portions moving in opposite directions with hydraulic coupling.

The version of this concept which provided the best packaging approach is shown by the rough sketches in Figures 5 and 6.* A central 10.16-cm-diameter

*Necessary leakage makeup systems and other design subtleties are not included in these figures or in the other design sketches to follow. Such details are addressed for the final configuration.

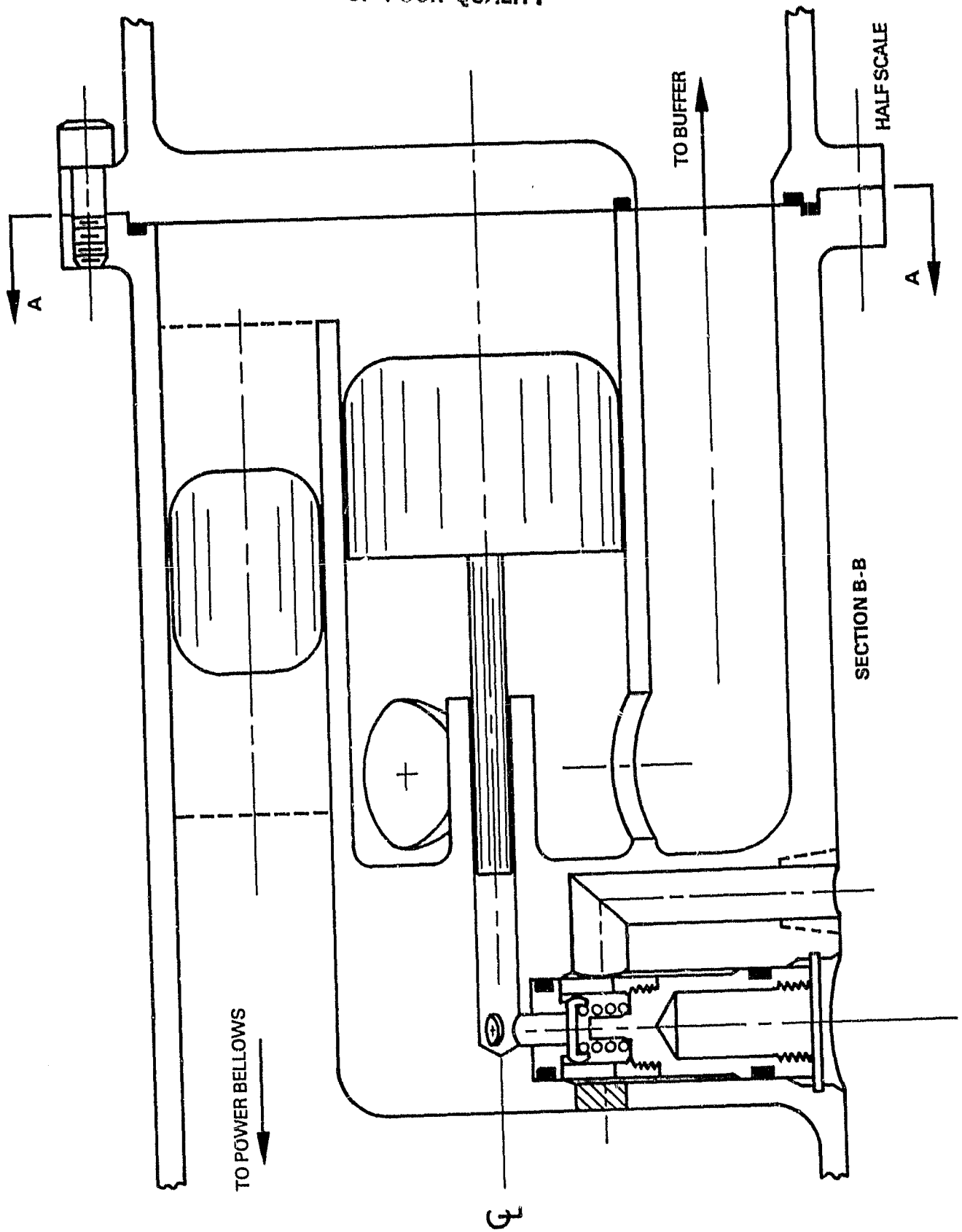

Figure 5. Concept Sketch with Three Counterbalancing Pistons.

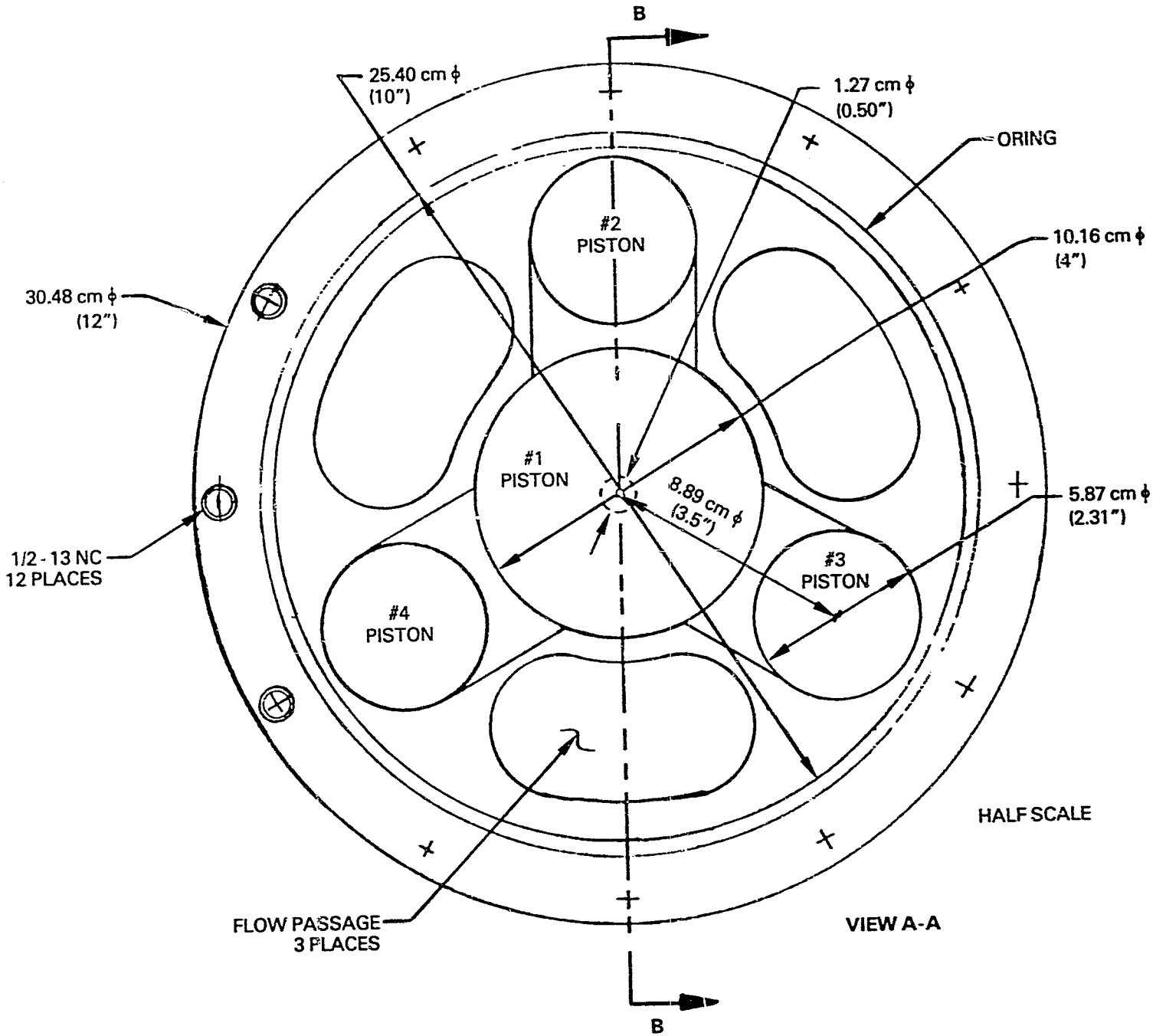

Figure 6. Section View of Figure 2.

cross-sectional area and same total mass as the central piston. Hydraulic flow passages are manifolded around to enable incorporating the entire assembly between the buffer and engine regions while balancing all forces and introducing no couples. The basic impracticality of this approach became clear, however, when hydraulic flow losses in the interconnecting passages were evaluated. Flow friction losses were inconsequential, but $v^2/2g$ velocity head losses in the main flow stream were totally unreasonable. The fluid manifolding and direction reversals would result in several head losses and the flow loss for each head loss was on the order of 15 kW.

The magnitude of one head loss was reduced by about a factor of ten by returning to the increased cross-sectional area and reduced velocity of the 17.8-cm-diameter piston of the original reference design. This magnitude of loss is manageable since the primary hydraulic flow path is unidirectional, and careful tailoring of the flow passages can maintain essentially constant flow area. It is possible, though perhaps expensive, to tailor the flow passages accurately enough to provide a relatively small fraction of one head loss in this configuration. Taking this approach, however, effectively eliminates the option of counterbalancing, unless two independent piston-buffer assemblies are used back-to-back.

It is clear that flow loss per velocity head is very high when shuttling hydraulic fluid with the same volumetric displacement as the engine gas. Simple analysis shows that the head loss problem is greatly diminished if the fluid flow diameter is significantly reduced without a corresponding increase in velocity. Capitalizing on this fact is possible since the actual power delivery stream is on the small intensifier diameter, with the large-diameter flow used only for coupling between the power bellows and the buffer bellows.

A means for accomplishing this is conceptually illustrated in Figure 7. The large-diameter section of the power piston is extended and attached to the buffer bellows with a hydraulic equalization region around the buffer bellows similar to that around the power bellows. This concept eliminates the considerable fluid inertia between the power piston and buffer bellows together with its attendant velocity head problems. It is therefore termed a "dry-inertia" configuration. Other advantages include increasing the axial distance between power piston outside bearing surfaces and being able to use the region formerly occupied by the hydraulic fluid for buffer bounce chamber gas. The latter result allows the overall converter size and weight to be reduced by roughly a factor of two relative to the Figure 4 baseline design. All sliding surfaces remain immersed in hydraulic fluid with this approach and side loads are still minimized. It is necessary to add a seal bellows to the intensifier piston, with an effective bellows diameter equal to that of the piston. Overall, the Figure 7 dry-inertia concept is a significant step forward from the Figure 4 baseline design, but it still retains the unbalanced piston inertia forces.

A variation on the dry-inertia concept is shown in Figure 8. This introduces some additional complexity, but accomplishes the major advance of fully counterbalancing the inertial piston forces. An extra step in area is added to the intensifier portion of the piston. The volume displaced by this differential area is transmitted hydrostatically to the bottom of a coaxial annular counterbalance piston. This piston slides on an inner support member and is shown with a floating seal on the outside diameter of its seal region.

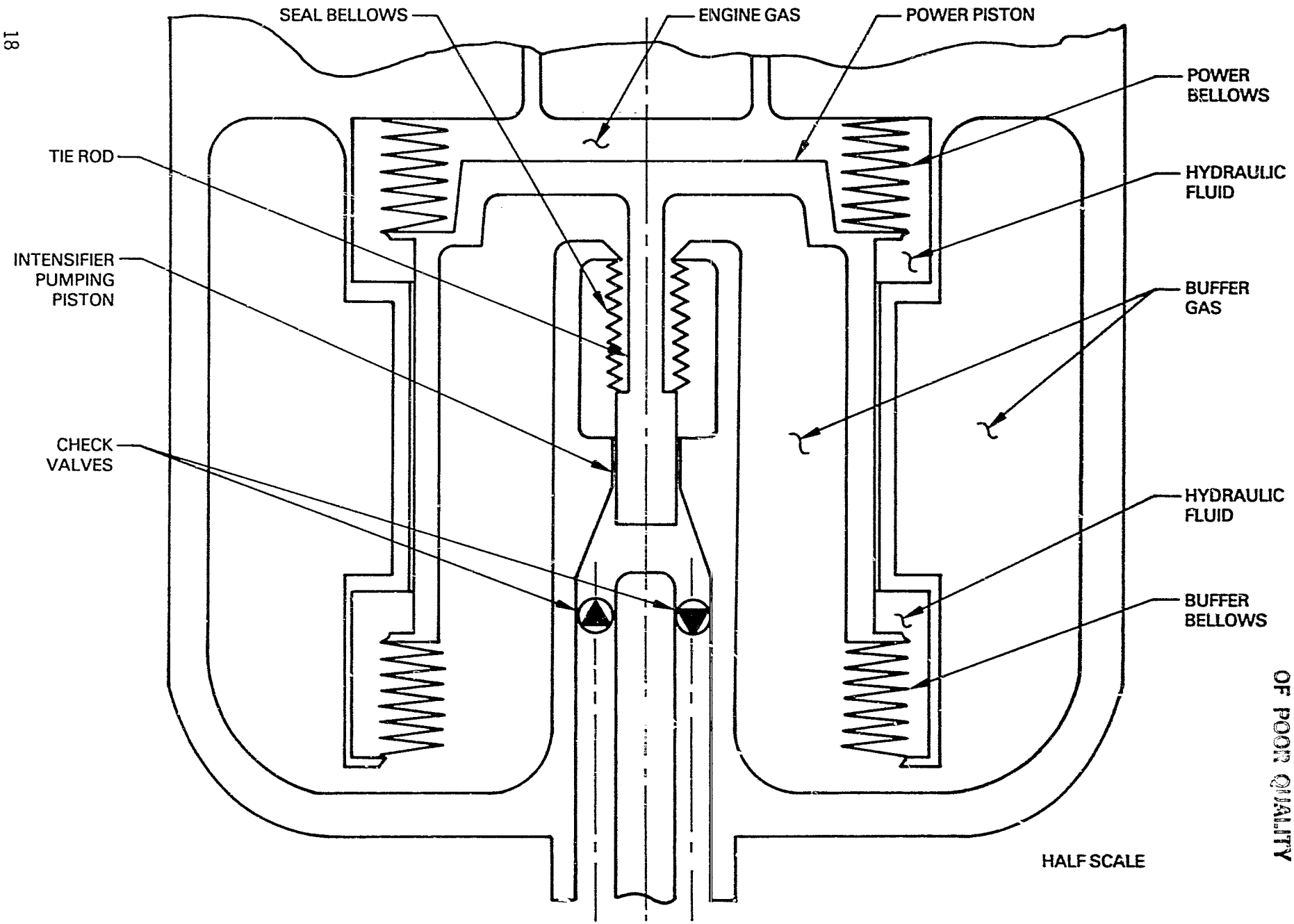

Figure 7. Concept Sketch of Hydraulic Converter with "Dry" Inertia.

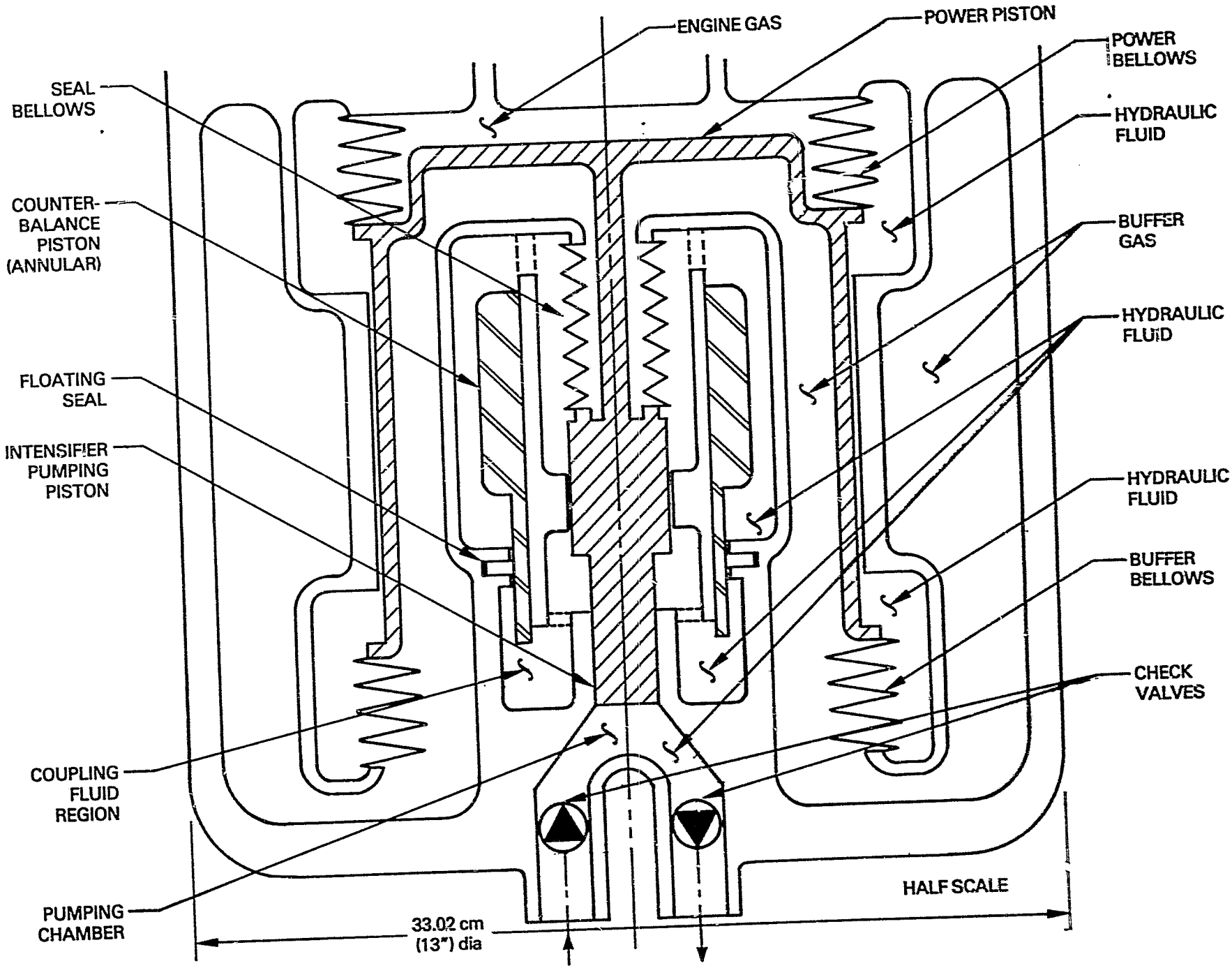

Figure 8. Concept Sketch of Hydraulic Converter with "Dry" Inertia and Counterbalancing

The cross-sectional area of the counterbalance piston between the seals is nominally equal to the step area on the intensifier piston, and its mass is equal to that of the overall intensifier/power piston assembly.

Further optimization of the reference design with consideration for manufacturing practicalities led to replacing the annular counterbalance piston with two cylindrical pistons deployed on opposite sides of the intensifier piston. Analysis of this design for practical consistency disclosed one major shortcoming. The seal bellows has the same effective diameter as the intensifier pumping piston. A minimum practical value of the bellows span limits the diameter of the tie rod inside the seal bellows to about 0.635 cm (0.25 in.). This size rod can easily carry the loads imposed by pumping chamber pressures. These induce compressive stresses of 235 MPa (34,000 psi) and tensile stresses of 41 MPa (6000 psi) in the tie rod. The inertial forces which result from accelerating the counterbalance pistons superimpose an additional 380 MPa (55,000 psi) of both compressive and tensile stresses. Problems caused by these marginal stress levels were compounded to unacceptable levels when ball joints were added to each end of the tie rod. These are necessary to permit disassembly and to remove the possibility of side loads resulting from reasonable manufacturing tolerances.

The solution to this problem was to remove the counterbalance piston driving area from the central intensifier piston to the power piston region between the buffer bellows and power bellows. This was accomplished by incorporating a floating seal midway between the buffer bellows and power bellows on the 17.78-cm (7.0-in.) piston OD as described in detail in Section 3.1.3.

Design trades were evaluated over a range of piston diameters. The results show a relatively narrow range of interest betweeen about 15 cm and 20 cm (6 in. and 8 in.) diameter. For larger diameters, the reciprocating mass becomes excessive and pressure vessel size and weight increase rapidly. At smaller diameters several adverse factors appear. Flow losses increase, the number of bellows convolutions (and therefore cost) increases rapidly, and the optimum piston mass becomes too small to satisfy structural requirements. The final compromise diameter selected was 17.8 cm (7.0 in.), which is fortuitously the same diameter as the power piston in the Reference 4 engine/linear generator, so the nominal stroke length in the present case remains the same as that in Reference 4.

o Power Bellows Design Trades

The power bellows (or metal diaphragm alternative) is one of the most critical system components. The metal diaphragm analysis was conducted as an independent task and is summarized in Section 3.1.4 and Appendix A. Elastomeric diaphragms are discussed later in this section. An analytical design trade study for the reference design metal power bellows was conducted to provide visibility for critical parameters. An effective diameter of 17.8 cm (7.0 in.) was assumed for a standard nesting ripple welded metal bellows configuration. Material properties for AM-350 precipitation hardening stainless steel (selected for reasons described below) were used, and all configurations had a peak stress level of 200 MPa (30,000 psi). This stress is composed of a 100 MPa (15,000 psi) mean stress and a 100 MPa (15,000 psi) alternating stress. These values are chosen to avoid tensile stresses and maintain a peak stress sufficiently low to provide essentially infinite life.

With the above conditions, independent parameters are chosen as material thickness t and bellows span S defined as (OD - ID)/2. Calculated results include number of convolutions N, static pressure difference support capacity P_s and natural surging frequency f_s. Dead volume is also calculated for the standard nested ripple configuration. If the higher cost HIPRES™ proprietary bellows design is used, the gas dead volume is essentially eliminated. Previous experience with miniature Stirling hydraulic engines (Ref. 3) has shown the HIPRES™ configuration to be essential to prevent major performance compromises from excess dead volume. With the 15-kw design, however, dead volumes with a standard nesting ripple power bellows can be as low as 16 cm^3 (1.0 in^3). The total engine dead volume is more than 2000 cm^3 (122 $in.^3$). The performance impact caused by using a standard bellows does not, therefore, justify the extra cost.

General objectives to consider in selecting a power bellows configuration are

1) a natural surging frequency (frequency for axial oscillation of central convolutions with the ends fixed) as far above the 60 Hz operating frequency as practical (although oil damping in the convolutions will reduce potential problems),

2) a minimum number of convolutions to reduce cost,

3) a low gas side dead volume, especially where it is low enough to avoid the extra cost of a HIPRES™ bellows,

4) a narrow bellows span to reduce hydraulic flow losses external to the bellows, and

5) a high static ΔP tolerance.

The last item is of minimal importance since no feasible design can take the full ΔP and the reference configuration virtually eliminates the possibility of ΔP's induced by transient operating conditions.

The results of the power bellows design study are summarized in the array of points shown in Figure 9. The location on the array specifies bellows span and convolution dead volume. Other pertinent data are listed adjacent to each point. Perusal of Figure 9 allows several general observations to be made.

1) Other parameters remaining equal, increasing material thickness has a positive effect on the minor factor of static ΔP tolerance but a negative impact on both dead volume and the number of convolutions required.

2) Decreasing bellows span improves all parameters except the number of convolutions required.

3) The larger bellows spans considered have surging frequencies uncomfortably close to the operating frequency.

4) At wide spans, the dead volume is nearly independent of span, but it decreases fairly rapidly with span for relatively narrow spans. This effect is most pronounced with thicker material.

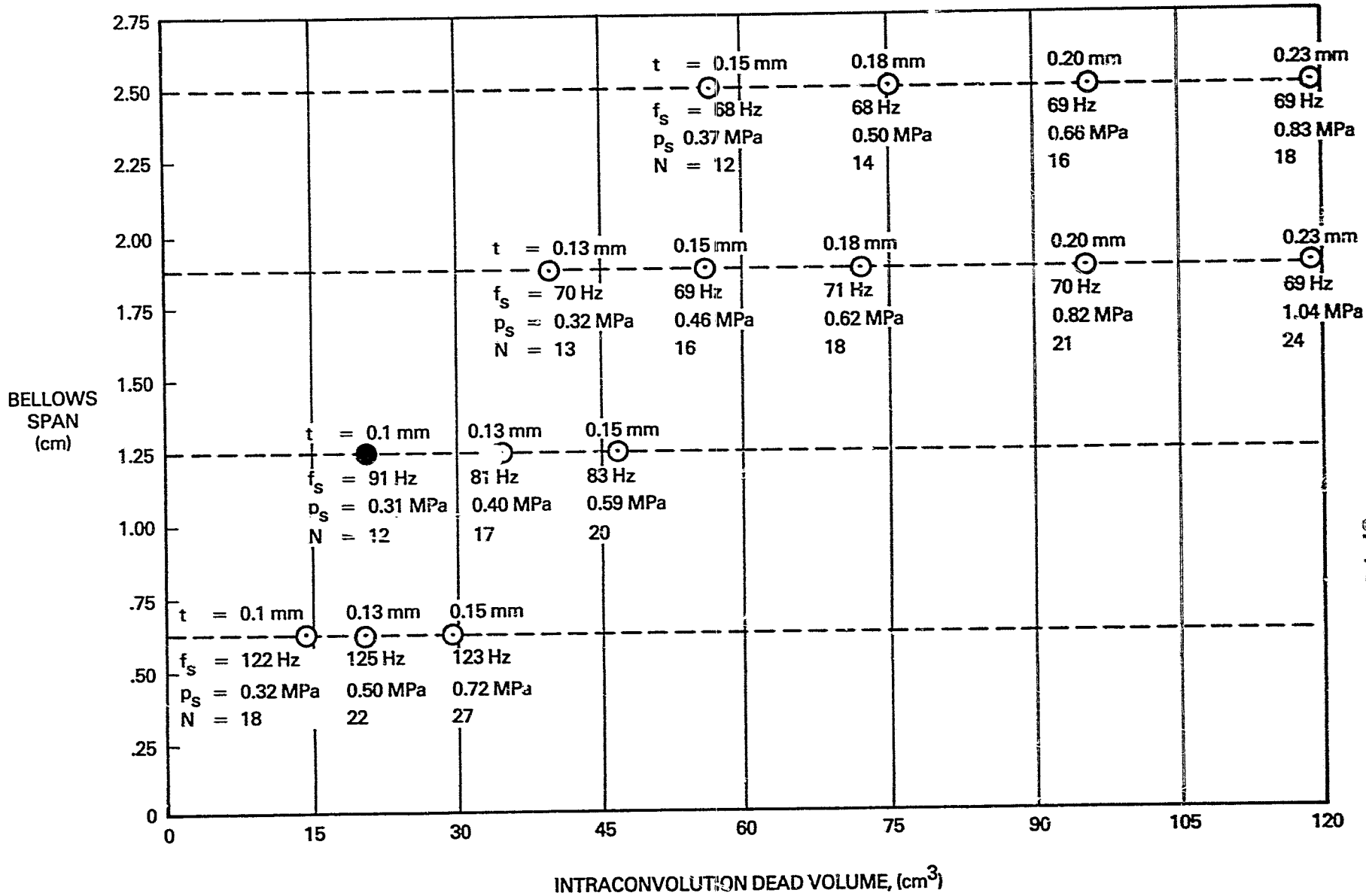

Figure 9. Results of 17.7 cm Effective Diameter Power Bellows Design Study

All factors considered, the region of primary interest appears to be material 0.10 mm (0.004 in.) thick with a span between 6.35 mm (0.25 in.) and 12.70 mm (0.50 in.). Slightly thinner material might be considered, but there is some danger of making the bellows too fragile. Conversely, a slightly thicker material could be utilized if it is desired to make the power bellows more rugged.

o Material Choice for Metal Diaphragm or Bellows

Several metals are commonly used by metal bellows manufacturers to form bellows convolutions. These have been selected to meet a variety of strength and cost requirements while providing reasonable welding and forming properties. Occasionally operating environments require some specific material such as titanium which requires a great deal of extra fabrication effort as well as higher material costs. Since no such requirement exists for the Stirling hydraulic engine in the solar application, materials considerations were primarily limited to preferred materials choices.

The highest strength properties are found with Inconel 718 which has a yield strength of 1030 MPa (150,000 psi) and an endurance limit of 720 MPa (104,000 psi). The overriding problem with this material in the present application is that its grain structure allows helium permeaton in thicknesses below 0.152 mm (0.006 in.) The optimum material thickness is about 0.102 mm (0.004 in.) for bellows and 0.127 (0.005 in.) for a diaphragm.

The lowest cost materials commonly used for welded metal bellows are 347 and 410 stainless steels. Their low strength provides little or no net cost advantage in this application, however, since more convolutions are required in order to reduce the stress levels while maintaining required stroke volume.

The clear choice for either metal bellows or diaphragm material is AM-350 precipitation hardening stainless steel. It is strongly preferred by the bellows manufacturer as the best all around high strength steel. It is considered very easy to form and weld and has a moderate material cost which amounts to about $10 for a buffer or power bellows. This represents about 10% of the total bellows cost. It also has good mechanical properties with a yield strength of 520 MPa (75,000 psi) and an excellent endurance limit of 565 MPa (82,000 psi).

o Evaluation of Elastomers

The practicality of using elastomeric materials for a diaphragm or possibly even a bellows was considered. Materials costs and especially fabrication costs are potentially much lower than for their metal counterparts. In the solar application, it is likely that the inevitable permeation of helium into the hydraulic region could be collected in a bubble trap and periodically vented without imposing unmanageable constraints. Lifetime limitations, however, effectively rule out elastomers except for low-cost short-term demonstration projects. The stated system lifetime objectives are 50,000 hours of operation at 60 Hz. This represents slightly over 10^{10} cycles of operation, more than an order of magnitude higher than known published lifetime data for elastomers. Moreover, as shown below, there is not an endurance limit characteristic for elastomers as there typically is for metals, in which essentially infinite life can be achieved by keeping stresses sufficiently low.

Some of the longest cycle lifetimes found in the literature for elastomers were reported for rolling sock seals. The University of Washington (Reference 3) reported 2.7×10^8 cycles for a roll sock used to seal a pump actuator in their artificial heart system. Philips Laboratories (personal communication, Jerry Pritchard, North American Philips) achieved 3×10^8 cycles for a roll sock used as an absolute seal on a Stirling refrigerator. It should be emphasized that both of these groups utilized extreme care at all stages from material compounding to fabrication to installation and testing. The above lifetimes also represent the single best test in each case. Many duplicate or similar tests resulted in earlier failures, often with only the order of one-tenth the best cycle life.

One of the most extensive collections of data available on engineering uses of rubber is given in Reference 6. Figure 10 shows some remarkable results for dynamic fatigue life measurements as a function of minimum strain for rubber vibration mountings with various stroke lengths. One of the most unexpected results is that optimum fatigue life is obtained when the rubber is oscillated in constant tension, with the minimum strain at two to four times the unstretched length. As the minimum strain is reduced from the optimum level, fatigue life decreases. As the minimum strain approaches zero, i.e., stretching cyclically occurs from the relaxed state, the life drops rapidly and may be two orders of magnitude or more lower than the cycle life at optimal minimum strain. As the minimum strain decreases still further so that the oscillations occur partially or totally with the rubber in a compressed state, cycle life again increases dramatically and peaks sharply before dropping rapidly to zero. This effect is most dramatically illustrated by the top curve in Figure 10 which is plotted on a linear scale. The shape is changed significantly when this curve is replotted as the topmost curve on the lower semilog plot.

The lower plot in Figure 10 also includes several additional curves which show the effect of increased dynamic amplitude (strain) which is proportional to induced stress levels. These relative stress levels are plotted as a function of dynamic fatigue life at optimum minimum strain in Figure 11. The significance of presenting the data in this manner is that no indication of an endurance limit type of relationship exists. That is, in contrast to most metals, there is not any significant stress level below which the cycle life increases to virtually infinite levels. For these data in fact, it appears quite possible that 10^{10} cycles will not be achieved even with virtually negligible stress levels.

In light of the above, unless some specific elastomeric material is found with consistently demonstrated cycle life in excess of 10^{10} cycles in conditions similar to those encountered in the Stirling hydraulic application, elastomers are considered unsuitable for this application.

3.1.3 Final Reference Design Configuration

The original baseline design and its evolutionary development were described above. This section provides a detailed description of the final design configuration and shows how the internal fluid charging and makeup systems function. Three figures are used to support the discussion. Figure 12 is an unsymmetrical cross section through the hydraulic converter with identifying flags for key components. Figure 13 is a reduced size two-view version of the converter layout which identifies the section location for Figure 12.

4.0

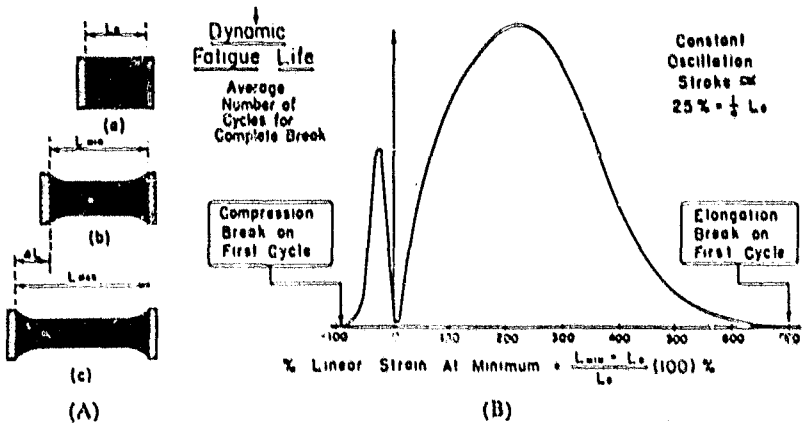

Fig. 5.31. (A) Shape of rubber parts vibrated in tension. (B) Dynamic fatigue life as a function of strain. Oscillation strokes of the order of 25 per cent of unstretched length.

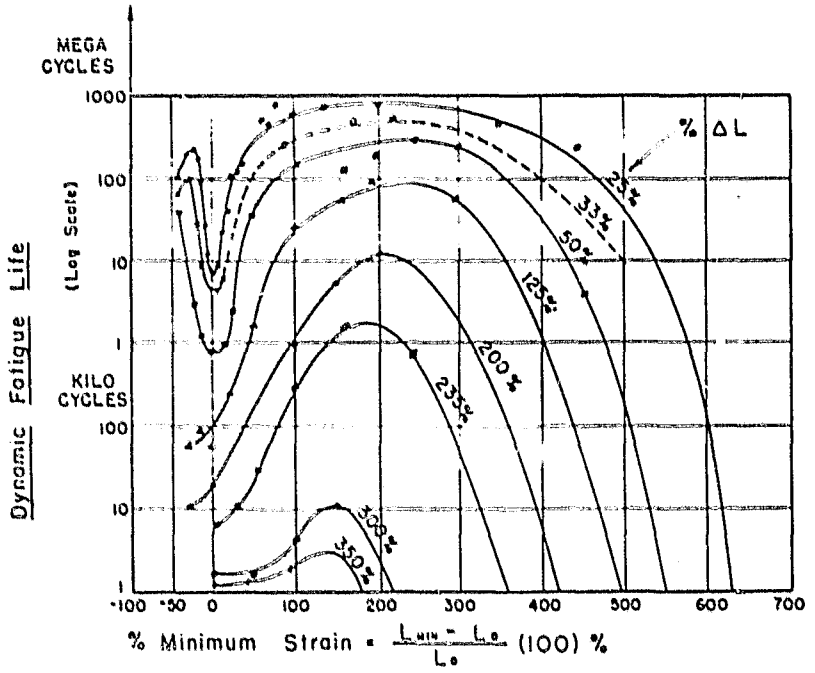

Fig. 5.32. Dynamic fatigue life for oscillation strokes from 25 to 350 per cent of unstretched length.

Figure 10. Dynamic Fatigue Life of Rubber (From Reference 5).

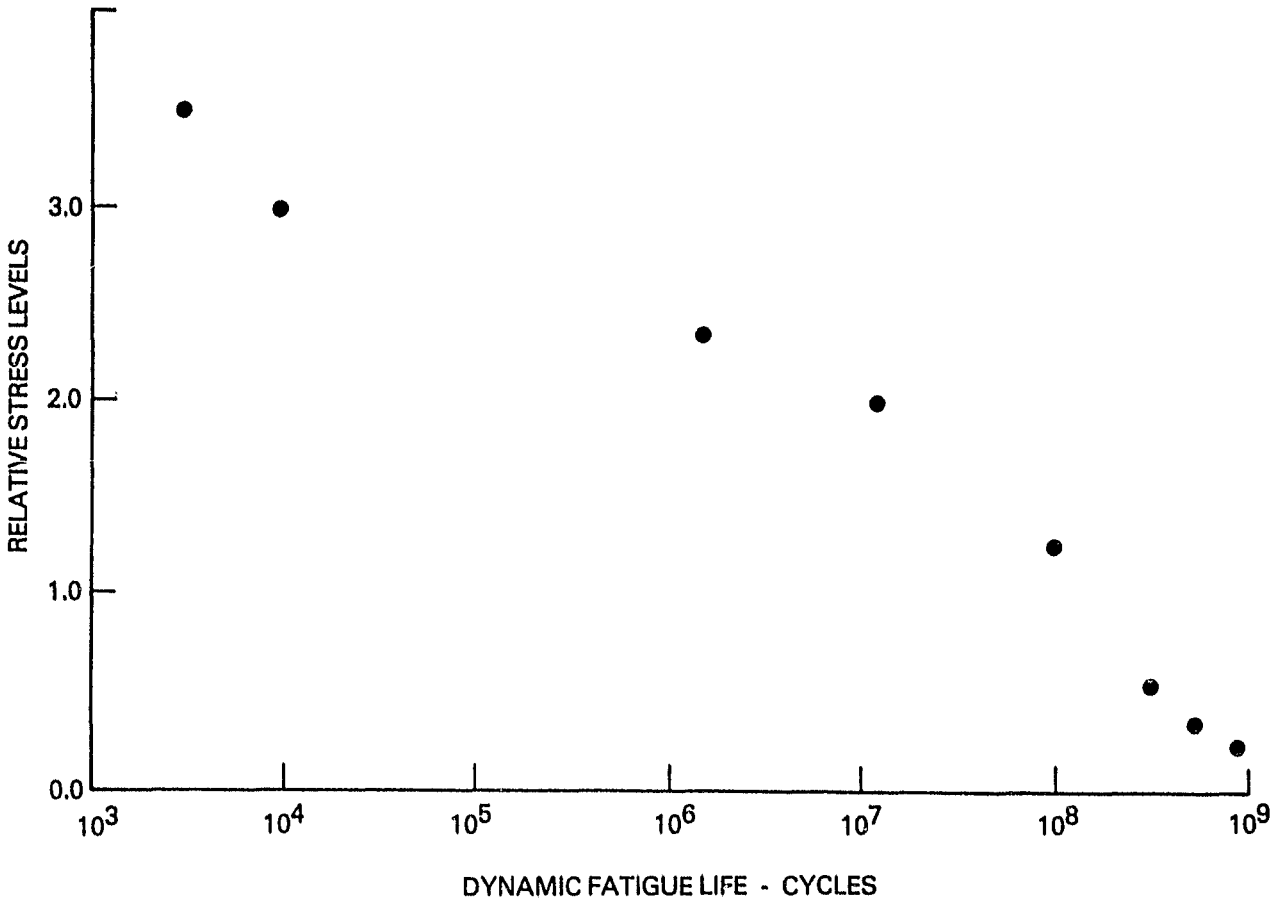

Figure 11. Lifetime Data for Rubber Vibration Mountings at Optimum Strain.

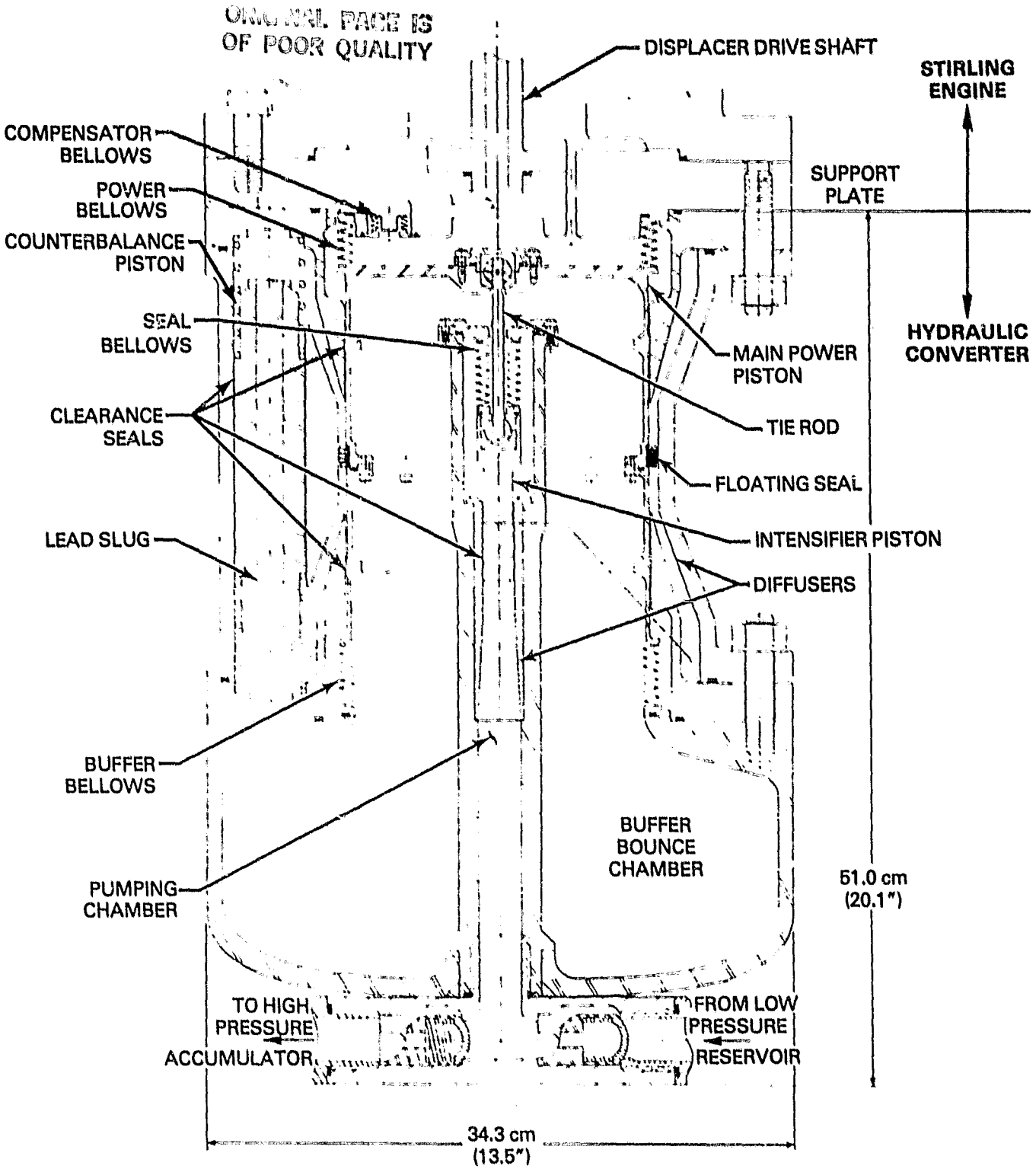

Figure 12. Hydraulic Converter Layout, Final Design Configuration

Figure 14 includes balloon identifiers for all converter components as used for the costing studies reported in Section 3.4. It also semi-schematically shows the necessary porting and valving required for making up internal fluid leakages and for achieving an initial vacuum fill of the hydraulic regions.

o Functional Hardware Description

In Figure 12, a portion of the cold end of the Reference 4 Stirling engine is shown to illustrate how it interfaces with the hydraulic converter. More engine details are available for reference purposes in Figure 4. The engine support plate is the support base for the cantilevered displacer drive shaft on which the posted displacer rides. The support plate incorporates minor modifications to accomodate converter interface components including the power bellows and compensator bellows. The compensator bellows accomodates any mismatch between the power bellows effective area and main power piston area and assures that the power bellows will always be pressure balanced, as with the reference design. In this case, however, the compensator bellows is not required to actuate a leakage makeup valve.

The main power piston is comprised of the power bellows end terminal, the sleeve which connects the power bellows to the buffer bellows and the tie rod which drives the intensifier piston. The outer sleeve is made in two parts for assembly purposes. A five-piece solid ring floating seal is used adjacent to the sleeve assembly point with an effective area that allows it to drive two diametrically symmetric counterbalance pistons. An annular diffuser is employed at each end of the seal stroke region to reduce the velocity head in the fluid before it is manifolded to the ends of the counterbalance pistons. The floating seal has three alternate rings which fit tightly to the piston on their inside diameter and two with a close clearance to the central cylinder section on their outside diameter.

This allows a good seal to be maintained without imposing side loads or requiring extremely tight and expensive concentricities between mating parts of the housing.

Coil springs are provided to maintain the counterbalance pistons in an average position near midstroke in response to shifting gravity loads or preferential fluid leakage past the pistons. A lead slug is used in the pistons to keep the optimum diameter pistons to a length which fits comfortably within the minimum package length established by other component requirements. The optimum counterbalance piston diameter is determined by the allowable pressure swings in the hydraulic regions adjacent to the floating seal (relative to sidewall flexing at the clearance seals on the main power piston) and the dynamic inertia of the pistons. The mass of each piston must be 2.5 kg (5.5 lbs) which is one-fourth the optimum total converter piston resonant mass of 10.0 kg (22.0 lbs). With reference to Figure 13, it can be seen that the counterbalance pistons are contained in appendages on each side of the converter housing, formed as part of the casting for the housing.

Side loads are avoided without any stringent concentricity requirements for the intensifier piston sleeve relative to the main power piston cylinder by connecting the pistons with a tie rod having a ball joint at each end. The chrome-plated steel ball joints are located in the buffer gas region, so they do not have the advantage of operating immersed in hydraulic oil as do all other converter

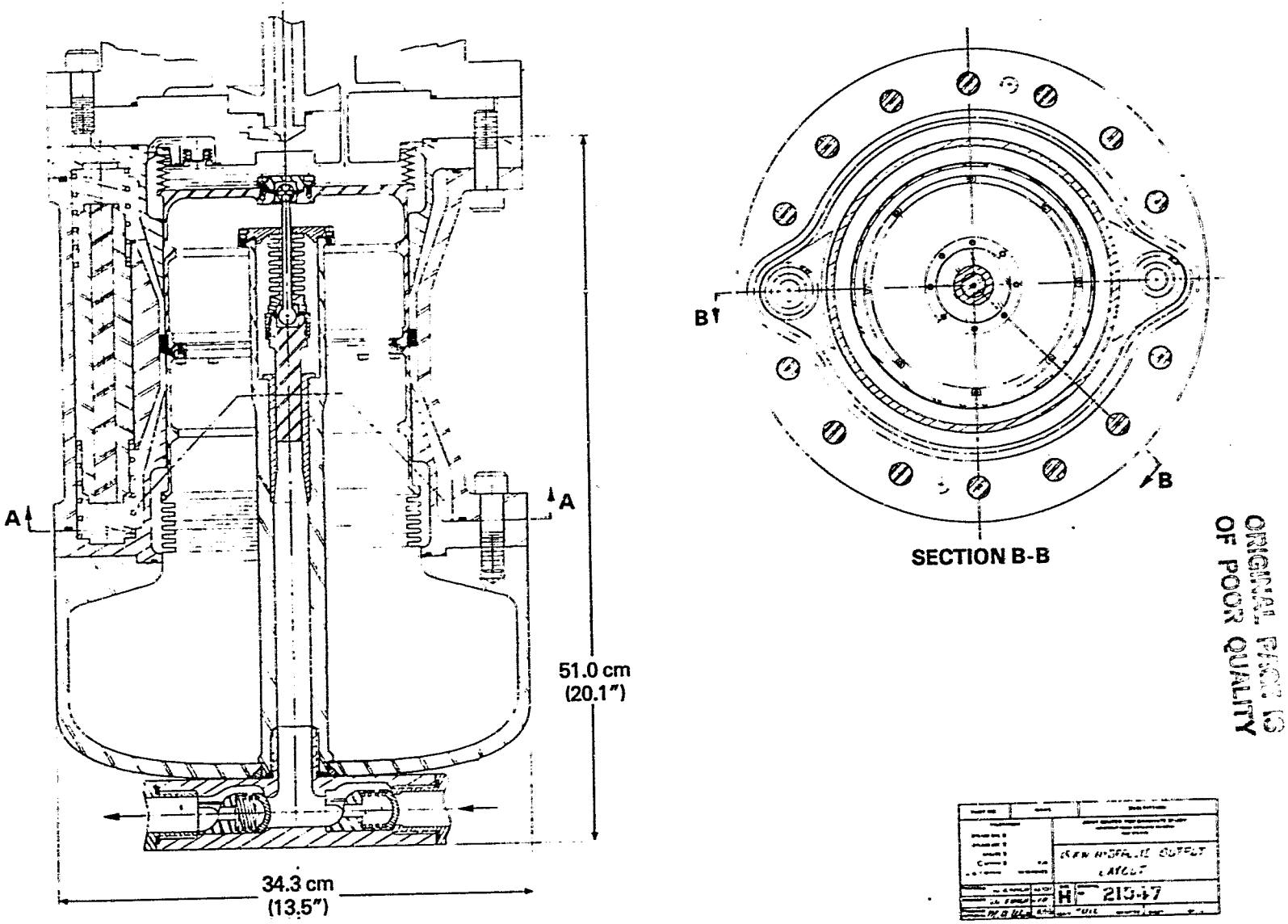

Figure 13. Two-View Hydraulic Converter Layout, Final Design Configuration

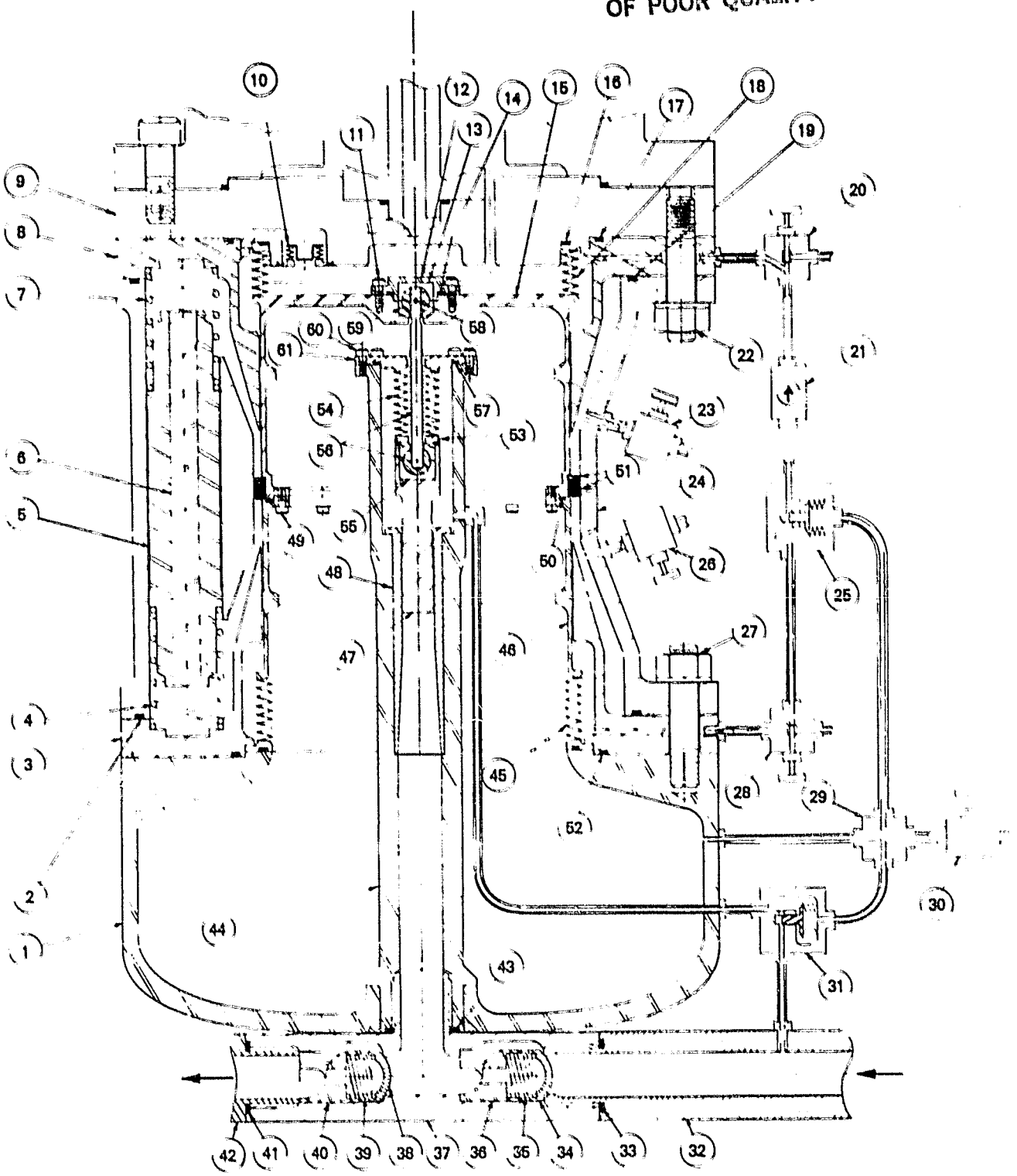

Figure 14. Hydraulic Converter Showing Part Numbers and Makeup Systems.

components which experience any sliding or rubbing action. Little or no relative motion between ball and socket is anticipated, but any potential wear problem is addressed by using a knitted Nomex/Teflon epoxy composite bearing material for the mating sockets. With peak stresses in the composite held to 44 MPa (6400 psi), these joints should have infinite life with the expected neglible sliding motion in the sockets. The published static load capacity is 240 MPa (35,000 psi) and the dynamic load capacity is 100 MPa (15,000 psi). The sockets can be replaced, if ever necessary, with moderate disassembly effort and nominal parts cost.

The intensifier piston pumps hydraulic fluid from a low pressure accumulator to a high pressure accumulator, which comprises the output mechanism for the Stirling hydraulic engine. The fluid displaced by the intensifier piston is first routed through a diffuser section to reduce its velocity. This minimizes the velocity head losses encountered with changing flow direction and flowing through check valves.

The seal bellows has the same nominal effective area as the intensifier piston so that no net fluid displacement occurs in the region around the intensifier piston and seal bellows. Minor differences due to manufacturing tolerances are handled as described below for the makeup systems. The seal bellows, as with all bellows in the system, is of a welded configuration. Hydroformed bellows were considered for those applications where their excess dead volume was not a problem. They proved to be impractical, however, because of length constraints and/or a natural surging frequency (frequency for axial oscillation of central convolutions with the ends fixed) too near the operating frequency. Two small compensator bellows used in makeup systems could still use hydroformed bellows because of their negligible strokes, but potential cost savings are miniscule when the larger housing requirements are considered.

o Fluid Charging and Makeup Systems

Figure 14 illustrates the hydraulic fluid charging and makeup components in a semi-schematic fashion. The converter has two independent hydraulic circuits which are hermetically separated from one another. One sealed circuit consists of the regions outside the buffer bellows and the power bellows, the regions between the floating seal and the counterbalance pistons, and adjoining hardware and fittings. The other hydraulic circuit consists of the region around the seal bellows, the pumping chamber between the intersifier piston and check valves, and the external hydraulic circuit including accumulators, hydraulic motor and associated plumbing.

Initial converter charging with hydraulic fluid is required before the system is first operated and after any major disassembly. The geometry of the hydraulic regions, especially those in the sealed circuit, is not amenable to attaining a high quality gas-free hydraulic charge except by means of a vacuum fill. Valves 20, 23, 26, and 28 are provided to connect the four regions in the sealed circuit to an external manifold which is first evacuated and then back-filled with hydraulic oil and the valves sealed and capped. The other hydraulic circuit, which includes the external flow components, may be adequately charged without resorting to vacuum fill procedures. If required, however, the region around the seal bellows and the pumping chamber may be vacuum filled.

After the hydraulic system has been charged, the engine and buffer gas regions are charged in preparation for operation, the latter through valve 30. During operation, internal leakage past clearance seals occurs and must be made up or disposed of as appropriate. These makeup systems, which are functionally similar to those routinely and successfully used for years in several hardware generations of artificial heart Stirling hydraulic engines (Reference 3), are illustrated in Figure 14.

As shown in Section 3.1.1, the average buffer pressure is lower than the average engine pressure. As also described there, compensator bellows 10 maintains instantaneous (and therefore average) engine pressure in the hydraulic region surrounding power bellows 18. In an analogous way, the hydraulic region around buffer bellows 45 is maintained at buffer gas pressure by means of the buffer compensator bellows in item 25. Net leakage flow past clearance seals will thus occur from the power bellows region to the buffer bellows region. The intermediate counterbalance regions will stabilize at appropriate intermediate average pressures as the leakage flow slowly occurs. The resulting fluid buildup in the buffer hydraulic region will act on the buffer compensator bellows and begin to open the valve which is integral with that bellows. The excess fluid needs to be returned to the power bellows region where the average pressure is higher. The engine pressure cyclically swings well above and below buffer pressure, however, so check valve 21 enables flow to return to the power bellows region during the low pressure interval, until the valve on the buffer compensator bellows is again closed. This valve must, of course, have a lower static leak rate than that past the clearance seals.

With a proper initial hydraulic charge, this bellows/counterbalance hydraulic region can thus be charged and sealed with no further attention required, provided no leakage occurs. The system will protect both power bellows and buffer bellows from experiencing adverse pressure differences even in the event of a sudden loss of engine or buffer gas. The gas pressures would, of course, have to be equalized after some moderate period of time (probably measured in minutes or hours) before resultant leakage past clearance seals exceeded the stroke capacity of the two appropriate compensator bellows.

The hydraulic region around the seal bellows experiences a net inflow leakage of oil from the pumping chamber which has a much higher average pressure. This excess fluid actuates the seal region compensator bellows in housing 31 to enable dumping the fluid to the low pressure reservoir. This compensator bellows also maintains an instantaneous pressure balance across the seal bellows in the same manner as the other two compensator bellows do for the power bellows and buffer bellows.

3.1.4 Metal Diaphragm Alternative Design

The design studies described above were based on the use of welded metal bellows to separate the engine helium from the hydraulic fluid. This function can also be accomplished with a corrugated metal or elastomeric diaphragm. The elastomer was shown to be inappropriate in Section 3.1.2. Advantages of a corrugated metal diaphragm relative to welded metal bellows include a significant potential for cost saving in production quantities, and inherently low gas dead volume.

A diaphragm may demand more axial length than a bellows, and always requires a larger diameter to achieve a given stroke volume. Evaluation of how a diaphragm could be integrated into the Stirling hydraulic engine was included in this contract effort and a design analysis was conducted in order to develop a specific configuration and specifications.

The conclusion reached is that a metal diaphragm is a viable alternative to the power bellows. A full cost comparison of the two alternatives including necessary interface hardware was not completed, but it is clear that inherent labor and materials cost for the basic diaphragm would be lower than those for the bellows capsule. The power bellows approach was selected as the reference design for reasons outlined below, but the diaphragm concept merits a more definitive evaluation of manufacturing realities prior to any future quantity manufacturing decision. The reasons for this approach are:

1) The bellows can be provided by an established vendor using standard production techniques applied routinely for generally similar configurations. A diaphragm would require some fabrication development effort to be assured of meeting specifications and no supply source with a proven track record has been identified.

2) While the developed cost of the diaphragm is expected to be lower than that for the bellows, bellows cost is not a major portion of the energy system cost.

3) Flow loss analysis indicates that the bellows version will have a slightly higher efficiency than the diaphragm version. This conclusion may possibly be modified with a more refined analysis of diaphragm losses.

4) Excellent lifetime has been demonstrated for both metal bellows and metal diaphragms (Reference 3). Metal bellows data, however, includes a much broader range of configurations and many more units on life test. This gives bellows a slight edge in confidence level.

5) The bellows configuration has a more foolproof inherent protection mechanism to handle unusual transient conditions without damage than does the diaphragm configuration.

Scoping analysis was conducted for metal diaphragms prior to full computer analysis to bracket the region of interest. Hand analysis techniques based on the Haringx approach, as developed in support of the artificial heart program (Reference 3), were used for these studies. This approach is fully described in Appendix A. The ranges of parameters used in the scoping studies were diameters of 30.5 cm to 45.7 cm (12.0 to 18.0 in.) and corrugation depth to material thickness ratios of 3.0 to 8.0. Stroke volumes from the relaxed position of 426 cm^3 and 852 cm^3, corresponding respectively to bidirectional and unidirectional stroking, were considered. Parameters of specific interest are circumferential and meridinal stresses, and pressure differential required to deflect the diaphragm to maximum extension.

The hand analysis narrowed the region of specific interest to diameters near 35.5 cm (14.0 in.) for the bidirectional case and 45.7 cm (18.0 in.) for unidirectional stroking. The depth-to-thickness ratio was also narrowed to a

range of 5.0 to 8.0. Test cases were set up on the JCGS 32-bit digital computer using the NONLIN (nonlinear) version of the DIAN (Diaphragm Analysis) computer program. This program was developed by Battelle for the Air Force (Reference 7). It uses direct numerical integration to solve the differential equations which represent the physical configuration of the diaphragm (or bellows). The geometry is represented by conical and toroidal shells of revolution, and the program is capable of linear elastic axisymmetric and nonsymmetric deformations, and of nonlinear axisymmetric deformations. Very good correlation between analytical prediction and strain gage testing has been achieved by Battelle in their evaluation of the method.

A preliminary layout showing how a diaphragm could be used to replace the power bellows is shown in Figure 15. This shows only enough of the interface region to illustrate key features. The engine support plate has been modified to accept a retainer plate with an integral poured elastomer backup support for the diaphragm. The elastomer is poured on a master diaphragm which is hydrostatically deflected to the proper position in a suitable fixture, and the retainer plate is added. After curing, the parts are separated with the retainer/elastomer assembly available for installation in a diaphragm final assembly fixture where welding occurs. The elastomeric backup provides a soft cushion for the diaphragm during transient collisions at startup or when gas charges are not optimized. Its accurate conformance to the diaphragm shape also minimizes gas dead volume. The diaphragm is protected at its other end of stroke by the same makeup system used with the power bellows configuration, assuming that a proper total quantity of hydraulic fluid is maintained in the makeup circuit.

The converter interface end of the diaphragm assembly in Figure 15 does not correlate exactly with comparable parts in Figure 12. The reason is that Figure 15 was based on an earlier converter layout in which the counterbalance pistons were driven off the intensifier. It is not difficult to visualize how the Figure 15 preliminary layout could be adapted to the final configuration.

Specific design details for a diaphragm, as determined by computer optimization, are shown in Figure 16. The edge tilt and corrugation geometry are selected to maintain stresses as uniform as possible. This provides the required volumetric displacement with a minimum diameter. The design is conservative, with a 50% margin of safety used for stress levels. Details are given in Appendix A. The diaphragm is formed against a metal female die using hydrostatic pressure applied through a rubber pad by a metal ram in a hydraulic press (Ref. 3 p. 60 ff.). The forming takes place in stages. The tilt edge is formed first, then the corrugations are formed to about 80% of their final depth. After annealing, final forming is completed. This is followed by a trigger annealing operation, straightening and tempering. The resulting diaphragm blank is then trimmed and finally electron-beam welded into its retaining rings. Based on hardware experience, it may prove necessary to perform a final straightening operation following the girth weld, to avoid inducing excess stresses as the diaphragm passes through its midstroke position.

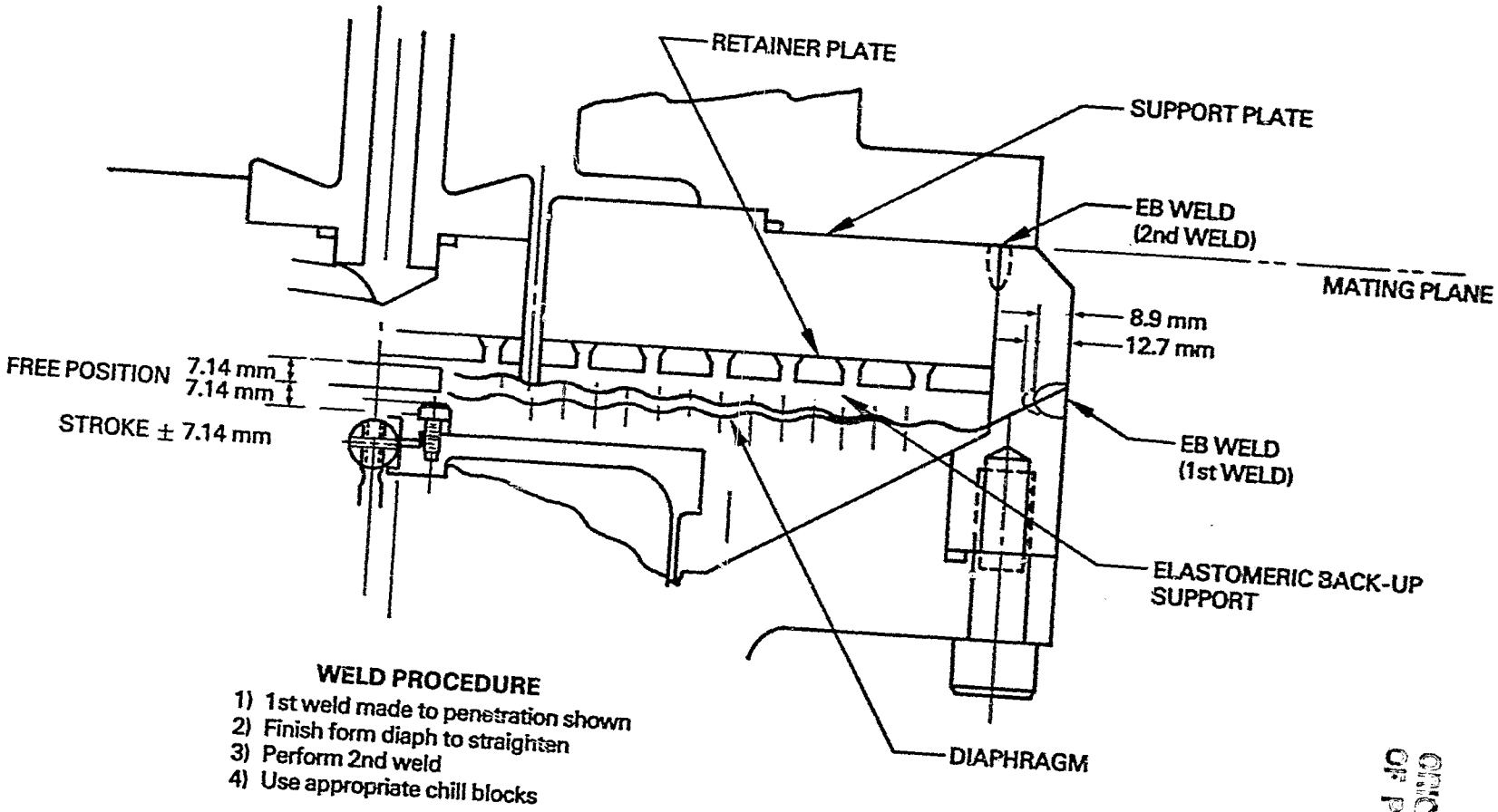

Figure 15. Diaphragm Assembly Preliminary Layout.

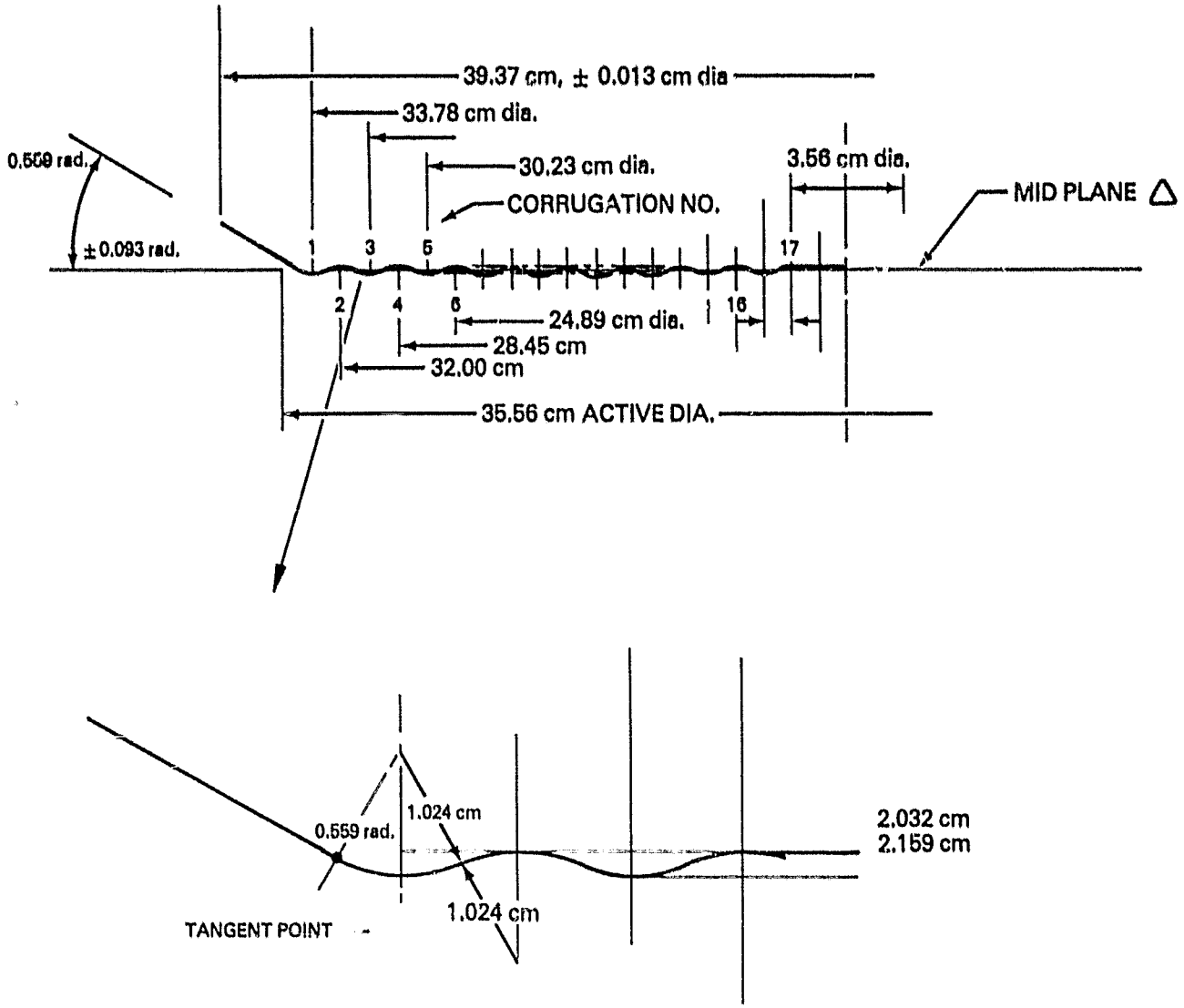

GENERAL NOTES

1. MAT'L AN350 SHEET 0.013 cm THICK - MUST BE FREE OF SCRATCHES - FULLY ANNEALED CONDITION
2. PREFORM USING RUBBER PAD AGAINST METAL DIE FORM
3. ANNEAL BETWEEN FORMING STAGES
4. FINAL SIZING BETWEEN METAL DIES
5. HEAT TREAT TO SCT 850 CONDITION PRIOR TO GIRTH EB WELD
6. TOLERANCES UNLESS NOTED
   xxx - 0.013 cm
   CONCENTRICITY 0.025 cm
7. CORRUGATIONS 1 THRU 8 SHOULD BE HELD TO 0.013 cm BALANCE OF CORRUGATIONS MAY BE 0.025 cm
8. CONCENTRICITY THIS CORRUGATION ONLY
9. MIDPLANE TO BE FLAT WITHIN 0.114 cm AFTER WELD - FINAL FORM TO STRAIGHTEN MAY BE NECESSARY

Figure 16. Diaphragm Details

3.2 Hydraulic Converter Losses

Calculations were made to evaluate all of the energy losses within the hydraulic converter. Such analysis proved very useful during the evolutionary development of the layout design in order to achieve a low loss design. Where approximations were required, attempts were made to be conservative so that the actual losses would be smaller than the calculated values. The final results show an overall hydraulic converter efficiency of 93.5%. Most of the losses are associated with the counterbalancing pistons. The same basic converter without the counterbalancing feature would have an overall efficiency of 97.0%. With the alternative diaphragm to replace the power bellows, the efficiencies are respectively 92.8% and 96.3%. Converter efficiency and power density would also be significantly enhanced by coupling to a more optimal engine design with a higher charge pressure and lower stroke volume, since converter losses are independent of pressure but strongly dependent on stroke volume. Specific cases evaluated showed that converter efficiencies as high as 99.6% are possible with a counterbalanced system.

3.2.1 Clearance Seal Losses

The final layout design in Figure 12 incorporates six clearance seals. Elimination of the counterbalance system could reduce the required number of clearance seals to two, and one of those would experience significantly lower pressure drop and therefore lower leakage.

The clearance seal optimization and performance analysis, as developed in the Flow Industries subcontract, is based on the following assumptions:

1. Flow in the annular gap is laminar.
2. The axial temperature distribution is uniform.
3. The flow responds instantaneously to piston motion.

The velocity distribution across the annular seal gap is determined by integrating the fundamental momentum equation and applying suitable boundary conditions.

Incorporation of the velocity distribution into the continuity equation and integration across the gap yields an expression for the pressure gradient along the seal length. Integration of the pressure gradient equation along the seal yields a relationship betwen total pressure drop and leakage flow as a function of seal geometry, oil viscosity and relative velocity at the two sides of the seal. The effect of the pressure dependence of viscosity is also included, but this is negligible for all seals except the intensifier pumping piston. The power loss due to seal leakage is the product of the overall seal leakage rate and the total pressure drop.

The shear force on a differential element of fluid in the seal region is a function of seal geometry, oil viscosity, relative seal wall velocity and pressure gradient along the seal length. Total shear force is found by integrating along the length of the seal. Frictional drag power loss is the product of the total shear force and the relative seal wall velocity.

Total power loss for an annular hydraulic clearance seal is the sum of the leakage power loss and the frictional drag power loss. After combining these loss terms and with a fortuitous cancelling of terms, the expression for total clearance seal power loss $\hat{P}_L$, in watts, becomes

$$\hat{P}_L = \frac{\pi D H^3 (\Delta P)^2}{12 \mu_a L} + \frac{\pi D \mu_a L V^2}{H} \tag{1}$$

where

D = Primary seal diameter (cm)
H = Radial seal clearance (cm)
ΔP = Pressure drop across seal (MPa)
L = Length of seal (cm)
V = Relative velocity of adjacent seal walls (cm/sec)

and

$$\mu_a = \mu_o \frac{\alpha(P_2 - P_1)}{e^{-\alpha P_1} - e^{-\alpha P_2}} \tag{2}$$

where

μ_a = Effective average viscosity of oil in seal (MPa sec)*
μ_o = Oil viscosity at ambient pressure (MPa sec)*
P_2 = Pressure at high pressure end of seal (MPa)
P_1 = Pressure at low pressure end of seal (MPa)
α = Pressure correlation coefficient for viscosity (MPa^{-1})

is an empirical factor for the oil viscosity at pressure P defined by

$$\mu = \mu_o e^{\alpha P} \tag{3}$$

Typical values of α for many oils range from .015 MPa^{-1} (10^{-4} psi^{-1}) to .03 MPa^{-1} (2×10^{-4} psi^{-1}). Equation 1 may be used to obtain either instantaneous or average power loss, depending on whether instantaneous or time average values are used for the independent parameters. ΔP and V will normally be the time dependent parameters, although and L can also vary over an operating cycle for some cases.

Optimum values for H, L, or μ_a may be obtained by differentiating Equation 1 with respect to the appropriate variable and setting the result equal to zero. Each case can provide valuable insights, but generally speaking practical limits establish actual values. For example, reasonable cost effectiveness in manufacturing and functional practicality dictate something near a class 3

*One MPa sec = 10^7 poise

medium fit (Reference 7) for the clearance seals. For the 17.8-cm (7.0-in.) piston, a class 3 fit gives a diametral clearance of .0122 ± .0038 cm (.0048 ±.0015 in.). Another factor to consider is that oil viscosity must be maintained in a relatively narrow range specified by the hydraulic motor manufacturer. This last condition need not necessarily apply to the counterbalance and main power piston region of the layout design since that oil system is independent of the main power train; however, since total loss is independent of viscosity at optimum seal geometries and optimum seals have reasonable sizes for typically used viscosities near 20 cp, there is no advantage to using an alternate oil.

Analysis of the total seal loss for all seals in the system was conducted over a range of conditions including tolerance limits and seal clearance cyclic changes from breathing effects where appropriate. In the case of the intensifier piston, operation during one half-cycle exhibits about 29 MPa (4200 psi) pressure difference with about 5 MPa (700 psi) during the other half-cycle. This results in significantly different optimum seal geometry for the two cases and necessitated many trial-and-error computations to reach a good compromise seal with reasonable tolerances.

A given clearance seal diameter produces a total loss which is directly proportional to clearance, if the optimum seal length is chosen for each clearance. For fabrication ease and minimal cost, a straight class 3 fit and tolerance specification was initially tried for all seals. This was maintained intact for both the counterbalance pistons and the intensifier piston. Strong consideration was given to tightening the clearances and/or tolerances on these seals. The magnitude of these losses are substantially less than those for the large diameter piston, however, so the relatively small gains in overall efficiency did not appear to warrant the extra hardware problems associated with reducing those losses.

The greatest difficulty was encountered with the seals at each end of the main power piston. These seals have the added complication that cyclic pressure changes cause breathing of the piston in the seal region. This breathing improves seal performance over part of the cycle and degrades it during part of the cycle. When all these factors are applied to the main piston seals, cycle averaged losses range from 123 W to 228 W at each end of the piston, depending on where in the tolerance band a given seal lies.

These losses were judged to be excessive and too uncertain, so other alternates were considered. For some time, split piston rings were thought to be an excellent choice in this application. That conclusion was unfortunately based on an erroneous reference for the coefficient of friction between the ring and the cylinder. When the correct coefficient was determined, the loss proved to be several times that for the class 3 clearance seal, rather than less than half as first thought.

With ring seals out of the picture (solid rings would have reasonable losses but housing them would increase piston weight which is already something of a problem), variations on clearance seals were evaluated. The final compromise was to tighten up both the fit and the tolerance somewhat from the class 3 fit. On the 17.8 cm (7.0 in.) piston this entailed changing the diametral clearance from 0.0122 ± 0.0038 cm (0.0048 ± 0.0015 in.). to 0.0076 ± 0.0025 cm

(0.0030 ± 0.0010 in.). This change reduced total power losses for the two end seals from 350 ± 100 W to 200 ± 20 W.

The central floating seal on the main piston was adopted to avoid severe alignment problems with three guiding surfaces on one moving member. As an added benefit, the solid rings can easily be ground to a tighter tolerance and clearance than is practical for the piston itself. Thus the friction problem with split rings is avoided but the seal losses are about the same as for the end seals despite experiencing twice the pressure differential. The added weight associated with housing the floating seal precludes its use on the end seals.

The final results with key dimensions and power losses for all clearance seals are summarized in Table 1. Tolerances on seal losses are determined by the losses at extremes of the dimensional tolerances. The nominal loss figures shown are for the average loss between extremes, although the loss at the nominal clearance is typically somewhat less than this median value. The total loss for the six clearance seals is 460 W with tolerance limits of ± 65 W. Relative to the 15 kW net output of the system, this amounts to 3.1% ± 0.4% of the total.

The seal lands specified for most seals are typical engineering practice for such applications. What they generally amount to is circumferential grooves cut in the sealing surface to break the seal up into lands. This provides pressure equalization at intermediate points along the seal to prevent potential problems caused by eccentricities or other seal anomalies.

Table 1

SUMMARY OF SEAL DESIGN DATA

Seal Location/ Seal Type	Number Required	Nominal Diameter (cm)	Diametral Clearance (cm)	Total Seal Length (cm)	No. of Seal Lands/ Rings	Peak Pressure Difference MPa (psi)
Main Piston-Ends/ Clearance with Lands	2	17.78	.0076 ±.0025	0.97	2	2.07 (300)
Main Piston-Center/ 5 Solid Ring Floating Chrome Plated Steel	1	18.77	.0051 +.0112 -.0025	0.64	2 OD 3 ID	4.14 (600)
Counterbalance Pistons/ Clearance with Lands	2		.0058 ±.0025	0.091	2 each end	4.14 (600)
Intensifier Piston/ Clearance with Lands	1		.0112 ±.0152	3.18	10	28.98 (4200)

3.2.2 Fluid Flow Losses

The hydraulic converter has two regions in which appreciable fluid flow losses occur. (Fluid losses associated with bellows or the optional metal diaphragm will be treated separately in the next section.) Primary flow losses occur in the coupling fluid which drives the counterbalance pistons. Much lower losses occur in the main power train where the intensifier piston pumps fluid to and from external accumulators. In the geometries of interest, the power loss due to wall friction is generally smaller than the velocity head or inertial flow losses due to changes in the cross-sectional flow area.

The pressure drop ΔP due to one velocity head loss is $\rho V^2/2$ where ρ is the mass density of the fluid and V is the fluid velocity at the flow area of interest. The associated power loss is the product of fluid flow rate and pressure drop, with suitable cycle averaging. Frictional power loss is also determined. This depends on the length and circumference (or length, width and height) of the flow channel as well as fluid velocity and the appropriate friction factor. The latter is a function of Reynolds Number and, in the case of turbulent flow, the surface finish of the flow channel.

The layout design minimizes flow losses where practical by incorporation of diffusers. These increase flow area (without incurring velocity head losses) and therefore reduce the velocity at which head losses occur. Flow from the intensifier piston enters a conical diffuser which requires 6.1 cm (2.4 in.) length to expand from a diameter of 1.8 cm (.70 in.) to 2.5 cm (1.00 in.) with an included angle of .123 rad (7°). A total of five head losses are assigned in this region for change of direction and flow through check valves.

Flow from the counterbalance driving region (step between the center seal and either end seal on the main power piston) is directed into an essentially one-dimensional diffuser section with a total included angle of .175 rad (10°). The thickness of this annular region increases from .50 cm (.195 in.) to 1.38 cm (.545 in.) in the available flow length of 5.1 cm (2.0 in.). Fluid at the outlet of this diffuser is manifolded circumferentially to the ends of the diametrically opposite counterbalance pistons. It is conservatively assumed that three velocity heads are lost in the manifolding process. It is further assumed that an additional 1.5 head losses occur on the smaller area of the pistons themselves, as a result of their motion through the fluid.

Pertinent information about these fluid flow loss terms and the magnitude of the power losses are summarized in Table 2. The total loss of 317 W is 2.1% of 15 kilowatts.

3.2.3 Bellows/Diaphragm Flow Losses

Fluid flow losses in bellows are associated with hydraulic flow 1) between convolutions, 2) between weld beads at the exit from convolutions and 3) between the bellows outside diameter and the surrounding enclosure. Both friction and inertial losses were evaluated. Previous experience in evaluating flow losses for miniature bellows used in Stirling hydraulic engines has been based on crude analyses that intentionally produce very conservative results. This approach has been adequate to verify the fact that these losses are inconsequential.

Table 2

FLUID FLOW LOSS SUMMARY

Flow Region	Flow Area (cm^2)	No. Head Losses	Friction Loss (W)	Head Loss (W)	Total Loss (W)
Pumping Chamber (Intensifier Piston)	5.1	5.0	1.0	11.0	12.0
Counterbalance Coupling Region					
° Manifold	77.4	3.0	25.0	52.0	77.0
° Pistons	27.7	1.5	2.0	202.0	204.0
° Diffuser/Main Piston	0	0	24.0	0	24.0
Totals			52.0	265.0	317.0

Effects of scale, however, result in calculated losses for the 15-kW power bellows on the order of a kilowatt. It was thus deemed important to develop a refined analytical model to more accurately determine these losses and to provide design support data. This assignment was made as part of the Flow Industries subcontract.

A very sophisticated analytical model was developed from first principles for the most significant two of three loss regions. Application of this model requires numerical solutions to be generated using a specialized computer code. No time was available to develop such a code, so several simplifying but conservative assumptions were made to enable the equations to be integrated and produce an approximate closed form solution. This was successfully accomplished and several geometries near the reference design power bellows were analyzed. Since all approximations were made conservatively, actual losses should be less than the calculated values. The losses were found to be very sensitive to bellows span, which reinforced the earlier choice of the narrowest practical bellows span based on dead volume. The layout design power bellows has an effective diameter of 17.8 cm (7.0 in.), a span of 0.95 cm (0.375 in.), and uses sixteen convolutions of 0.010 cm (0.004 in.) thick AM-350 stainless steel. It has an effective dead volume of 20 cm^3 (1.2 $in.^3$). The power bellows housing has a radial clearance of 0.76 cm (0.30 in.) around the bellows outside diameter.

The calculated losses for the various regions are summarized in Table 3.

Table 3

POWER BELLOWS FLOW LOSS SUMMARY

Region	Friction Loss (W)	Inertia Loss (W)	Total Loss (W)
Inside Convolutions	20.8	62.0	82.8
Across Weld Beads	1.8	41.0	42.8
Outside Bellows	4.8	11.1	15.9
Along Surrounding Wall	3.3		3.3
Total Bellows	30.7	114.1	144.8

A worst case calculation for the peak pressure difference across a bellows convolution shows that it is less than 0.017 MPa (2.5 psi). This is sufficiently low that it presents no compromise on bellows lifetime.

Hydroformed bellows were first planned for the buffer and seal bellows applications, since dead volume was of no concern there and costs are substantially lower. Bellows design analysis, however, showed that they were too long to be practical and also had a surging frequency problem. Conventional nested ripple welded bellows are therefore specified for both the buffer and seal bellows. Minor reductions in power loss for the buffer bellows can be achieved by increasing the pitch. The gain is so slight, however, that for first order purposes the buffer bellows loss will be set equal to the 145 W power bellows loss. The much smaller seal bellows, however, has a greatly reduced power loss. Combining the four friction and three inertia loss terms described above for the seal bellows gives a total of 6.6 W loss. Of this, 5.1 W is inertia loss and 1.6 W friction loss.

The three compensator bellows will be off-the-shelf welded bellows. The welded choice is made for dead volume reasons on the compensator bellows which interfaces with the engine gas. The other two enjoy a significant packaging advantage relative to hydroformed bellows, with a minimal cost disadvantage. The power loss associated with all the compensator bellows is virtually zero, since their strokes are nominally zero.

The metal diaphragm alternative to the power bellows presents a much different loss characteristic than does the bellows. There is only one loss term of significance here, and that is the inertial loss in the coupling fluid between the diaphragm and the power piston. These losses are difficult to analyze accurately because they involve a fluid flow transition from the 17.8-cm (7.0-in.) diameter power piston to the approximately spherical deflection of the 35.6-cm (14.0-in) diameter corrugated diaphragm. The losses can be bracketed by limiting case calculations, however.

Spherical deflection of the diaphragm produces a total centerline stroke of 1.71 cm (0.675 in.). The best limiting case for velocity head pressure at the diaphragm would thus be where all stroke volume occurred at this stroke length, which implies an effective diameter of 25.1 cm (9.88 in.). One velocity head expanding from the 17.8-cm piston diameter to a diameter of 25.1 cm would consume 24.8% of a total expansion velocity head, or 302 W. The other limiting case is established by assuming the flow expands to the full 35.6-cm diaphragm diameter. In this case, one velocity head consumes 686 W. This is 56% of the full velocity head expanding into a stagnant plenum, which amounts to 1219 W. The average of these limiting cases (494 W) is therefore a reasonable number to use. The extreme limits differ from the average by 39%.

During the engine compression stroke when oil flow is expanding from the power piston diameter to the effective diaphragm diameter, one full velocity head between those areas will be lost. On the return stroke, the loss can be no more than 0.5 velocity head. With a well-rounded entrance to the cylinder bore, the loss can be as low as 0.05 velocity head. Averaging this best value with the oil expansion loss gives an overall average of 0.525 head losses, or 259 W with bracketing limits of ±100 watts. This represents 1.7% ± 0.7% of 15 kW.

In the above analysis, it was assumed that the power piston always moves within its cylinder bore, and that the fluid stream exits the cylinder en route to the diaphragm region. In an alternate approach, the piston could always be allowed to protrude frm the cylinder. If it had a slightly rounded end, it would normally be subject to drag forces that produce virtually the same loss as the head losses calculated above. It is possible, however, that the unusual flow situation, in which the diaphragm motion follows the piston motion, would significantly reduce the wake and therefore the major drag force which occurs during the gas expansion stroke. An accurate analysis of such an effect is a complex three-dimensional flow problem which is beyond the scope of the present effort. The above loss figures will therefore be assumed for the diaphragm case, with the recognition that these losses might be significantly reduced in real hardware.

3.2.4 Bounce Chamber Losses

There are two loss mechanisms which occur in the converter bounce chamber or buffer gas region. The first is the irreversible thermodynamic loss which occurs in pneumatic bounce chambers and the other loss results from reciprocating flow of the bounce chamber gas. Irreversible thermodynamic losses in pneumatic bounce chambers are often cited as a major loss mechanism for free-piston Stirling engines. In order to avoid potential efficiency problems in the selected design concept and to gain a basic understanding of how to minimize this loss, a fairly extensive analytical study was conducted. The results show that although in some designs this is a major loss consideration, it can be reduced to a negligible level in the current design concept.

If the gas compression and expansion due to volume changes in a bounce chamber could be made either purely isothermal or purely adiabatic, there would be no loss to consider. This follows from the fact that cyclic compression and expansion would retrace a single isothermal or adiabatic curve with no open area on a pressure-volume diagram. In reality, the heat transfer coefficient between the bounce chamber gas and its surroundings is always somewhere between the limits of zero and infinity, which represent respectively adiabatic and isothermal

changes. Consequently the cyclic compression and expansion occur with some limited heat transfer which causes the bounce chamber indicator diagram to open up. This is caused by heat tranfer from the gas during compression at a higher temperature than heat return during expansion.

Various schemes have been suggested for isothermalizing variable-volume gas accumulators. Isothermalization provides the dual benefit of reducing both thermal losses and pressure swings. One of the simplest methods, which is also apparently very effective, was tested by Otis (Reference 8). He introduced plastic foam materials into the gas region. These function in a manner somewhat analogous to a regenerator matrix in a Stirling engine in that the foam remains in intimate thermal contact with the gas during compression and expansion. If the foam has a heat capacity substantially in excess of the gas heat capacity, the process will be nearly isothermal. The presence of the foam detracts slightly from the available gas volume which increases the pressure swing, but the isothermalizing effects more than offset this in Otis' tests. In what was cited as a typical test, the cyclic hysteresis loss was reduced from 15% of the total compression work without foam to only 1.4% with foam. His tests were run with holding periods at the end of each expansion or compression phase, which tends to maximize losses as compared with the rapid cyclic processes encountered in a Stirling engine bounce chamber. This technique is simple and effective, and may well prove useful in any case, whether the specific accumulator losses are relatively high or low. Metallic isothermalizers have also been used in a similar way. The foam is simpler and cheaper if it can achieve the necessary heat capacity, possibly using coating enhancements such as Otis described.

An analytical model for gas spring hysteresis losses was reported by Breckenridge et al. (Reference 10) and highlighted by Beale (ref. 11). An experimentally determined enhancement factor is utilized to account for boundary layer effects which were not included in the analytical model. The expression as provided by Beale is shown in Equation 4, which gives the gas spring hysteresis loss in W.

$$\text{Hysteresis Loss} = F(.353)Z^2 \left(\frac{K_g\ \omega\ P_o T_o \gamma}{Z}\right)^{\frac{1}{2}} \left(\frac{\Delta V}{V_o}\right)^2 A_s \qquad (4)$$

where

F = enhancement factor
γ = gas exponent (ratio of specific heats D_p/C_v)
Z = $\gamma - 1$
K_g = conductivity of the gas (W cm^{-1} K^{-1})
ω = circular frequency (rad/sec)
P_o = mean gas spring pressure (MPa)
T_o = mean gas spring temperature (K)
ΔV = amplitude of the volume change (cm^3)
V_o = mean gas spring volume (cm^3)
A_s = internal gas spring surface area (cm^2)

Breckenridge reported an enhancement factor F of 2.6 for a particular case, but Beale has found it to run between about 5 and 8 for many of his small Stirling engines. It should be emphasized that this expression is subject to various

unspecified limitations. These include operating frequency effects and geometrical factors since, for example, the addition of foam for isothermalization would greatly increase the internal surface area A_s. The magnitude of this increase is such that it significantly reduces the losses, although in the range of application of the equation the losses increase directly with A_s.

This expression nevertheless provides a good deal of useful information about how to optimize a bounce chamber and what the relative value of various improvements might be. It can also be used to approximate the losses for most typical accumulators, although an accurately validated figure would require additional information or experimental verification. The primary controllable factors determining the loss are the ratio $\Delta V/V_0$ of half-stroke volume to mean volume and the selection of an operating gas where possible. The volume ratio should simply be made as small as practical within size and weight limitations on the system. This reduces the effective gas spring constant as well as the hysteresis losses, the latter as a strong square law effect.

In a system such as a free-piston Stirling engine linear alternator where an absolute seal is not provided between the engine and bounce chamber regions, the designer is constrained to use the engine working fluid in the bounce chamber. This limits the practical choices to helium or hydrogen, both of which are poor performers in bounce chambers. With the bellows seal of the Stirling hydraulic engine, however, a much wider choice of bounce chamber gas is available. For hysteresis losses, the parameters of interest are thermal conductivity and specific heat ratio. The other key factor to consider is to assure that the gas does not change phase in the operating pressure and temperature ranges of interest. The only exception to this would be the case where total volume limitations were so severe that one would accept the temperature control requirements and additional losses involved in using a two-phase accumulator system.

The thermal conductivity appears as a square root function in Equation 4, so it has limited impact on losses. The conductivity of hydrogen is 21% higher than that of helium, so the hysteresis losses are a modest 10% higher with hydrogen, based on conductivity alone. With a very low conductivity gas such as xenon or some of the Freons, conductivity is 90% lower than for helium or hydrogen, which can result in about 1/3 to 1/5 the hysteresis loss.

The principal opportunity to reduce hysteresis losses, however, is provided by the specific heat ratio γ. In Equation 4, γ and $Z = \gamma - 1$ take the form of $(\gamma Z^3)^{\frac{1}{2}}$. This function, normalized to 100 for monatomic gases with $\gamma = 1.67$, is plotted as a function of γ in Figure 17. The dramatic dependence of hysteresis losses on γ is illustrated by the fact that they are reduced by more than 50% when using hydrogen instead of helium. When using Freon 14, 90% of the hysteresis losses are eliminated on the basis of specific heat ratio only. When the thermal conductivity is also considered, Freon 14 reduces losses by about 97% relative to helium. Estimates of absolute numerical losses are given below.

Properties of well over a hundred industrial gases were investigated as potential candidates for use in the buffer bounce chamber/accumulator. A low specific heat ratio was, of course, a primary consideration. The most difficult criterion to satisfy with a low specific heat ratio gas was the necessity for a very high vapor pressure at anticipated operating temperatures, or preferably a critical

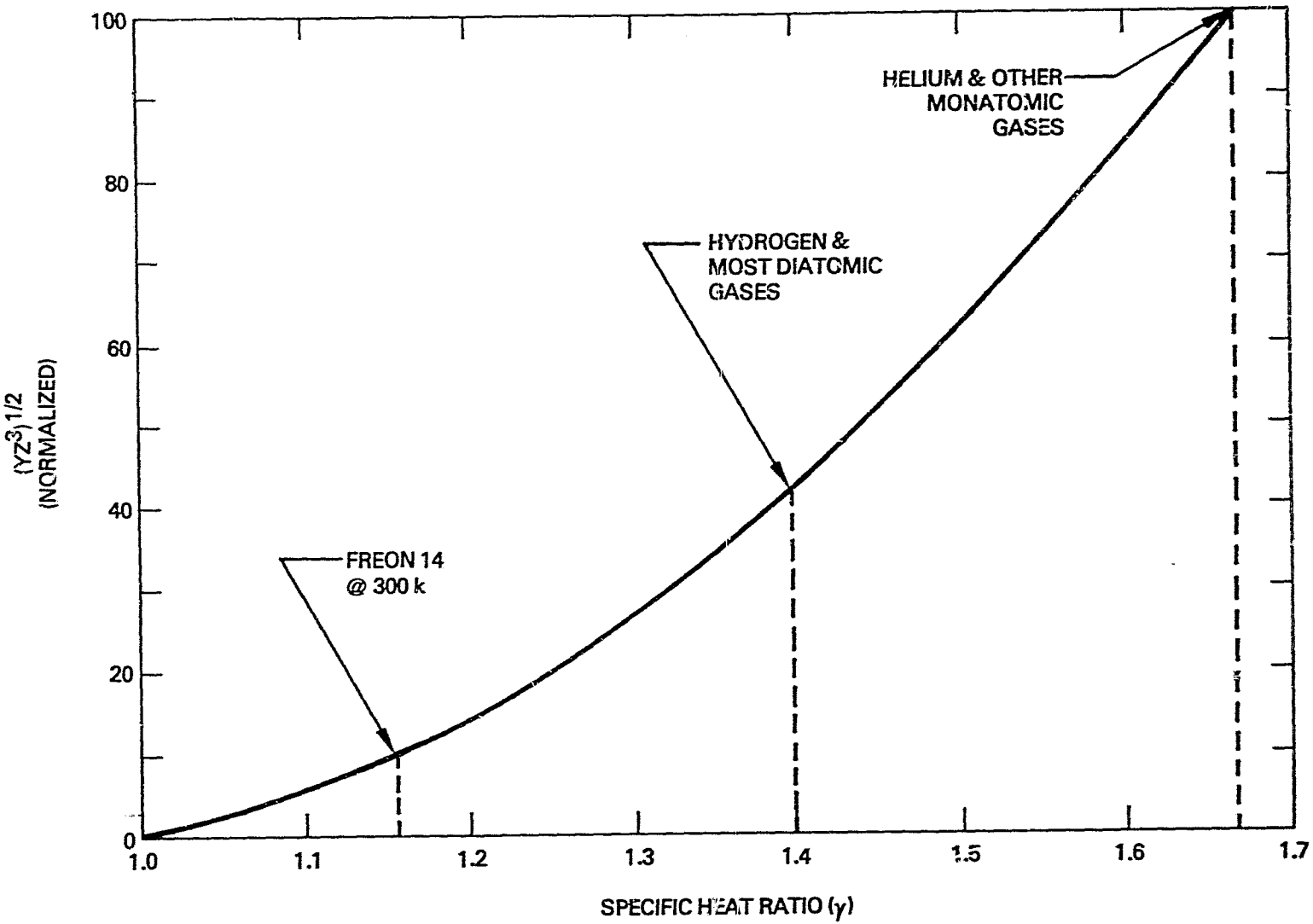

Figure 17. Relative Bounce Chamber Hysteresis Loss as a Function of Gas Specific Heat Ratio.

temperature lower than any anticipated operating temperature. The latter characteristic assures that no condensation will occur at any pressure as long as the temperature remains above the critical temperature.

The clear choice was tetrafluoromethane, CF_4, more commonly knon as Freon 14. It has a very reasonable critical temperature of 227.6°K (-45.5°C or -50°F), which is lower than should be encountered in any anticipated operating regime. Freon 14 has an acceptably low specific heat ratio of 1.159 at 25°C. It is further identified as being inert, colorless, nonflammable, noncorrosive, and nontoxic, except that in high concentrations it could act as an asphyxiant. Thermal conductivity is 1.58×10^{-4} W/(cm K) at 25°C. This value is slightly over 10% of helium conductivity. Several other candidate gases had lower specific heat ratios (as low as 1.067), but were substantially inferior to Freon 14 in at least one other parameter.

To obtain a rough idea of the absolute magnitude of hysteresis losses involved with various configurations, some sample calculations were made using Equation 4 with an enhancement factor F of 6.5 (average of the range 5 to 8 as reported above by Beale). First to be considered was the Reference 4 linear alternator bounce chamber using the specified helium working fluid and operating parameters. The major uncertainties in this calculation were values for the gas spring surface area A_s and volume V_0. These were estimated using dimensions scaled from the final layout design presented in Reference 4 for those regions interpreted as being included in the bounce chamber. The parameters used were as follows:

$F = 6.5$

$\gamma = 1.67$

$Z = 0.67$

$K_g = 0.000158$ W/(cm K)

$\omega = 377$ rad/sec (f = 60 Hz)

$P_0 = 5.82$ MPa

$T_0 = 310$ K

$\Delta V = 424$ cm^3

$V_0 = 6360$ cm^3

$A_s = 3360$ cm^2

When used with Equation 4, these values yield a hysteresis power loss of 774 watts, which represents a loss of 5.2% relative to the net electrical output. Subsequent information (personal communication between George Dochat and Maurice White) indicates that the correct bounce chamber volume is actually 19,300 cm^3. This amount of bounce chamber volume is difficult to conceptualize from the Reference 4 layouts, but assuming it to be correct and with a minimum possible corresponding area $A_s = 4460$ cm^2, the bounce chamber loss for that system drops to 183 watts or 1.2% of the net output. This is more than 4 times the loss of

43.7 W reported in Reference 4. The difference probably results from the value of the empirical enhancement factor which was used. If this design could utilize Freon 14, the calculated loss would be about 5 watts.

When the above analysis is applied to the bounce chamber in the hydraulic converter, the calculated loss is 5.6 watts. This number is based on an enhancement factor of 6.5 and the use of Freon 14 in the buffer. With a fluid this dense, flow losses within the Freon gas must also be considered. The volume of the buffer chamber is 15,000 cm^3 of which approximately 5,000 cm^3 is inside the 17.3 cm (6.8 in.) diameter piston shell and 10,000 cm^3 inside the 32.5 cm (12.8 in.) diameter lower end region. Therefore 2/3 of the volumetric flow expands from the smaller to the larger diameter. With all factors considered, the average fluid flow power loss is calculated at 6.1 W. Therefore, the total buffer chamber power loss is 12 W or 0.08% of 15 kW.

3.2.5 Loss Summary and Overall Hydraulic converter Efficiency

The four sections immediately above detail the power losses in the hydraulic converter. The general rule of thumb in arriving at calculated results was to use conservative assumptions whenever approximations were required. It can therefore be reasonably anticipated that actual losses might be somewhat lower than those presented. The only area where this observation does not hold is in the power output requirement. This is because the stroke volume at the power piston interface, used to determine flow for loss calculations, was taken from the Reference 4 engine specifications. The reported efficiency for the linear alternator of 90% is essentially equal to the 90.2% combined efficiency for the hydraulic motor (95%) driving a rotary alternator (95%). Taken together with a 93.5% efficiency for the hydraulic converter, the net efficiency downstream from the engine is 84.4%. This implies an engine indicated power requirement of 17.8 kW to the hydraulic converter which compares with 16.6 kW to the linear alternator. The resultant higher throughput to the hydraulic converter reduces its efficiency from 93.5% to 93.2% as iteratively determined from the data in Figure 18, Case I (see below). This minor difference essentially disappears when the non-counterbalanced version is considered, and the latter is more directly comparable to the non-counterbalanced linear alternator.

Scaling studies were done to determine part load efficiency of the hydraulic converter. It was assumed that power reduction by throttling resulted in equal drops in frequency and stroke, with the charge pressure remaining fixed. Results in Section 3.3.4 show this assumption to be approximately correct, but even a significant difference in throttling approach would have little impact on the results since most loss terms scale similarly in frequency and stroke. Results of the part load loss scaling at reference design conditions are illustrated in Figure 18 as Case I. Hydraulic converter efficiency is seen to improve significantly as power level is reduced.

An even more significant efficiency factor is also indicated in Figure 18 by the designations Case II and Case III. Case I represents the engine design parameters as specified in Reference 4 where the piston stroke volume at design output, ΔV_{po}, is 845 cm^3. The actual stroke volume ΔV_p, of course, decreases as the system is throttled to part power conditions. In Case II, it is assumed that the average engine pressure, $\bar{P}_E$, is tripled to a level more typical of high-technology Stirling engines. There is a corresponding decrease in ΔV_{po} by a

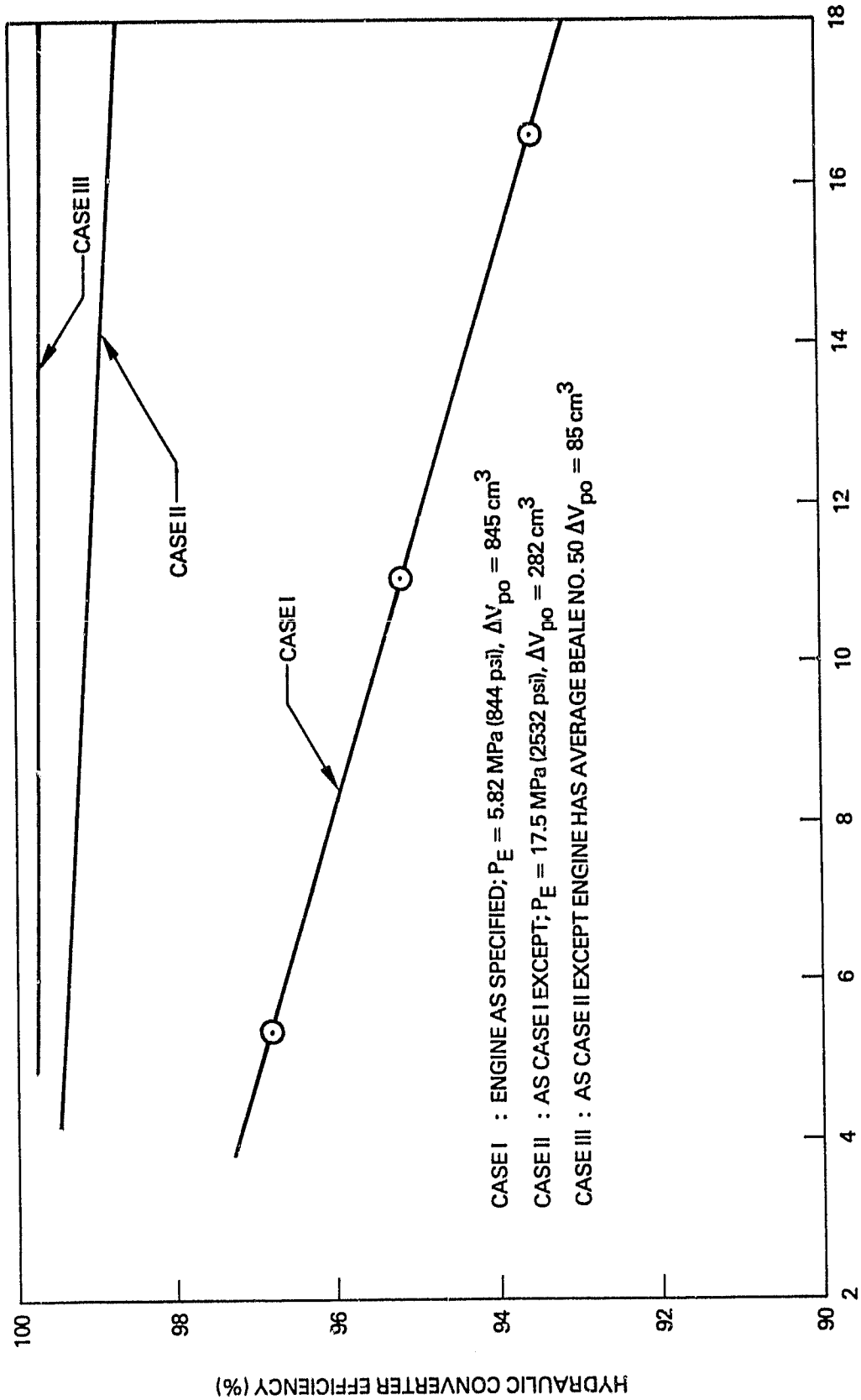

Figure 18. Hydraulic Converter Efficiency as a Function of Power Throughput.

factor of three to maintain power output constant. Since most of the loss terms are independent of absolute pressure but decrease with typically the first or second power of stroke volume, the converter losses are greatly reduced. The resulting efficiency increases to 98.7% at full load from 93.5% for coupling with the specified engine design.

Case III represents another major increment in converter efficiency. This case assumes the same charge pressure as for Case II, but in addition assumes that the engine is designed to exhibit a typical Beale number (see Section 3.3.3 for definition) of 0.015. In this case, the stroke volume is further reduced by slightly more than another factor of three. This issue is more fully discussed in Section 3.3.3. In this case, the full power counterbalanced hydraulic converter efficiency reaches the phenomenal level of 99.6%.

The overall hydraulic converter loss figures are summarized in Table 4. Performance without the counterbalance pistons is included for Case I since this provides a more rational basis for comparison to the Reference 4 linear alternator which not only has no counterbalance for the reciprocating motion but also incorporates a more massive piston which will adversely affect Stirling engine efficiency to an unspecified degree.

It should be noted that this represents a very early stage of development for this concept. Innovative design and/or manufacturing techniques may very likely result in significant reductions of seal and fluid flow losses. The conservative approximations made with the bellows and diaphragm loss calculations suggest that these losses may actually be significantly lower than presented. Finally, the outstanding increase in converter efficiency at higher charge pressures illustrates that the hydraulic output Stirling engine has a very high efficiency potential when used at more typical operating pressures for high technology Stirling engines. Compared with friction losses in kinematic engines, hydraulic converter losses are probably lower. Of course hydraulic motor efficiency must also be considered when shaft power is required.

Table 4

HYDRAULIC CONVERTER LOSS SUMMARY

	Counterbalanced System Loss (W)				Unbalanced System Loss (W)	
	Power Bellows			Power Diaphragm	Power Bellows	Power Diaphragm
Loss Type	Case I	Case II	Case III	Case I	Case I	Case I
Seals	460	73	29	460	172	172
Fluid Flow	317	35	3	317	12	12
Bellows/Diaphragm	296	99	30	410	296	410
Bounce Chamber	12	1	0	12	12	12
Totals	1085	208	62	1199	492	606
Overall Efficiency	93.5%	93.7%	99.6%	92.8%	97.0%	96.3%

3.3 Computer Simulation and Engine Analysis

The dynamic and thermodynamic characteristics of Stirling engines are quite complex and require validated computer codes to develop high confidence designs. For the present purpose, the thermodynamic results are primarily for reference purposes since the engine thermal design is specified (Reference 4). The need for an accurate dynamic simulation is especially important with free-piston engines. The nature of the load affects system dynamics significantly. In the present case, this requires comparing results using a hydraulic converter load (equivalent to Coulomb friction) with results for a linear generator (approximated by a viscous load).

In this section, the background and current status are described for the programs used to analyze the specified free-piston Stirling engine coupled to both a hydraulic converter and a linear generator. Modifications to the preexisting codes are also described. These were incorporated to more accurately model the given engine which has some unique gas flow passages which impact dead volume, gas flow windage and thermal performance.

The effect of Stirling engine characteristics on system performance is analyzed on an overall basis. Results indicate that stall and instability problems could be reduced or eliminated with engine modifications. The relatively low Beale number (see Section 3.3.3 for definition), charge pressure and phase lag, and high dead volume ratio, lead to a low power density and limit efficiency. Efficiency of the hydraulic converter is especially impacted by the large stroke volume requirements imposed by the low charge pressure, as outlined in Section 3.2. Functionality of both the linear alternator and hydraulic systems would be enhanced by coupling to an engine with operating parameters more in line with typical high technology Stirling engines.

Finally, results of the simulation study are presented with the aid of numerous plots. These results show the hydraulic and linear generator loads to be generally comparable in overall impact, although significant detail differences exist. Results of the thermal analysis obtained by Martini Engineering using proprietary codes are also discussed.

3.3.1 Program Description

o Background

The dynamic simulation and thermodynamic analysis computer programs utilized in this study are the result of more than ten years of continuous model development for free-piston Stirling engines. Systems have been analyzed using free-piston Stirling engines coupled to linear generators, piezoelectric generators (Reference 11, 12), pneumatic thermocompressors (Reference 13), and hydraulic pumps (Reference 3). Extensive validation with experimental results from seven generations of hardware has been achieved at low power levels and measured performance of the latest system agreed almost identically with previously published performance curves (Reference 3, p. 95 ff.).

The first extensively developed program was a digital version which included freepiston dynamics and third order thermodynamic analysis. This program proved useful in correlating experimental data from given engines, but running times were far too long to utilize the program as a viable design tool. An analog computer simulation was therefore developed to model free-piston dynamics. Capacity limitations on the analog computer required linearization of some equations, but the model proved eminently useful in surveying a wide range of design options and providing valuable insights into the characteristics including instabilities of free-piston engines. It also did an excellent job of identifying design points and predicting performance envelopes for two generations of Stirling hydraulic engines.

In 1979, a state-of-the-art 32-bit virtual memory minicomputer with a CSMP (Continuous System Modeling Program) digital/analog simulator software program became available. This enabled the basic analog system equations to be modeled in their more accurate nonlinear form. An added bonus is the addition of several refinements, notably an option which analyzes the case where power density is enhanced by allowing overlap of piston and displacer motions. A major side benefit results from development of an auxiliary FORTRAN V digital program designated ASHES (Analysis of Stirling Hydraulic Engine Simulation). This program uses the CSMP output file for input and computes all important dynamic and second order thermodynamic data on a cycle-by-cycle basis. It greatly improves the visibility of transient behavior and eliminates much of the drudgery otherwise involved in reducing analog or CSMP results.

o Program Specifics

The versions of the computer programs used in this study were modified as described in the next section to reflect specific needs of the 15 kW system and were designated MCP.6 and ASHES.7. The dynamic simulation MCP.6 is set up for convenient data entry, calculation of important Stirling engine system constants and initial conditions, dynamic simulation of the system, and standardized output data format. Output of the dynamic simulation includes all input data (57 items), all constants calculated and used by the program (typically 190 items), and a table of specified outputs, which normally include system pressures and piston positions versus time. The output data from the simulation are usually not printed but rather are stored on disc for use as an input file for subsequent FORTRAN digital programs for plotting and/or thermodynamic analysis. A print plotting routine and a drum-type x-y plotter allow the generation of pressure-displacement plots and plots of simulation output variables versus time.

The ASHES.7 code allows convenient and cost-effective evaluation of the results of the dynamic simulation. The output of ASHES provides a compact, comprehensive summary of

1) Static data:

   a) The simulation case name.

   b) Complete input data for the case.

   c) All calculated constants.

2) Dynamic data; a cycle-by-cycle analysis of:

   a) Kinematic data, including operating frequency, piston strokes, and piston approaches to stroke limits.

   b) Thermodynamic data, including power output, displacer drive power, second law heat input, reheat losses, and fixed heat losses.

Among the calculated constants are parameters which at a glance tell the user of MCP and ASHES whether the case under study represents an engine with enough vitality to operate and whether the drive spring rate has been specified low enough to allow the engine to self-start and run, but high enough to prevent engine stall at the displacer end-of-stroke position.

Figure 19 shows the ASHES.7 input and output for the Reference case No. C-16D. The first page (Figure 19A) repeats the data array used as input to the MCP.6 dynamic simulation. The second page (Figure 19B) provides a summary of all parameters initially calculated at time zero. Figure 19C provides a cycle-by-cycle summary of the ASHES.7 output and shows how transients stabilize out very rapidly.

3.3.2 Program Modifications

The specified Stirling engine configuration (Figure 4 and Reference 4) has several features which distinquish it from the configurations previously modeled in the existing computer codes. The engine features which are new to this analysis method are:

1) The central flow tube between the engine and the annular heater.

2) The fixed annular heater.

3) The fixed porous annular regenerator.

4) The multi-tube cooler.

5) The separate displacer pneumatic bounce spring.

The required code modifications were completed prior to running test cases. Among the more important new computations performed are those which determine the windage force coefficients for the displacer and the main reheat loss. These are discussed briefly in following paragraphs.

The windage coefficients are used by the CSMP dynamic simulation routine in the equations of motion for the displacer. There are two windage coefficients. These are B_1, which is the force coefficient of displacer velocity, and B_2, which is the force coefficient of displacer velocity squared. The total force is expressed as:

$$\text{Displacer windage force} = B_1 V_{\text{displacer}} + B_2 V^2_{\text{displacer}} \qquad (5)$$

```
****              ASHES - FALLOUT FROM CSMP                ****
****  ANALYSES OF THE STIRLING HYDRAULIC ENGINE SYSTEM     ****

INPUT FILE WAS CSMPOU.C16D
OUTPUT FILE IS ASHES.OUT.C16D

                    ***PROBLEM INPUT STATEMENTS***
*      CSMP PROGRAM TO ANALYSE MOVING COLD PLATE STIRLING ENGINE
*                       FOR THE NASA CONTRACT DEN3-212
*
*              SYSTEM 8 MOVING COLD PLATE - VERSION 6
*         COMBINE MCP-5 AND M/FCP-2 FOR ABSOLUTE STROKE LIMITS,
*          ASHES COMPATIBILITY AND FIXED OR MOVING COLD PLATE
*            ALTERNATIVE BY REDEFINING INPUT VALUE FOR DPBE
*
*            ------ C O U L O M B      L O A D -------
*                              CASE : C16D    DATE 5-17-81
*
CONSTANT  ABCE = 4.050,   ARE  = 17.35,   B1V  = 0.0,    B2V  = 0
CONSTANT  BVL  = 0.0,     C1   = 68947,   C2   = 175125, C3   = 2.54
CONSTANT  CL   = 1.2,     DBUFE= 7.000,   DCENE= 1.30,   DCLRE= 0.138
CONSTANT  DCPEE= 7.000,   DDISE= 3.960,   DDPE = 1.114,  DPBE = 7.088
CONSTANT  DWIREE=0.003,   ETAX = 0.84,    FANT = 60.0,   GAMBC= 1.67
CONSTANT  GAMMA= 1.16,    GE   = 0.020,   GHE  = 0.12,   K1E  = 0.00
CONSTANT  K3E  = 24.2,    KBUFE= 24.2,    KDBE = 0.0,    LCENE= 8.00
CONSTANT  LCLRE= 4.0,     LDE  = 12.60,   LHTRE= 14.82,  LRE  = 5.00
CONSTANT  M1   = 1474,    M2   = 10000,   NCLR = 200,    PEOE = 844.0
CONSTANT  PHE  = 5000,    PLE  = 100,     QFIX = 1012,   RACP = 1.009
CONSTANT  SDISE= 3.014,   SPBE = 2.0,     START= 1.0,    TCM  = 320.5
CONSTANT  THM  = 1089,    V80  = 16000,   VBC  = 327,    VCDO = 56
CONSTANT  VHDO = 9,       VOID = 0.88,    XOE  = 2.375,  X1BE = 0.2
CONSTANT  X30E =-0.85,    XK1E = 0.0,     XK3E = 0.0,    XNE  = 0.0
CONSTANT  SHORT= 1.0,     ZZZZ2= 0.0,     ZZZZ3= 0.0,    ZZZZ5= 0.0
*
*
```

Figure 19A. Input Data Block for Dynamic Simulation.

INITIAL CONDITIONS

A2	A23	A3	7.3978E+01	1.0000E+00	1.7430E+02
ABAR	ABARE	ABC	8.0266E+01	1.2441E+01	2.6129E+01
ABUF	ACEN	ACLR	2.4829E+02	8.5633E+00	1.9299E+01
ACPB	ACPE	ACPEE	2.4607E+02	2.4829E+02	3.8484E+01
ACPP	ADIS	ADISE	2.2146E+00	7.9460E+01	1.2316E+01
ADP	ADPE	AECY	6.2882E+00	9.7467E-01	8.1073E+01
AFLOW	AHTR	AMAT	9.8503E+01	1.0312E+01	8.9548E+04
APB	APBE	AR	2.5457E+02	3.9458E+01	1.1194E+02
B1	B2	B2T	1.3933E+04	1.3497E+01	1.3497E+01
C4	DBUF	DCEN	1.5500E-01	1.7780E+01	3.3020E+00
DCLR	DCPE	DDIS	3.5052E-01	1.7780E+01	1.0058E+01
DDP	DELPE	DELTA	2.8296E+00	8.2675E+06	9.8603E+00
DHHTR	DHMAT	DPB	6.0960E-01	5.5880E-02	1.8004E+01
DWIRE	ETAC	ETACE	7.6200E-03	7.0569E-01	5.1444E-01
FANCEN	FANCLR	FANHTR	4.8884E-03	9.1578E-03	7.8123E-03
FANMAT	FDP	FFCEN	8.8327E-01	0.0000E-01	3.6071E+05
FFCLR	FFHTR	FFMAT	2.5518E+05	3.9886E+06	1.2800E+07
FLCEN	FLCLR	FLHTR	3.5973E+06	7.0822E+05	2.4805E+06
FN1	FN2	G	6.1807E+01	6.8703E+01	5.0800E-02
GH	K1	K11	3.0480E-01	0.0000E-01	3.0549E-02
K1DKS	K1DKST	K3	2.7299E+00	1.1931E+02	4.2380E+06
KBUF	KD	KDB	4.2380E+06	2.2230E+08	0.0000E-01
KDT	KHEAV	KHLOGM	2.2230E+08	6.9735E-03	6.6185E-03
KP	KSTIK	LCEN	6.7909E+06	1.1191E-02	2.0320E+01
LCLR	LD	LHTR	1.0160E+01	3.2004E+01	3.7643E+01
LR	MD	MS	1.2700E+01	7.5798E+01	6.3165E-01
MUBAR	MUC	MUH	3.3854E-04	2.4859E-04	4.2849E-04
NOR	P4	PBO	3.1903E+08	7.8540E-01	5.7133E+07
PBOE	PBCJ	PBCK	8.2865E+02	9.9905E+07	3.4774E+07
PEO	PH	PI	5.8191E+07	3.4473E+08	3.1416E+00
PL	PSIO	PSIJ	6.8947E+06	5.4824E+00	5.0949E+00
PSIK	RATE	RATE1	5.8700E+00	1.8634E+09	1.6042E+09
RATE2	RATE3	RATE4	2.5081E+08	4.2382E+06	4.1628E+06
RHOBAR	RHOC	RHOH	1.4758E-03	2.5499E-03	1.0384E-03
RNCEN	RNCLR	RNHTR	6.8210E+04	5.5379E+03	1.0457E+04
RNMAT	SCP	SCP2	1.2701E+02	5.0799E+00	2.5399E+00
SCPNEG	SCPPOS	SDIS	-2.1589E+00	2.9209E+00	7.6556E+00
SDIS2	SPB	SUMF	3.8278E+00	5.0800E+00	1.1390E+07
TBAR	TC	TH	7.0475E+02	4.0788E+02	1.0016E+03
TR	VO	VBAR	6.6088E+02	8.2259E+02	6.7761E+02
VCD	VDIS	VDISS	2.5208E+02	9.1867E+02	6.1448E+02
VDP	VEFFO	VGD	4.6140E+01	2.2362E+03	5.1374E+01
VHD	VHDT	VRD	5.7120E+02	5.7120E+02	1.2510E+03
VSOVE	WINDO	XO	2.7479E-01	7.6556E-02	6.0325E+00
X1B	X1I	X3	5.0800E-01	-3.8278E+00	0.0000E-01
X30	XK1	XK3	-2.1590E+00	0.0000E-01	0.0000E-01
XN	XSHORT		0.0000E-01	9.5100E-08	

CSMP TIMING

FINTIM = 0.75 PRDEL = .00020 DELT = .000025

Figure 19B. Summary of All Parameters at Time Zero.

ANALYTICAL RESULTS

CYC NO	FREQ	2D LAW HOT PV	PUMP POWER	INTGL POWER	***STROKE*** DISP	P BEL	*CLOSEST APPROACH** DISP	P BEL	D/PB	CONTACT TIME	SHUTTLE LOSS	MAIN REHEAT	TOTAL INPUT	NET EFFIC	AVG PRESS
	HZ	********KILO-WATTS********			***INCHES***		*******INCHES*******			%CYCLE	********KILO-WATTS**********			%	PSIA
1	58 6	23 55	8 03	10 66	2 71	0 72	0 14	0 42	1 05	0 0	0 31	6 58	31.45	25 5	851.87
2	59 2	41 25	13 79	21 32	2 75	1 22	0 10	0 19	1 25	0 0	0 32	6 81	49.39	27 9	854 14
3	59 9	47 69	17 92	24 68	2.88	1 57	0 01	0 04	1 43	0 0	0 35	7 41	56 46	31 7	852 51
4	63 3	48 09	20 91	24 76	2 93	1 73	0 00	0 00	1 57	0 0	0 37	8 24	57 72	36 2	839 72
5	62 6	40 87	20 69	21 08	2 91	1 74	0 00	0 00	1 65	0 0	0 37	8 03	50 28	41 2	839 31
6	60 8	34 09	19 37	17 72	2 88	1 68	0 02	0 02	1 70	0 0	0 36	7 56	43 02	45 0	844 65
7	60 7	33 12	18 79	17 25	2 85	1 63	0 04	0 05	1 69	0 0	0 35	7 44	41 93	44 8	844, 49
8	60 7	32 95	18 30	17 12	2 83	1 59	0 05	0 06	1 67	0 0	0 34	7 34	41 64	43.9	844, 57
9	60 6	32.95	17 97	17 16	2.81	1.56	0 06	0 08	1.66	0 0	0 34	7.27	41.57	43 2	844.77
10	60 6	33 44	17 81	17 37	2 80	1 55	0 07	0 08	1 64	0 0	0 33	7 23	42 02	42 4	845 00
11	60 5	33 76	17 81	17 59	2 80	1 55	0 07	0 08	1 64	0 0	0 33	7 22	42.32	42 1	845 23
12	60 5	34 21	17 88	17 76	2 80	1.55	0 07	0 08	1 64	0 0	0 33	7 23	42 79	41 8	845 35
13	60 6	34 28	17 97	17 88	2 81	1.56	0 06	0 07	1 64	0 0	0 34	7 25	42.88	41.9	845.42
14	60 6	34 30	18 06	17 89	2 81	1.57	0 06	0 07	1 64	0 0	0 34	7 27	43.11	41.9	845 40
15	60 6	34.31	18 12	17 94	2 81	1.57	0 06	0 07	1 64	0 0	0 34	7 28	43 14	42.0	845.40
16	60 6	34 39	18 16	17 90	2 82	1 58,	0 06	0 07	1 65	0 0	0 34	7 29	43 04	42 2	845 32
17	60 6	34 41	18 17	17 88	2 82	1.58	0 06	0 06	1 65	0 0	0 34	7 30	43 06	42 2	845 29
18	60 6	34 25	18 17	17 83	2 82	1 58	0 06	0 07	1 65	0 0	0 34	7 29	42.89	42 4	845 27
19	60 6	34 28	18 15	17 80	2 82	1 58	0 06	0 07	1 65	0 0	0 34	7 29	42.92	42.3	845 27
20	60 6	34 15	18 13	17 78	2 81	1.57	0 06	0 07	1.65	0 0	0 34	7 29	42.79	42.4	845.25
21	60.6	34.30	18 12	17 81	2 81	1.57	0 06	0 07	1 65	0 0	0 34	7 29	42.94	42 2	845.26
22	60 6	34 18	18 12	17 81	2 81	1 57	0 06	0 07	1 65	0 0	0 34	7 28	42.82	42.3	845.28
23	60 6	34 29	18.11	17 80	2 81	1.57	0 06	0.07	1 65	0 0	0 34	7.28	42.93	42 2	845.27
24	60 6	34.23	18 12	17 84	2.81	1.57	0 06	0.07	1 65	0 0	0.34	7.29	42 87	42.3	845.29
25	60 6	34 33	18 13	17 81	2 81	1.57	0 06	0 07	1 65	0 0	0 34	7 28	42.97	42.2	845 30
26	60 6	34 22	18 13	17.84	2 81	1.57	0 06	0.07	1 65	0 0	0 34	7 29	42 85	42.3	845.30
27	60 6	34.34	18.13	17.81	2 81	1.57	0 06	0.07	1 65	0 0	0.34	7 29	42 98	42.2	845.26
28	60 6	34.27	18 13	17 82	2 81	1 57	0 06	0 07	1 65	0 0	0 34	7.29	42 91	42.2	845.29
29	60 6	34 16	18 12	17.77	2 81	1 57	0 06	0 07	1 65	0 0	0 34	7.28	42.79	42.3	845.25
30	60 6	34.24	18 11	17 80	2 81	1.57	0 06	0 07	1 65	0 0	0 34	7 28	42 87	42.2	845.27
31	60 6	34 19	18 11	17 79	2 81	1.57	0 06	0 07	1 65	0 0	0.34	7.28	42.82	42.3	845.25
32	60 6	34 30	18 11	17 82	2 81	1 57	0 06	0 07	1 65	0 0	0 34	7 28	42 93	42 2	845 29
33	60 6	34 19	18 11	17 80	2.81	1 57	0 06	0 07	1 65	0 0	0 34	7.28	42 82	42 3	845.28
34	60 6	34 30	18 11	17 81	2 81	1 57	0 06	0 07	1 65	0 0	0 34	7 28	42 93	42 2	845.26
35	60 6	34 18	18 12	17 81	2.81	1 57	0 06	0 07	1 65	0 0	0 34	7 28	42 81	42 3	845.30
36	60 6	34 31	18 11	17 81	2.81	1.57	0 06	0 07	1 65	0 0	0 34	7 28	42.94	42.2	845.28
37	60 6	34 24	18 12	17 85	2 81	1.57	0 06	0 07	1 65	0 0	0.34	7 29	42.88	42.3	845.29
38	60 6	34 32	18.13	17 81	2 81	1.57	0 06	0 07	1 65	0 0	0.34	7 28	42 96	42.2	845 29
39	60 6	34 19	18.12	17 83	2 81	1.57	0 06	0.07	1 65	0 0	0 34	7 29	42.82	42.3	845.30
40	60 6	34.31	18 12	17 79	2 81	1 57	0 06	0 07	1 65	0 0	0 34	7 28	42 94	42 2	845.26
41	60 6	34.27	18 12	17 82	2 81	1 57	0 06	0 07	1 65	0 0	0 34	7 29	42.91	42 2	845.30
42	60.6	34.17	18.11	17.78	2 81	1.57	0 06	0 07	1 65	0 0	0 34	7 28	42.81	42.3	845.26
43	60.6	34.25	18.11	17 80	2.81	1.57	0 06	0 07	1 65	0 0	0 34	7 28	42.89	42 2	845.27
44	60 6	34.19	18.11	17.79	2.81	1.57	0 06	0.07	1 65	0.0	0.34	7 28	42.82	42.3	845.26
45	60.6	34.29	18.11	17 82	2.81	1.57	0 06	0.07	1 65	0 0	0 34	7 28	42.93	42.2	845.29

END OF REPORT

Figure 19C. Cycle-By-Cycle Output Data From ASHES 7.

The regenerator matrix operates in the laminar regime and produces a displacer windage force which is better described by a B_1 coefficient than a B_2 coefficient. All other flow passages of interest operate in the turbulent regime, and produce a windage force that is better described by a B_2 coefficient than a B_1 coefficient. The B_2 coefficient includes contributions from wall friction and local flow pressure drops for the engine/heater flow tube, the annular gas heater, and the multi-tube gas cooler. The Fanning friction factors, f, for these regions are computed from the Reynolds number N_R using the equation

$$f = 0.079\ N_R^{-.25} \tag{6}$$

which represents the low end of the turbulent flow range and is appropriate for the design under consideration. This relationship is shown in Figure 20 which, together with Figures 21 and 22, is taken from Reference 15. The Fanning friction factor for the matrix was determined from curve fits representing pressure drop for flow through an infinite randomly stacked woven screen matrix, as presented in Figure 21. The friction factor depends upon Reynolds number and matrix porosity. The analytical curve fit used in the simulation was taken through the center of the data in Figure 21, disregarding the porosity effect, because the porosity effect is complex and difficult to fit. The effort required to include porosity effects is not justified by the moderate improvement in accuracy for the scoping objectives of this study.

The B_1 and B_2 coefficients were computed by assuming that the displacer operates full stroke at constant linear speed at an anticipated frequency. These coefficients are then used with instantaneous velocity to determine the gas pressure forces upon the displacer. The coefficients are defined as

$$B_1 = \frac{\text{gas pressure force from regenerator matrix pressure loss}}{\text{displacer average velocity}}$$

$$B_2 = \frac{\text{gas pressure force from other pressure losses}}{(\text{displacer average velocity})^2}$$

The optional engine speed control valve setting based on throttling cooler tube flow was modeled by an input parameter designated B_{2V} which is used as an additional variable component of the overall B_2 coefficient.

Main reheat was calculated from an approximate equation derived assuming constant and uniform gas pressure and a relationship between displacer position and time represented by sine wave motion with a dwell at each end of the stroke. This equation is

$$Q_m = \frac{\pi^2\ C_p^2\ \Delta T_m\ M^2\ f^2}{2\ hA_R\beta} \tag{7}$$

Friction factors for fully developed turbulent flow in a smooth-walled circular tube. Turbulent flow friction factors for rectangular and annular tubes do not differ significantly.

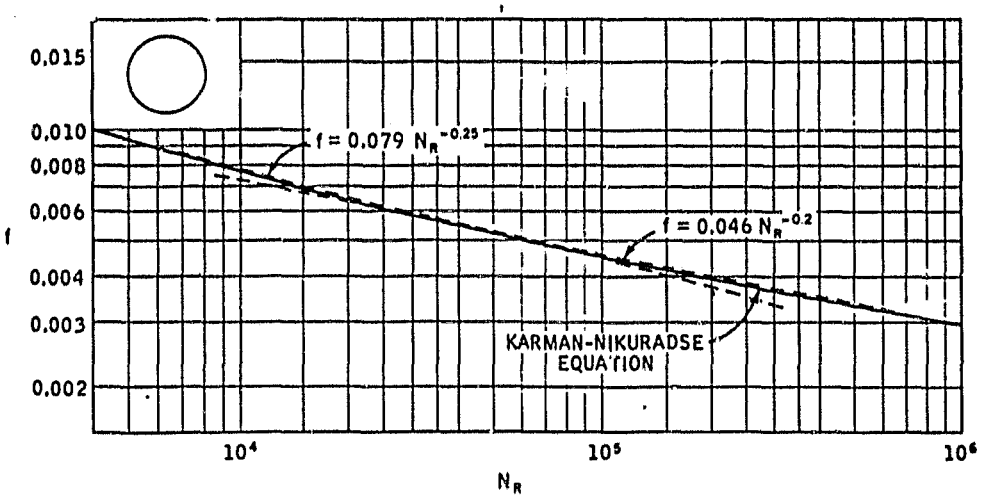

Figure 20. Friction in Tubes (From Reference 14)

Flow through an infinite randomly stacked woven-screen matrix, flow friction characteristics; a correlation of experimental data from wire screens and crossed rods simulating wire screens. Perfect stacking, i.e., screens touching, is assumed.

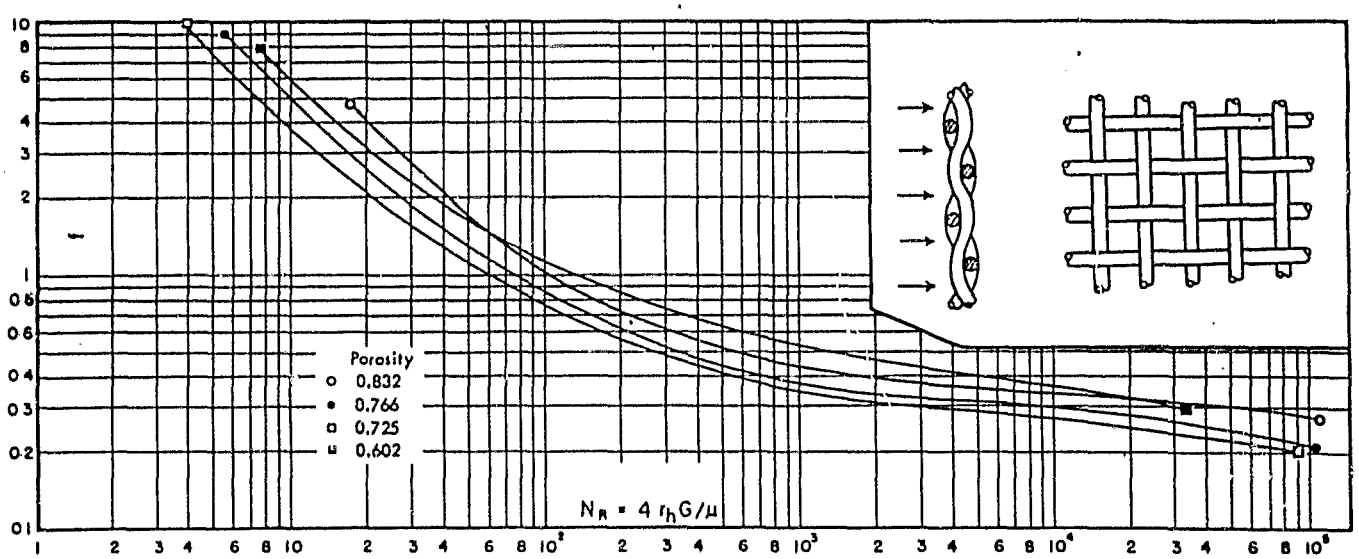

Figure 21. Friction in Woven Wire Screens (From Reference 14)

Gas flow through an infinite randomly stacked woven-screen matrix, heat transfer characteristics; a correlation of experimental data from wire screens and crossed rods simulating wire screens. Perfect stacking, i.e., screens touching, is assumed.

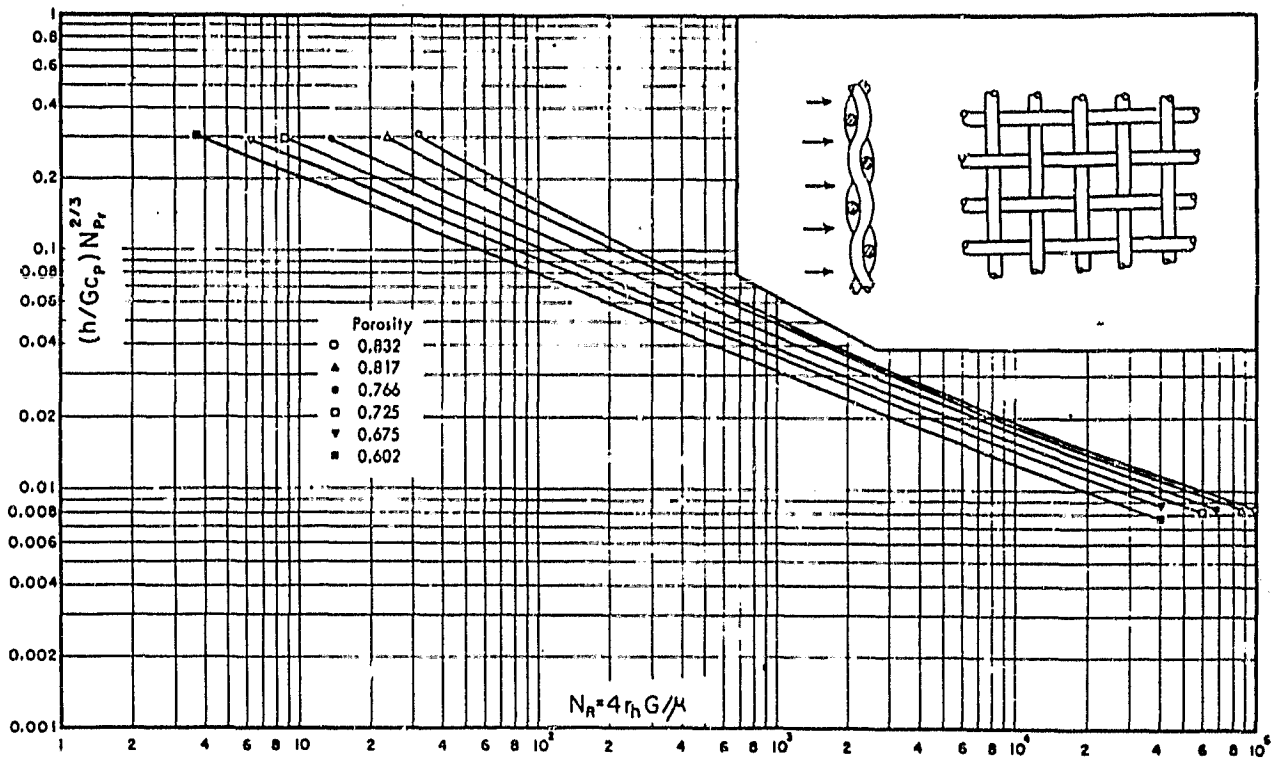

Figure 22. Heat Transfer in Woven Wire Screens (From Reference 14)

where

Q_m = main reheat (w)

C_p = specific heat at constant pressure = 5.2 J g^{-1} K^{-1}

ΔT_m = hot to cold metal temperature difference (K)

M_s = hot space swept mass (g)

f = operating frequency (Hz)

h = matrix film coefficient (W cm^{-2} K^{-1})

A_R = matrix heat transfer area (cm^2)

β = 1.0 - d/T

d = total dwell per cycle (sec)

T = cycle period (sec)

The matrix film coefficient, h, was computed from a curve fit to a relationship between Stanton number, Prandtl number, Reynolds number, and porosity. The curve fit is presented in graphical form in Reference 14. The curves are repeated for reference purposes as Figure 22.

Inputs to the curve fit for determination of the film coefficient are matrix Reynolds number and matrix porosity.

The windage coefficients and the appropriate pneumatic bounce chamber equations were incorporated into the MCP.6 dynamic simulation. The main reheat expression for a porous matrix regenerator was added to the ASHES.7 analysis program, together with other minor changes required to adequately address the 15-kW engine system. Most of these changes were added to take full advantage of the latest computer code improvements available at the time of this contract. They provided the best practical visibility and effectiveness when conducting the parametric survey described in Section 3.3.4, and provide a point of reference relative to the previously predicted Stirling engine/linear alternator performance.

3.3.3 Stirling Engine Characteristics

The characteristics of the Stirling engine mated with the hydraulic converter have a major impact on converter operation. In the present case, engine parameters resulted in a number of compromises in converter and system performance, relative to possible results. As shown in Section 3.2.5, higher engine charge pressure and/or a higher Beale No. would reduce converter piston stroke volume. This in turn greatly reduces converter flow losses resulting in an increase of converter efficiency from 93.5% to as high as 99.6% at 15 kW nominal output. This section will document the Beale number rationale used in Section 3.2.5 and highlight other characteristics of the specified Reference 4 interface engine.

The common denominator which pervaded the various aspects of system design and analysis was that system performance is compromised in several ways by characteristics of the Reference 4 engine. Establishment of a base case system design required far more effort than anticipated. The originally proposed power output control scheme using displacer windage variation proved to be efficient but unworkable from a stability standpoint and had to be abandoned. Power output control using displacer bounce chamber volume variations was shown to be feasible, but system operation remains very sensitive to several parameters. Small changes can cause power train motion to either increase amplitude leading to unacceptable power train collisions or decrease amplitude leading to stall.

These characteristics are a consequence of basic engine design and of the specified operating point for this engine. This point is just slightly below the resonance peak in frequency but at least a factor of three below it in power output. Operation on the leading edge of this very steep resonance peak was apparently chosen because the large dead volume to stroke volume ratio and the engine configuration do not allow stable operation at resonance without power train collisions.

A key result of this operating mode is that the engine operates well below its power output potential. This impacts efficiency and/or regenerator requirements since the gas heat exchangers process approximately the same mass flow rate of gas as they would at the higher output point. Hydraulic converter efficiency would also be greatly improved by operating nearer to resonance because the indicator diagram tends to become more open so that the stroke volume does not increase in proportion to power output (see Section 3.2.5).

The fact that the engine is indeed operating well below its design potential is illustrated by applying a refined Beale number analysis as described in Reference 15. The Beale number is defined as the power output in watts divided by the product of charge pressure in bars, operating frequency in Hz and piston swept volume in cm^3.

$$B = P/(pf\,\Delta V_{po}) \tag{8}$$

where

B = Beale number, Watt/sec/bar-cm^3

P = engine charge pressure, bars

f = operating frequency, Hz

ΔV_{po} = power piston swept volume, cm^3

For a typical modern Stirling engine an average Beale number is 0.015 Watt-sec/bar-cm^3. In the refinement by Walker in Reference 16, the Beale number is given as a function of operating temperature for typical Stirling engines and is bracketed by approximate limits for very well designed and relatively poorly

designed engines. At the specified hot gas operating temperature of 771°C (1044 K), a typical Beale number is 0.0174 Watt-sec/bar-cm^3 with bracketing limits of approximately 0.009 and 0.024. The actual Beale number for the specified operating conditions of the Reference 4 engine is 0.0054. This is less than one third the typical value and only a little over half the lower limiting value. This simple evaluation provides some quantitative support for the qualitative observations made earlier. It is also significant that the piston/displacer phase lag is specified in Reference 4 as 36.1°, when something much closer to 90° is known to be more optimal from general Stirling engine experience and analysis.

Another factor to consider is values of volume ratios in the engine. Reference 15 defines the dead volume ratio X of the Stirling engine as the total dead volume (unswept volume) in the engine divided by the swept volume in the expansion space. Typical values of X are near 1.0. Power density decreases monotonically with increasing X, so it is desirable to maintain X as low as practical, commensurate with adequate heat exchanger capacity. For the Reference 4 engine dimensions specified, X exhibits a very high value of 3.3. This fact significantly restricts the power density and contributes to the low Beale number.

A related ratio of significance discussed in Reference 15 is the volume compression ratio, defined as the ratio of maximum gas volume to minimum gas volume. At the lower limiting value of 1.0, no work is produced since no volume change occurs. A practical upper limit is about 2.5, though most engines have a value near 2.0 or a little less. The value of 1.3 for the Reference 4 engine is quite low, and again reflects the large amount of dead volume.

One additional characteristic of this engine is worth noting here. Previous hydraulic Stirling engines (Reference 3) similar in concept to the system which is the subject of this study have all been designed to be self starting. Self-starting engines operate very stably over a wide range of power outputs from zero power up to the maximum design power. Drop-outs do not occur. The self-starting characteristic is determined by a so-called self-start ratio, R, which relates the displacer spring restoring force to displacer driving force for essentially zero displacer velocity. Certain engine parameters establish upper and lower limits for R. If R is too low, the displacer will move to one end of its stroke and remain there unless some external force is applied, for example by motoring the engine. On the other hand, if R exceed its upper limit, the displacer drive spring is so stiff that any small motion of the displacer will be resisted and the displacer will return to its neutral static position. For the Reference 4 engine, R is much too high for self starting. As explained in the next section, this fact caused considerable confusion during the early simulation studies because it was tacitly regarded as violating an operating condition rather than just a self-start condition. The problem was solved for simulation purposes by selecting appropriate initial conditions which in effect motor the system so that inertial forces come into play and allow sustained operation. The practical consequences of a nonself-starting design, in addition to requiring motoring to achieve startup, dictate that a minimum output level always exists below which the system is subject to stall. This characteristic proved to be a troublesome factor which contributed to performance compromises to avoid either stall or overstroking modes.

The upper and lower limits which must be imposed upon the displacer spring rate to assure self starting and to avoid engine stall are shown in Figure 23. The upper limit is applicable to both Coulomb and viscous load engines. The lower limit is applicable only to Coulomb load engines. The ratio of the upper spring rate limit to the lower spring rate limit can be called the Start and Return Ratio. For successful self-starting designs the Start and Return ratio must be set sufficiently above unity to allow good margins beteween the drive spring rate and its upper and lower limits, at the lowest operating temperature of interest.

3.3.4. Simulation Results

The objectives of the computer simulation were to: 1) Aid in selecting key parameters for the hydraulic converter design, 2) determine piston and displacer motion together with performance and other operating parameters at full load and throttled to 3/4, 1/2 and 1/4 of full load, and 3) conduct a parametric survey about the reference design point to evaluate dynamic stability and establish system sensitivity with respect to parameter variations.

More than 200 dynamic simulation cases were run and analyzed on the specially modified versions of MCP.6 and ASHES.7, as described in Sections 3.3.1 and 3.3.2. This was more than twice the number of cases originally anticipated, a result at least partially caused by the items discussed in Section 3.3.3. Some engine parameters, primarily regenerator porosity, were varied to achieve acceptable results. Many cases were run with reduced porosity to improve efficiency, but other cases did not run well until porosity was returned to a nominal 92%. All changes were held to the minimum practical level in keeping with the objectives of this program, which were to design a hydraulic output unit but leave the engine design alone.

The results of the simulation study were organized into an extensive tabular format. Many runs involved parametric experimentation which provided few useful results, and are therefore not presented in this report. The more significant data were reorganized into both graphical and tabular formats for a concise presentation as given below. Some of the plots are quite complicated, but they do provide a good deal of insight into system operation. Many results would be very different if more latitude on changing engine parameters had been allowed.

The actual sequence of executing the simulation task is outlined below. Item 3 and the results and extent of item 2 were not anticipated before the simulation task was begun. The need for these items was a consequence of the operating character and sensitivities of the specified Stirling Engine. This is the primary reason for the excess computing load. The sequence of the simulation task is as follows:

1. The MCP.6 and ASHES.7 computer codes were modified to properly model features of the Reference 4 engine design which differed from previous engines. Additional equations were added to more accurately model windage and thermal performance of the gas heat exchangers.

2. Unsuccessful attempts were made to find suitable operating points with hydraulic converter (Coulomb) loads or linear generator (viscous) loads using parameters limited almost exclusively to those taken from Reference 4 or inferred from the engine layout in that document.

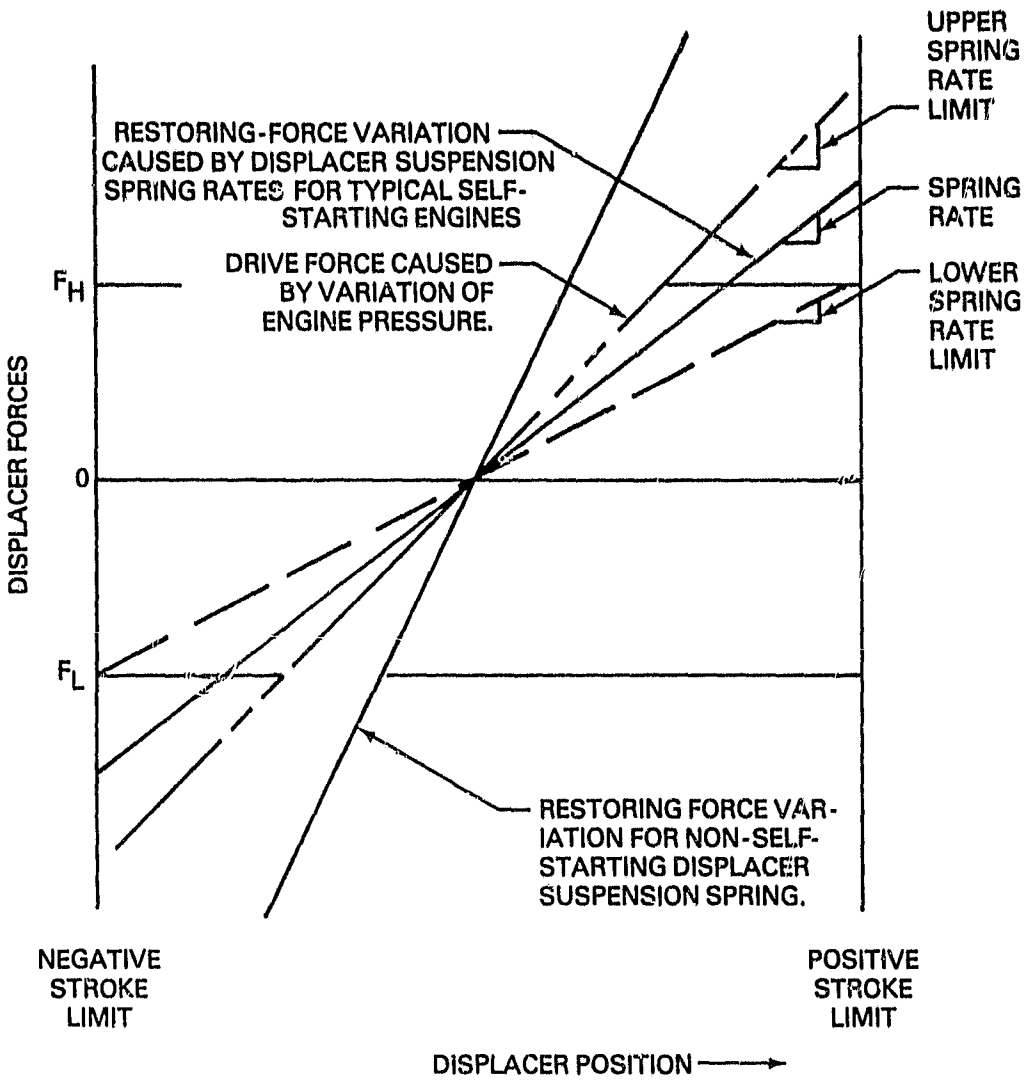

NOTES:

(1) F_H and F_L are drive force limits imposed by the converter low-frequency pressure limits.

(2) The dashed lines represent the upper and lower allowable limits of displacer restoring-force variation.

Figure 23. Displacer Spring Rate Criteria, Self-Starting Engine.

3. A more extensive evaluation of stability and control was conducted based upon minimum deviation from the Reference 4 engine design. Considerably more latitude was allowed than in item 2 above in attempting to find a stable reference case. This evaluation led to selection of variable displacer bounce chamber volume (variable displacer natural frequency) as the mechanism for achieving power output control. Varying displacer windage as originally proposed had some success but typically resulted in a relatively narrow control range before system stall occurred. Several base case parameters were modified in order to obtain moderately stable operating points.

4. A complete range of power output control cases from full power to very low power was run for both coulomb and viscous load cases.

5. Parametric variations on each side of the reference design case were run independently for several significant parameters to establish an operating sensitivity base.

In actual practice, it was necessary to iterate between items 3 and 5, because the first time item 5 was completed most of the parametric variations resulted in either amplitude blowup or engine stall. Somewhat better results were obtained with the reference case selected this time around, but the marginally acceptable performance envelope leads to concern about practical operational viability.

A thermodynamic computer analysis of the Reference 4 engine using the piston and displacer motions from MCP.6 was conducted by Martini Engineering. Results are detailed in Appendix B. Overall performance was relatively close to the ASHES.7 predicted performance for a reference test case. Unfortunately, major inconsistencies resulted when the Martini code was applied to a group of cases representing response curves for part power operation. Despite extensive efforts, the reason for the indicated performance variations could not be determined.

The major conceptual difference between the Martini code and ASHES.7 is the inclusion in the Martini analysis of a "pumping" or "appendix" loss. This occurs when working fluid is pumped in and out of the clearance region between displacer and cylinder walls over a cycle. This is a thermodynamic rather than fluid flow loss term. In the initial test case given in Appendix B, the appendix loss alone resulted in an excessive thermal input requirement of 7.2 kilowatts. This case used a displacer/cylinder gap of .0127 cm (0.050 in.), an arbitrary value since this parameter was not specified in Reference 4. The appendix loss decreases rapidly as the gap is reduced, while shuttle loss increases at a lower rate. There must consequently be an optimum clearance. This was evaluated by Martini Engineering in a series of cases for gaps between 0.0127 cm (0.005 in.) and 0.127 cm (0.05 in.). The results, plotted in Figure 24, show an optimum value near 0.0381 cm (0.015 in.). A reference value of 0.0508 cm (0.020 in.) was chosen for all since the efficiency is fairly flat in this region and the latter value is not near a precipitous drop in efficiency. The appendix loss for the initial test case with a gap of 0.127 cm (0.050 in.) was calculated at 7185 W with the Martini code. This dropped to 724 W when the gap was reduced to the reference value of 0.0508 cm (0.020 in.).

A complex but informative summary of many computer runs is given by the variable load efficiency curves in Figure 25. As shown by the symbol keys in the two legends on the figure, response curves are included for both Coulomb and viscous

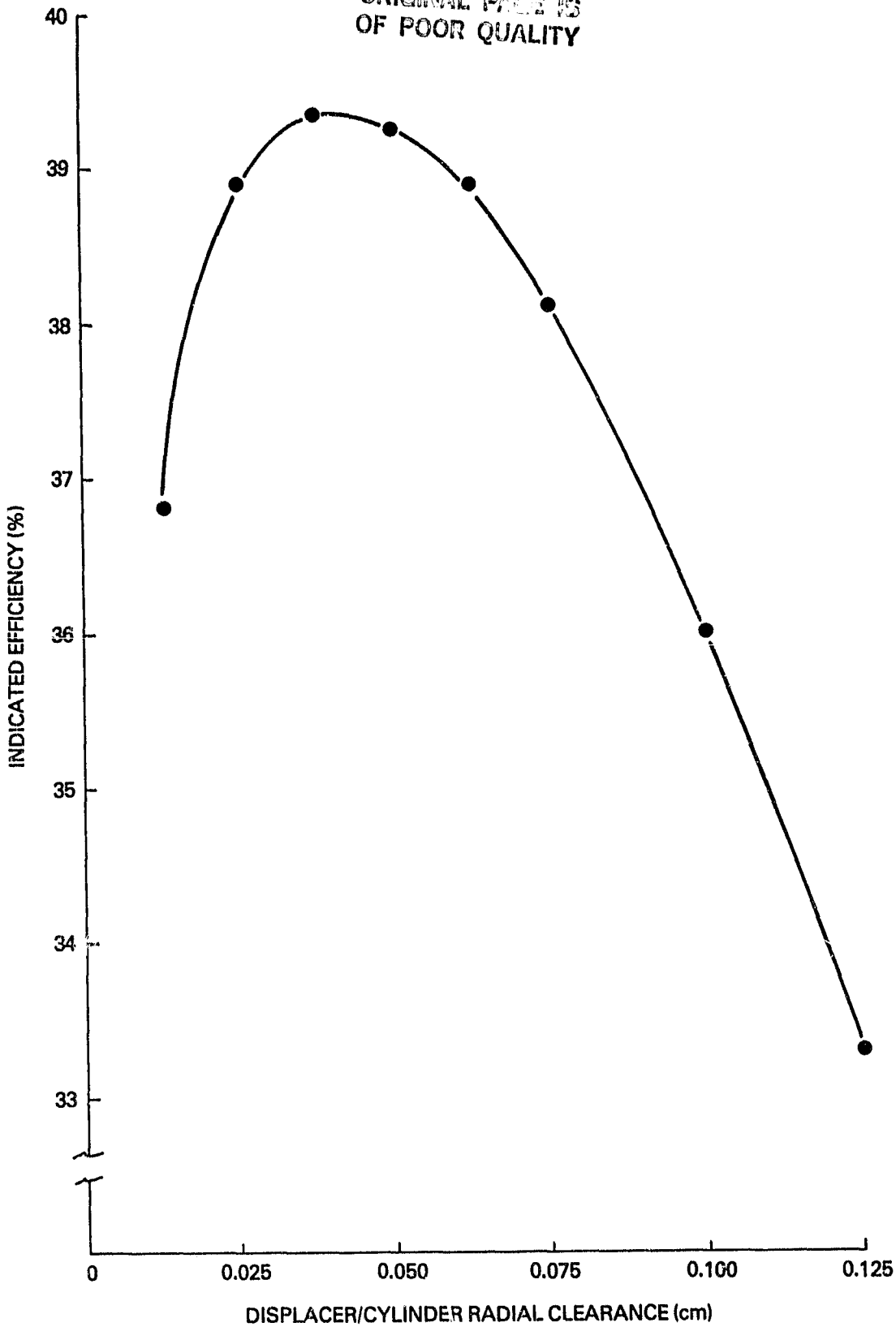

Figure 24. Optimization of Displacer/Cylinder Radial Clearance.

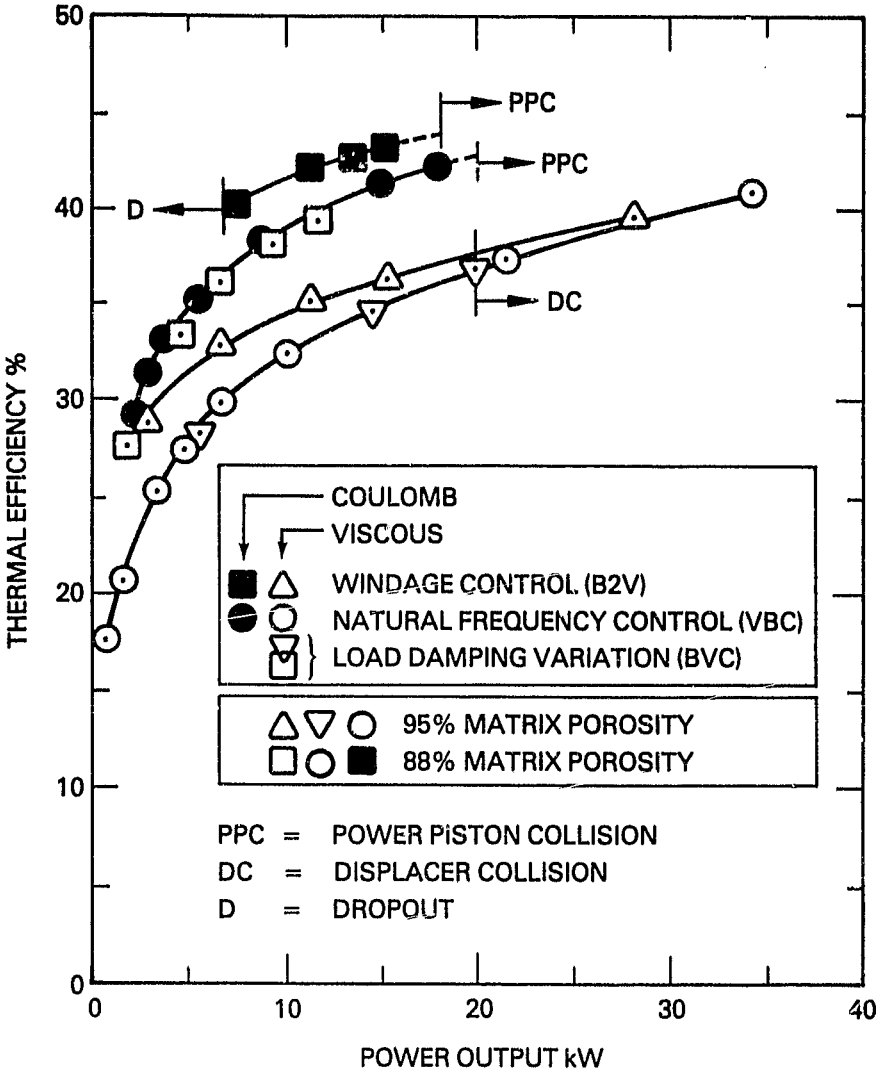

Symbol	Engine Load	Matrix Porosity	Parametric Variation	Case Designation
□	Viscous	0.88	BVL	V6
▽		0.92		V7
○			VBC	V10
△			B2V	V11
●	Coulomb	0.88	VBC	C16
■			B2V	C15

Figure 25. Overall Performance Summary.

load damping (hydraulic converter and linear alternator respectively) with two regenerator matrix porosities and three power output control concepts included. Only six of the twelve possible combinations were included in the simulation runs, but they provide enough information to draw several useful conclusions.

Points on several curves are indicated beyond which displacer or power train collisions occur.

An obvious conclusion is that the 88% porous regenerator provides higher efficiency than does the 92% porosity version. This is most directly compared by cases V6 and V7 where the only difference was in porosity. It is also supported by common Stirling engine experience. The reason for utilizing the higher porosity figure for most of the viscous load cases is that adequate power output could not be achieved with the lower porosity case V6.

The lowest curve correlates with computer data from cases V7 and V10 for power output control of the viscous load using load variation (BVL) and displacer bounce chamber volume (VBC) variation. This shows that these two control modes exhibit the same part load efficiency characteristics. The viscous load damping control mode results in displacer collision at a much lower power level than does bounce chamber volume control.

The third output control mode (Case V11) using heat exchanger windage (B2V) variation, as originally proposed, exhibits a significantly higher part load efficiency than do the other two control modes represented by similar configurations in cases V7 and V10. This observation correlates with previous experimental data for artificial heart engines (Rererence 3) which show that displacer windage control is conservative. In that case, part load efficiency drops only in response to fixed heat losses becoming a larger fraction of the total heat input. This efficiency control mode was abandoned for the Coulomb load case because it had a relatively narrow power range available. With some engine modifications, this may prove to be a viable control option.

Cases V6 and C16 follow the same response curve. These represent viscous and Coulomb load cases with 88% porosity but with different control parameters of BVL for the viscous case and VBC for the Coulomb case. Recalling the results for Cases V7 and V10 however, VBC and BVL control approaches also followed the same response curve. Combining these two observations, one can readily infer that viscous and Coulomb loaded engines exhibit the same basic efficiency characteristics.

As with the viscous load, Cases C15 and C16 combine to show that the Coulomb loaded engine also exhibits a superior part load efficiency when output control is accomplished by means of displacer windage control B2V.

It appears possible in retrospect that reasonably satisfactory operation may have been achievable for the viscous loaded (linear alternator) engine operating at 88% porosity if some minor engine parameter changes had been instituted. The combination of very limited and unsatisfactory function with the B2V load and the limited output regime shown in Figure 25 with the BVL load led to an early decision to adopt the higher porosity for the bulk of the viscous load studies. There was, however, no opportunity to explore this hypothesis.

The balance of the figures in this section illustrate more detailed looks at various cases, which typically show piston and displacer motions, frequencies of interest, power output and engine efficiency as functions of some output control parameter. Pertinent engine parameters are set off in a suitable format as part of each figure. The effects of parametric variations are given in tabular format later in the section. The natural frequencies referred to in Figures 26 through 29 and related tables, Tables 5 through 9, are the natural frequencies for undamped small amplitude free oscillations of the displacer and power piston.

Figure 26 provides a more detailed look at Case V11 which uses a viscous load to approximate the linear generator loading characteristic. Output control is by means of throttling flow through cooler tubes to increase displacer windage. For the parameters used, control is relatively smooth over a wide range of power output. Frequency is nearly constant over most of the range with power modulation reflected by strokes. As the nominal power output is approached from lower power levels, the sensitivity to throttle position increases dramatically accompanied by increased operating frequency and displacer stroke tending toward a collision. This represents an approach to fully resonant system operation with high power capability but lack of adequate control.

The response curves in Figure 27 (Case V10) represent the same basic operating parameters as existed for Figure 26, except that power output control is here achieved by varying displacer bounce chamber volume rather than displacer windage. This control mechanism was suggested as possibly the ideal alternative on page 3-14 of Reference 4, although, the discussion of power output control in Reference 4 was limited to qualitative speculation. The general response in Figure 27 is fairly similar to that in Figure 26, but several detail differences are apparent.

Most significant for a linear alternator load is that operating frequency varies over the full range, primarily because displacer natural frequency is dependent on displacer bounce chamber volume which is used as the control mechanism. The control sensitivity is somewhat less severe than for windage control, but displacer collision occurs at a lower power level. The curves are continued on well beyond both displacer and power train collision points, although these do not represent viable operating modes because of hardware limitations.

The third potential control mode for a viscous loaded engine is represented in Figure 28 (Case V7) where the control parameter is the viscous load damping coefficient. Other parameters are the same as in Figures 26 and 27. This type of control may be feasible in a stand-alone application, but not with a grid connected system. This control concept provides the smoothest response by far of the three control concepts evaluated for the viscous load. As shown in Figure 25, however, both this and the displacer bounce chamber volume control in Figure 27 result in less efficient operation than the displacer windage control used in Figure 26.

Coulomb load cases representing the hydraulic converter output were chronologically the first ones run. After debugging of program changes, it was determined that predicted engine efficiency ran somewhat below the Reference 4 values. To compensate for this, lower porosity values for the regenerator matrix were evaluated. A decision was made to use 88% porosity rather than the 92% value suggested in Reference 4 on the basis of general experience. This significantly increased

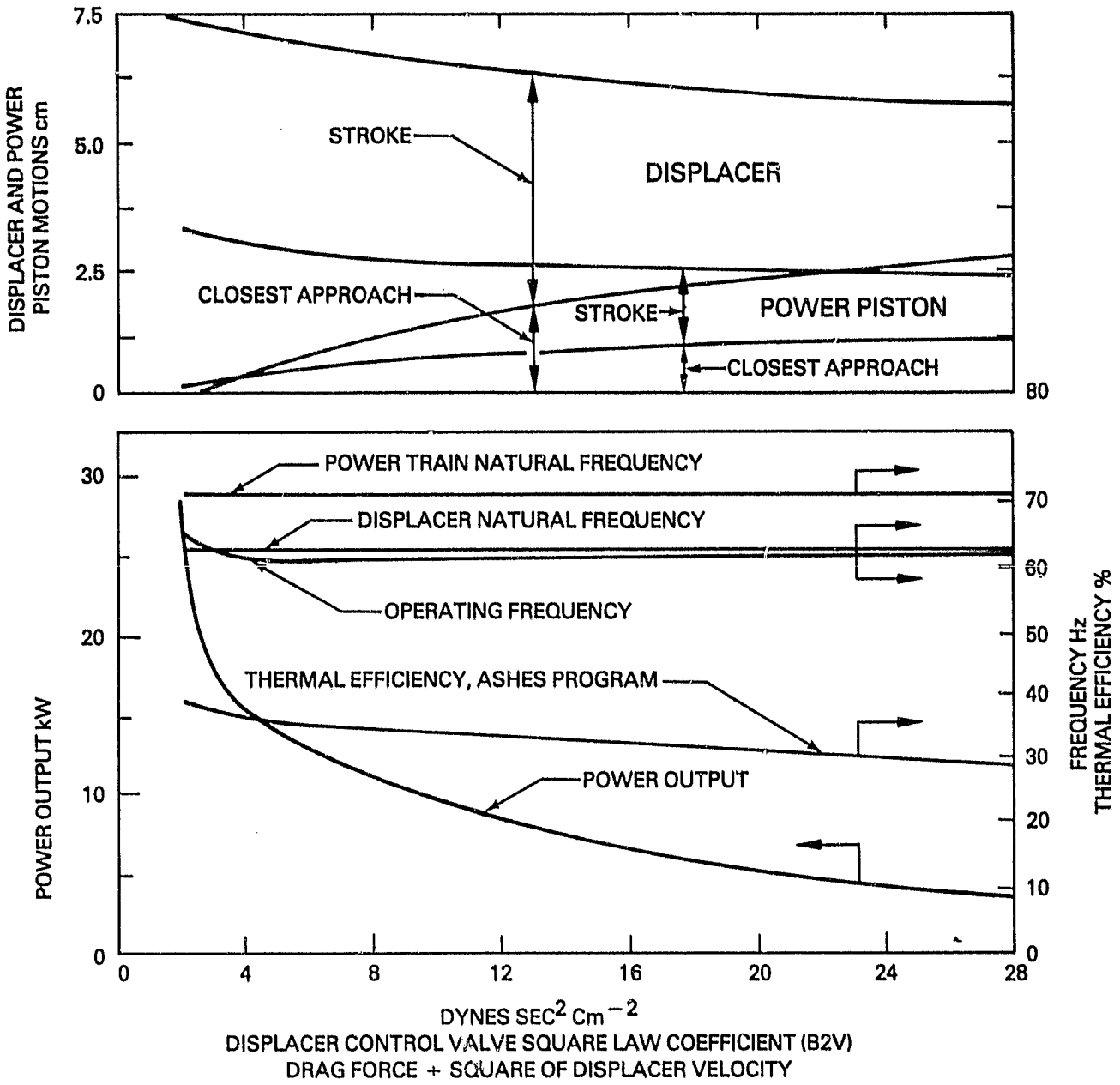

IMPORTANT PARAMETERS

Matrix Porosity	92%	
Viscous Load Damping Coefficient	1.4×10^6	Dyne Sec Cm^{-1}
Buffer Volume	16.0	liters
Power Piston Mass	10.0	kg
Displacer Bounce Chamber Volume	327	cc

CASES VIIS1, S2, S3, S4, S5

Figure 26. Response Curves, Viscous Load with Displacer Damping Control.

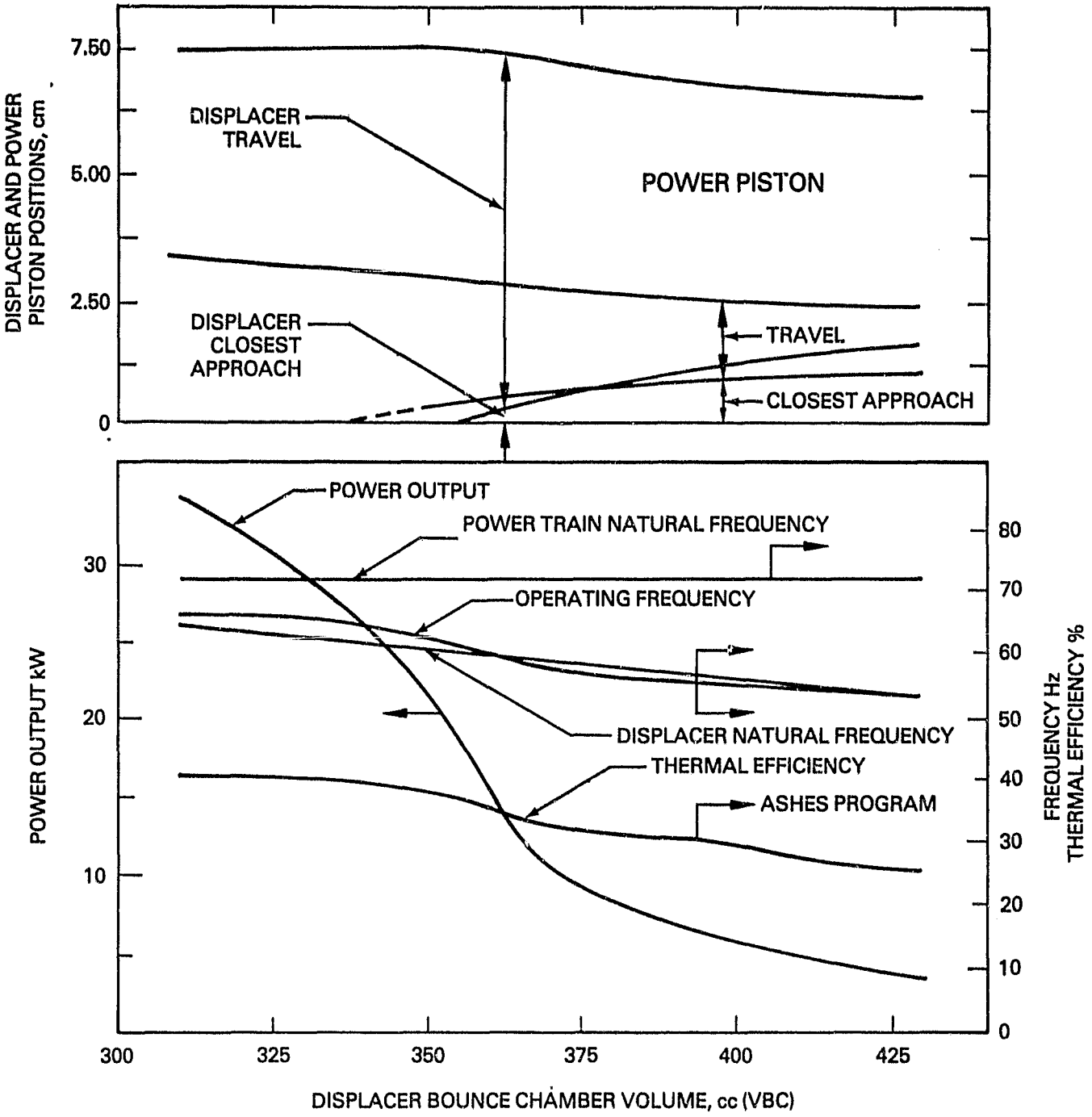

IMPORTANT PARAMETERS

Matrix Porosity	92%	
Viscous Load Damping Coefficient	1.4×10^6	Dyne Sec Cm^{-1}
Buffer Volume	16.0	liters
Power Piston Mass	10.0	kg

CASES V10AS1, S2, S3, S4, V10BS1, S2

Figure 27. Response Curve, Viscous Load, Bounce Chamber Volume Control.

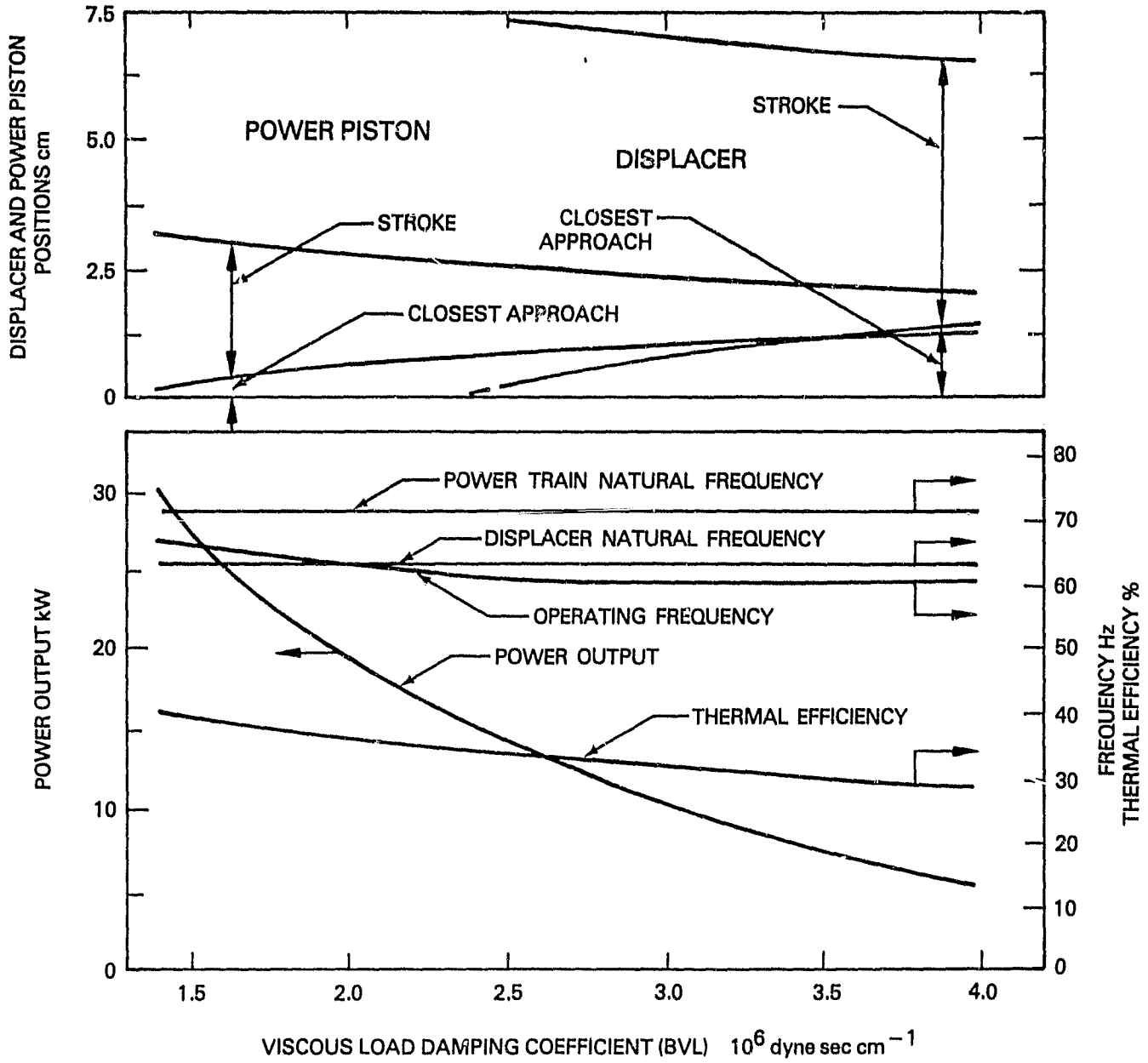

IMPORTANT PARAMETERS

Matrix Porosity	92%
Displacer Bounce Chamber Volume	327 cc
Power Piston Mass	10 kg
Buffer Volume	16 liters

CASES V2S1, V4S2, V7S1, S2, S?

Figure 28. Effect of Viscous Load Damping Coefficient.

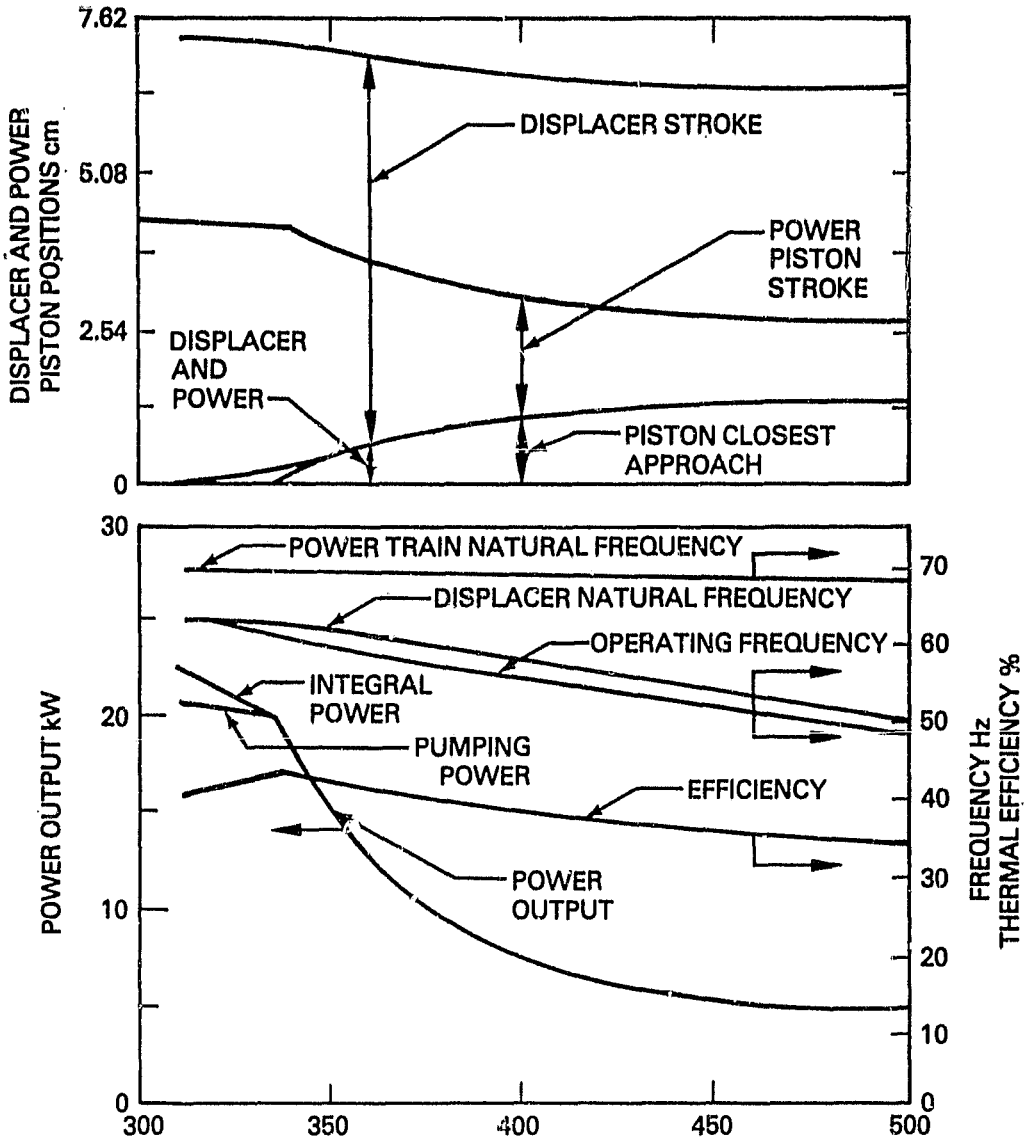

IMPORTANT PARAMETERS

Matrix Porosity	88%
Buffer Volume	16 liters
Power Piston Mass	10 kg
Displacer Mass	1.47 kg
Hot Metal Temperature	10.89 K

CASES C15-S1, C16

Figure 29. Response Curve for Stirling-Hydraulic Reference Design; Coulomb Load, Control by Bounce Chamber Volume Variation.

Table 5

SENSITIVITY ANALYSIS: EFFECT OF DISPLACER MASS ON HYDRAULIC SYSTEM PERFORMANCE

Displacer Mass (kg)	Power Output (kW) / Efficiency (%)	Operating Frequency (Hz)	Natural Frequencies (Hz)		Stroke / Closest Approach		End-of-Stroke Collisions	
			Displacer	Power Bellows	Displacer (cm)	Power Bellows (cm)		
1.62	9.8 / 39.2	57.0	58.9	68.7	5.97 / .89	2.31 / 1.02	None	+10% Displacer Mass
1.47	18.1 / 42.2	60.6	61.8	68.7	7.14 / .15	3.84 / .18	None	18.1 kW Reference Case
1.33	23.2 / 32.2	67.7	65.1	68.7	7.44 / 0	4.57 / 0	Displacer and Power Bellows	-10% Displacer Mass

Table 6

SENSITIVITY ANALYSIS: EFFECT OF POWER PISTON MASS ON HYDRAULIC SYSTEM PERFORMANCE

Displacer Mass (kg)	Power Output (kW) / Efficiency (%)	Operating Frequency (Hz)	Natural Frequencies (Hz)		Stroke / Closest Approach		End-of-Stroke Collisions	
			Displacer	Power Bellows	Displacer (cm)	Power Bellows (cm)		
11	22.8 / 31.6	64.8	61.8	65.5	7.47 / 0	5.0 / 0	Displacer and Power Bellows	+10% Power Piston Mass
10	18.1 / 42.2	60.6	61.8	68.7	7.14 / .15	4.0 / .18	None	18.1 kW Reference Case
9	8.8 / 38.6	59.7	61.8	72.4	5.46 / 1.19	1.8 / 1.19	None	-10% Power Piston Mass

Table 7

EFFECT OF BUFFER VOLUME ON HYDRAULIC SYSTEM PERFORMANCE; NATURAL FREQUENCIES HELD CONSTANT

Buffer Volume (liters)	Piston Power Mass (kg)	Power Output (kW)	Efficiency (%)	Stroke / Closest Approach		End-of-Stroke Collisions	
				Displacer (cm)	Power Bellows (cm)		
16.0	10.0	18.1	42.2	7.14 / .15	3.19 / .18	None	18.1 kW Reference Case
14.0	10.19	17.2	41.9	7.01 / .23	3.78 / .28	None	Reduced Buffer Volumes
12.0	10.44	15.9	41.6	6.80 / .36	3.53 / .41	None	
10.0	10.79	14.4	41.1	6.58 / .51	3.20 / .56	None	
8.0	11.33	12.5	40.4	6.22 / .74	2.77 / .76	None	

Displacer natural frequency = 61.8 Hz

Power train natural frequency = 68.7 Hz

Operating frequency = 60.1 to 60.5 Hz

Deviations from Reference Design:

Buffer volume, parameter of interest.

Slight variation of power piston mass to maintain Reference Power Train natural frequency.

Table 8

SENSITIVITY ANALYSIS: EFFECT OF HOT METAL TEMPERATURE ON HYDRAULIC SYSTEM PERFORMANCE

Hot Metal Temperature (K)	Power Output (kW) / Efficiency (%)	Operating Frequency (Hz)	Natural Frequencies (Hz)		Stroke / Closest Approach		End-of Stroke Collisions	
			Displacer	Power Bellows	Displacer (cm)	Power Bellows (cm)		
773			61.8	66.3				Dropout / Will not run
873	13.8 / 37.1	60.4	61.8	67.2	6.40 / .64	3.07 / .64	None	
973	16.7 / 39.9	60.4	61.8	67.9	6.88 / .33	3.68 / .33	None	
1089	18.1 / 42.2	60.6	61.8	68.7	7.14 / .15	3.99 / .18	None	Reference Case
1173	18.7 / 43.5	60.6	61.8	69.2	7.14 / .05	4.14 / .10	None	

Table 9

EFFECT OF LOAD PRESSURE ON HYDRAULIC SYSTEM PERFORMANCE

High Pressure Accumulator Pressure-- MPa (psia)	Power Output (kW)	Efficiency (%)	Operating Frequency (Hz)	Natural Frequencies (Hz)		Stroke / Closest Approach		End-of Stroke Collisions
				Displacer	Power Bellows	Displacer (cm)	Power Bellows (cm)	
34.5 (5000)	11.81	43.6	61.6	63.4	69.2	5.21 / 1.35	2.57 / .91	None
31.0 (4500)	11.82	43.7	62.0	63.4	69.2	5.16 / 1.37	2.84 / .79	None
27.6 (4000)	11.37	43.6	62.4	63.4	69.2	5.05 / 1.42	3.07 / .71	None
24.1 (3500)	10.79	43.6	62.8	63.4	69.2	4.90 / 1.52	3.30 / .86	None
20.7 (3000)	10.45	43.7	63.4	63.4	69.2	4.78 / 1.57	3.71 / .43	None
17.2 (2500)	11.04	44.6	64.6	63.4	69.2	4.78 / 1.57	4.67 / 0	Power Bellows

Power piston mass = 10.79 kg
Buffer volume = 10.0 liters
Bounce chamber volume = 321 cc

efficiency, as shown earlier in Figure 25, but probably also contributed to the stability and stall problems which were experienced. After marginally acceptable Coulomb cases were run, similar viscous runs were attempted. Acceptable stability results were not in general obtained using this porosity for the viscous load. Consequently, most viscous cases were run at 92% porosity where efficiency was sacrificed in exchange for much better stability and stall conditions. No time was available to rerun the Coulomb cases at 92% porosity and the computer budget was already greatly exceeded, so Coulomb cases are given only for 88% porosity. In view of the fact that big gains in stability were achieved by going from 88% to 92% porosity for the viscous cases, it is likely the same would hold true for the Coulomb cases. With engine changes suggested in Section 3.3.3, it is also likely that even greater stability than this can be achieved for the Coulomb system without sacrificing efficiency.

The overall results for the Coulomb cases representing the Stirling-Hydraulic Reference Design are shown in Figure 29 (Case C16) where output control is achieved by varying displacer bounce chamber volume. Parameters for the 18.1-kW Reference Case which represent one operating point of Figure 29 are presented without elaboration in the ASHES program listing of Figures 19A, 19B, and 19C presented earlier. Other than the higher efficiency resulting from lower porosity, the primary difference between this and the viscous load case is in the shape of the power piston stroke curve. This results in power piston collision occurring before displacer collision. This in turn causes a step change in the power output curve after collision. There is also a distinction between integral power (indicated engine output applied to the power bellows) and pumping power (ideal output of pumped hydraulic fluid) when the power piston collides. This is of course a destructively undesirable operating mode which would be avoided in actual practice. For the nominal design case in Figure 29, this only occurs above 20 kW output which provides a reasonable operating margin.

A parametric sensitivity analysis was conducted with the dynamic simulation to evaluate the impact of various parameter changes on performance of the nominal hydraulic output engine. These studies typically involved only a few discrete points which sometimes exhibit collisions or other discontinuities. The pertinent data are therefore presented in tabular rather than graphical format.

The first parameter change, shown in Table 5, evaluated the impact of changing displacer mass by +10% and -10% relative to the reference design. This had a major impact on system operation, as was anticipated for a parameter so closely tied in to the free-piston dynamics. The 10% increase in mass detuned the system enough by dropping displacer resonant frequency that power output dropped by nearly 50%. A 10% reduction in mass moved the system closer to full resonance so that higher power output was obtained, but both the displacer and power bellows were colliding with end stops. This latter condition would probably not occur with an engine designed to operate in a fully resonant mode to attain maximum power density. The study does, however, point out one of the design sensitivities which is the price a free-piston engine pays in exchange for eliminating many of the problems associated with a kinematic engine.

Very similar results were obtained when the power piston mass was varied by +10% and -10% from the nominal value. The results are summarized in Table 6. Essentially all the comments made with respect to Table 5 also apply here. It

should be observed that the piston mass changes had similar effects to displacer mass changes, but the changes occurred in opposite directions. The same result was obtained in either case by bringing the natural resonant frequencies of displacer and power train closer together or spreading them apart. Since power train natural frequency was higher than displacer natural frequency, opposite mass changes moved these frequencies closer together and therefore closer to full resonance. Again, in a fully resonant system any change would be away from resonance and therefore decrease power output.

Table 7 summarizes the results obtained when smaller buffer gas volumes were evaluated. The nonlinear gas springs represented by the engine and the buffer are the primary spring forces acting on the power piston. Therefore a change in the buffer gas volume affects the natural resonant frequency of the power train. In order to maintain comparable dynamic cases for evaluation, the power piston mass was thus varied with the buffer volume to maintain constant power train natural frequency. For the reduced volume cases evaluated, power output decreased substantially in response to decreased power bellows stroke while efficiency decreased moderately.

The stroke reductions occur because the "passive" or stroke restricting spring force produced by the buffer become relatively larger in comparison with the "active" or stroke producing spring represented by the engine. The effect would be less pronounced with an engine having lower dead volume since the equivalent stiffness of the engine spring would be larger. A smaller bounce chamber would also be capable of producing near limiting efficiency with an engine having a higher charge pressure and Beale number as described in Section 3.3.3. The reason for this is that stroke volume of the power piston would be greatly reduced.

The predicted impact of varying the heater temperature from 773 K (500°C) to 1173 K (900°C) is summarized in Table 8. At the lowest temperature, the simulation showed that the system was not capable of self-sustained operation. The power output is a relatively strong function of heater temperature, especially in the lower ranges of temperature. Efficiency is a somewhat weaker function of temperature, but it does increase monotonically with temperature over the range considered. Some change in power train natural frequency occurs with temperature, but operating frequency, which closely follows the fixed displacer frequency, changes very little.

The final presentation of data from the parametric survey is given in Table 9. This table shows the effect of reducing the high accumulator pressure and therefore the pressure delivery to the hydraulic motor. This is a very significant table since it illustrates the potential for using output pressure as part of the system power control capability. The system functions very well over a range of delivery pressure from the nominal level of 34.5 MPa (5000 psi) down to 17.2 MPa (2500 psi).

The power level at the nominal output pressure of 34.5 MPa (5000 psi) is reduced from that for the standard reference case because this series was conducted using a 10.0 liter buffer volume and a displacer bounce chamber volume of 312 cm^3 rather than the nominal 327 cm^3. This was initially done as an inadvertent data carry-over from the 327-cm^3 test series, but subsequent evaluation shows that more useful information was provided by this approach than would have been the case if varying only outlet pressure from the full reference case. This results from the fact as seen in Table 9 that if only outlet pressure is reduced, power bellows stroke

increases. In fact, beginning for the cases in Table 9, the lowest output pressure of 17.2 MPa (2500 psi) resulted in a slight power train collision at end of stroke. This would have occurred at a much higher output pressure if starting from the 18.1-kW reference case. Table 9 demonstrates that starting the pressure reduction from an 11.8-kW operating point allows a factor of two pressure reduction at nearly constant power output without collisions. A combination of output pressure variation with variation of bounce chamber volume to maintain constant flow rate provides a wide power output range using low-cost fixed-displacement hydraulic motors.

3.4 System Production Cost Analysis

One of the major tasks in this contract was to develop production cost estimates for three Stirling electric power generation systems at production rates of 25,000 units per year. This work was done as part of the Flow Industries subcontract. The three systems evaluated were:

1. The final version of the Stirling engine/samarium cobalt linear alternator system described in Reference 4.

2. The same engine design with a linear alternator using magnets without expensive and strategically scarce cobalt.

3. The same engine design driving an integral hydraulic pump as described in Section 3.1.3 connected to a remotely mounted hydraulic motor and electrical alternator as described in Section 3.0 above.

These three system costs were significantly higher than the estimate given in Reference 4. There are various reasons for the differences. First, prime costs (direct material and labor) as reported in Reference 4 cannot be used for direct comparison with manufactured and purchased components since such costing does not take into consideration overhead such as the costs of use of equipment and facilities during manufacture. This necessitates a different costing basis, as outlined in Section 3.4.1 below, when commercial items such as hydraulic motor and rotary alternator are included in the system. Another significant reason for cost differences is that the studies were separated by approximately three years of very high inflation rates.

The approach used to develop production cost figures is described next. Following that, the results of the cost studies are summarized in a tabular format. The hydraulic converter costing is more inclusive and more accurate than the Stirling engine and linear alternator costs because much more detailed information was available. The costing study still does an adequate job of producing reasonable comparative costs, which was the primary objective of this effort.

3.4.1 Basis for Cost Analysis

Many approaches to determine cost of goods can reasonably be used. Further, various stages in the manufacturing and marketing costs can be used as a cost basis. The most important criterion in selecting a cost basis for this program was to obtain consistency with comparative costs of various systems. The approach used here was selected as the best compromise to satisfy conflicting objectives.

The manufacturing cost estimates in Reference 4 were based on prime costs only, that is, direct material and labor costs. The approach used here was to include cost of shop overhead, which is an important element in the manufacturing cost of any article. If this cost is ignored, parts requiring expensive machinery to produce will be given an unfair cost advantage. For example, parts requiring complicated contouring on numerical control machinery would have a very low prime cost, but the value of the machine time may be many times the value of the operator's labor. Also, quotations from vendors will include these costs.

A second problem in the comparison arises when purchased components such as alternators and hydraulic motors are compared against manufactured parts. The price quoted by the manufacturer of such items includes many cost elements beyond the manufacturing cost as illustrated in Figure 30 which is taken from Reference 16. Two strategies are available to overcome this problem:

1. Back-calculate the manufacturing cost from the quoted price on purchased manufactured goods.

2. Calculate selling price for the entire system.

Of these two possibilities the first will perhaps yield the most consistent results. This is because pricing formulas and strategies used for pricing mixtures of manufactured and purchased parts are not as uniform and standard as methods for pricing items containing only manufactured parts. The hydraulic motor and alternator manufacturers are most likely to follow a common pricing formula as illustrated in Figure 30. For this reason the manufacturing costs for the hydraulic motor and alternator were back calculated from the price quoted by the vendors using a factor of 0.5 or 0.6 to relate quoted price to manufacturing costs. The factor of 0.5, as illustrated in Figure 30, was used when only low volume price quotes could be obtained. When high volume costs were quoted, the factor of 0.6 was used since it is expected that the vendor would offer a substantial discount on volumes of 25,000 per year.

The strategy which was followed then was to estimate both time costs as in Reference 4 and overhead costs for the three engines and to present the results in a tabular form which also allows comparisons with the prime costs alone as presented in Reference 4.

The starting points for the cost estimates were the conceptual drawings of the systems together with all design calculations which were available. The drawings and specifications for the hydraulic converter were considerably more detailed than those for the Stirling engine and linear alternator, so the former has a higher confidence level for the accuracy of the cost figures. The general approach used for costing used the steps outlined below.

1. For each system, rank the details by complexity and select approximately the top one-fifth for detailed cost study. A general rule for manufactured goods is that 80 percent of the costs lie in 20 percent of the parts. The remaining 80 percent of the parts, comprising an estimated 20 percent of the costs, were estimated approximately as described in items 7 and 8 below.

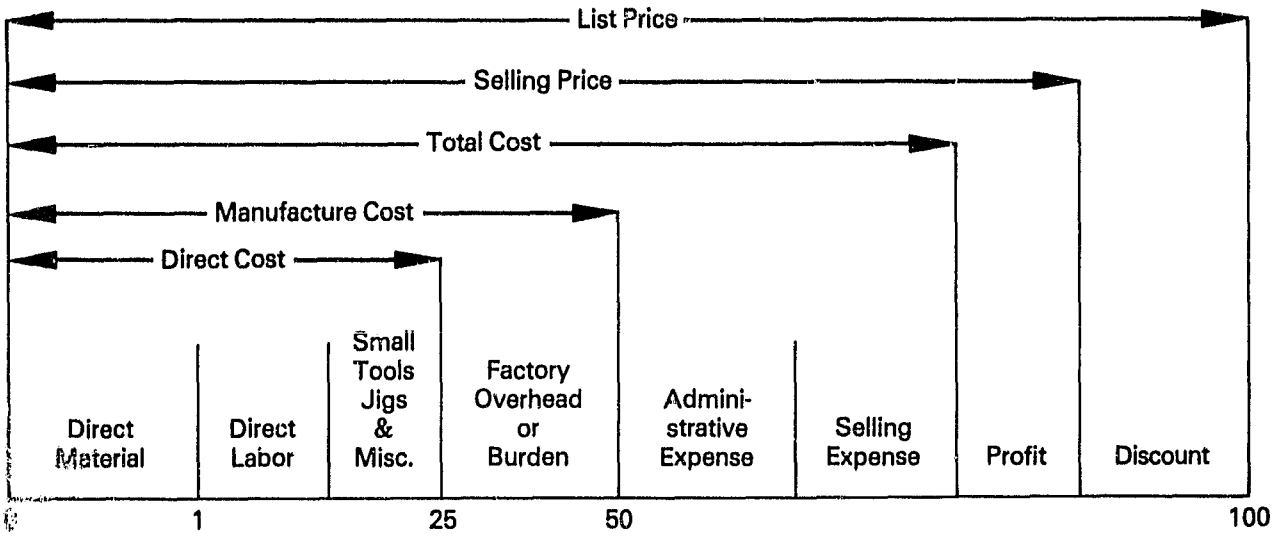

Figure 30. Breakdown of Cost Elements for Typical Manufactured Goods (from Reference 16).

2. Detail drawings which represent the complexity of parts and include critical dimensions and tolerances were prepared for each of the selected parts.

3. Drawings for castings, forgings, flame spraying and other nonmachine processes were sent to the appropriate vendors for bids.

4. Machinery, facility, and labor requirements for each machine part were estimated.

5. Costs for each part including labor, materials, and shop overhead were estimated.

6. The total costs and weight for the selected parts were estimated.

7. The costs of the remaining machine parts were estimated on the basis of weight for several categories with the same cost per unit weight figures as calculated for selected parts in each category.

8. Standard parts such as nuts and bolts were costed according to current commercial prices.

9. The total costs for each assembly were estimated by adding the parts cost and assembly costs.

3.4.2 Results of Cost Analysis

The size and detail of the Stirling engine/linear alternator conceptual layout drawing available for this costing study is shown in Figure 31. This is a copy of Figure 1-1 from Reference 4. Many specifications for materials, key dimensions, special processes and critical tolerances were also provided in Reference 4. Based on this information, crude but representative component detail drawings were produced under this contract to illustrate the critical parameters needed by cost estimators. Several such sketches were made for the engine components. Similar drawings produced for the linear alternator portion included the following.

1. Stator Support Sleeve/Stator Laminations/Stator Windings

2. Alternator Plunger/Permanent Magnet Assembly

3. Alternator Gas Bearing/Cylinder Assembly

4. Alternator Housing and Pressure Shell

Based on detailed costing of these components, estimates were extrapolated to other system components which fell into similar categories of material and complexity.

The results of the Stirling Engine costs are summarized in Table 10. As with other tabular summaries in this section, the costs for major components are broken down according to raw matrerial cost, direct labor cost for machining or other fabrication processes, shop overhead, and the total manufacturing

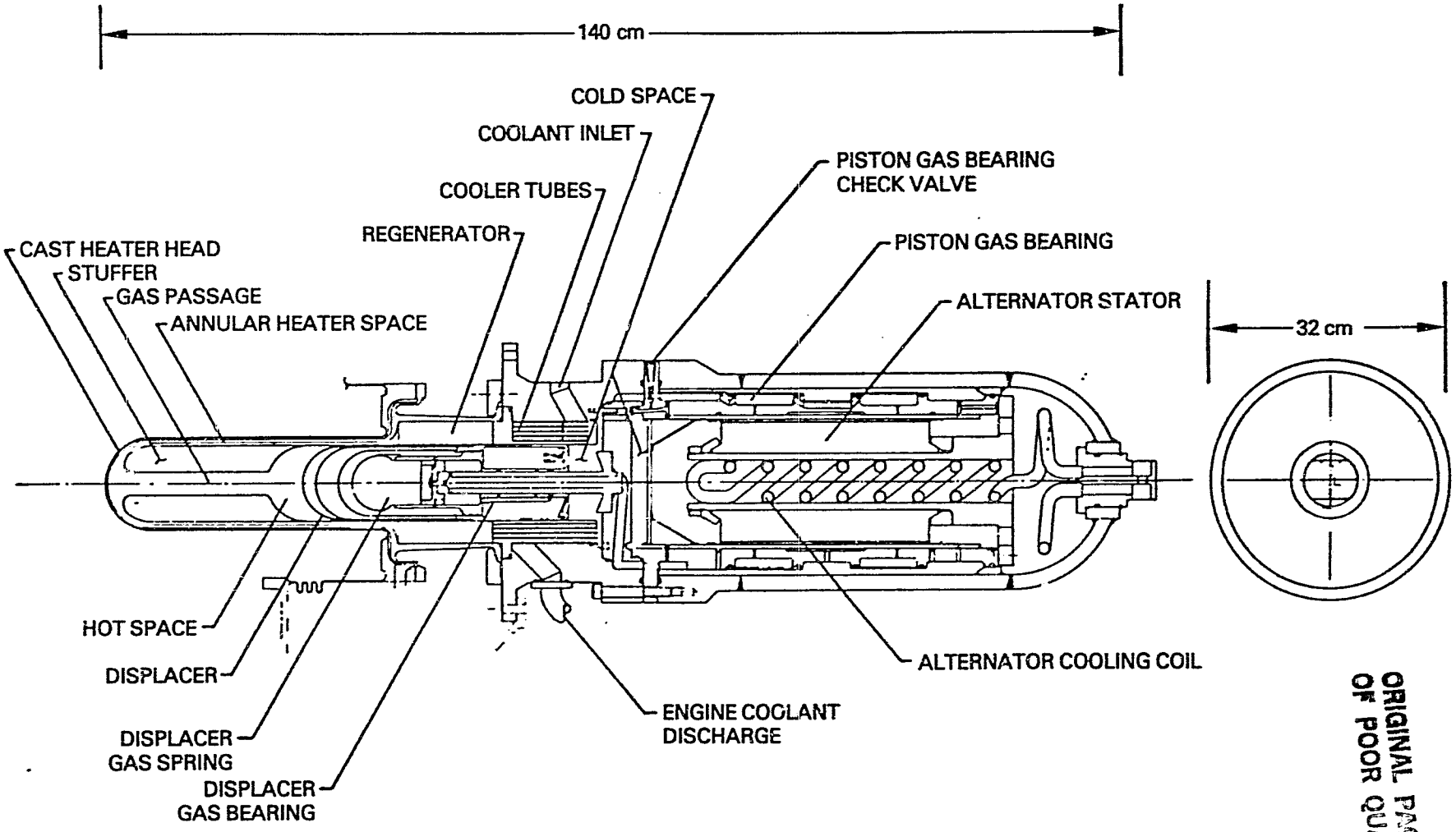

Figure 31. 15 kW Free-Piston Stirling Engine - Alternator Conceptual Design (Taken from Ref. 4, p. 1-6).

Table 10

STIRLING ENGINE COMPONENT COSTS IN DOLLARS

Component	Material Cost	Labor Cost	Overhead Cost	Total Mfg. Cost
Heater Head	145	194	291	630
Stuffer	293	20	30	343
Cooler	145	130	195	470
Cooler Housing	60	60	90	210
Displacer Front	40	118	177	335
Displacer Back	23	67	101	191
Displacer & Gas Bearing	52	152	229	433
Check Valve	1	2	3	6
Piston Rod	22	65	98	185
Displacer Guide	8	25	37	70
Support Flange	33	60	90	183
Regenerator	58	--	--	58
Misc. Bolts, Pipe Couplings	250	--	--	250
TOTALS	1130	893	1341	3364

cost which is the sum of the other three items. Also, as done with other tables in this section, items such as nuts and bolts which are purchased in a fabricated form are listed at purchase cost under materials. This approach does include cost elements beyond manufacturing costs otherwise provided, as shown in Figure 30, but any manufacturer would purchase such items to use directly in fabrication as would be done with materials.

The cost breakdown for the linear alternator is given in Table 11. One unusual item in this table is the high overhead cost for the housing. This results from the use of special equipment with a high net operating cost. The figures given for low cost magnets are representative of high quality permanent magnets other than cobalt-rare earth types. While the samarium cobalt magnet cost is roughly comparable to the magnet cost in Reference 4, greatly increased costs in other areas for reasons described in Section 3.4.1 make this cost a much smaller fraction of the total system cost. The low cost magnets therefore have much less impact on system cost than was the case in Reference 4.

The exercise of costing the linear alternator with low cost permanent magnets where the only change is substitution of the magnetic material has very little practical significance. A promising new technology magnet material using manganese, aluminum, and carbon was identified in Reference 4. The most definitive evaluation of this material to date was recently published in Reference 17. The material will not be available in production quantities for some time, if ever. Shapes are very limited and costs will probably never be as low as the raw materials would suggest, because expensive and difficult production procedures are required. The major technical objection to this material, in common with all other permanent magnet materials except cobalt-rare earth magnets, is the relatively low coercive force. This factor precludes their use in the configuration of the Reference 4 linear alternator design, which requires a magnet that is thin in the direction of magnetization.

Use of any alternative magnetic material would require a complete redesign of the alternator to maintain reasonable performance and plunger weight. The resulting design would probably cost significantly more except for the permanent magnets and would almost certainly exhibit lower performance. Similar comments are most likely applicable to an electromagnetic version.

Much finer detail was available for costing the hydraulic converter than for either the Stirling engine or linear alternator. Reported costs are therefore more inclusive and have a higher confidence level. The converter is shown here as Figure 32 which is repeated from Figure 14 for reference purposes. The balloon identifiers break the converter down into 60 components (61 balloons are shown, but item 9 is part of the engine).

Each of the sixty converter components are identified by number and name in Table 12. Also included in Table 12 are the material descriptions, special comments were appropriate, the number required per assembly if more than one, and the total weight of most components per assembly in kg. Individual weights are not given for nuts, bolts, and screws, but only for the total of 4.11 kg. Similarly, all seals, bellows capsules and socket liners are lumped as a total of 0.91 kg. The grand total for hydraulic converter weight is 114 kg (252 lb). Without the counterbalance feature, the total converter weight is estimated at 72 kg (159 lb).

Table 11

LINEAR ALTERNATOR COMPONENT COSTS IN DOLLARS

Component	Material Cost	Labor Cost	Overhead Cost	Total Mfg. Cost
Stator	180	400	600	1180
Housing	310	55	345*	710
Magnets: SaCo (Low Cost)	1050 (200)	--	--	1050 (200)
Plunger	75	158	237	470
Cooling coil	4	8	13	25
Gas bearing cylinder	196	414	621	1231
Gas bearing cover sleeve	26	5	7	38
Misc. bolts, etc.; water couplings for cooling coil	120			120
TOTALS	1961 (1111)	1040	1823	4824 (3974)

*Overhead rate is $75.00/hr.

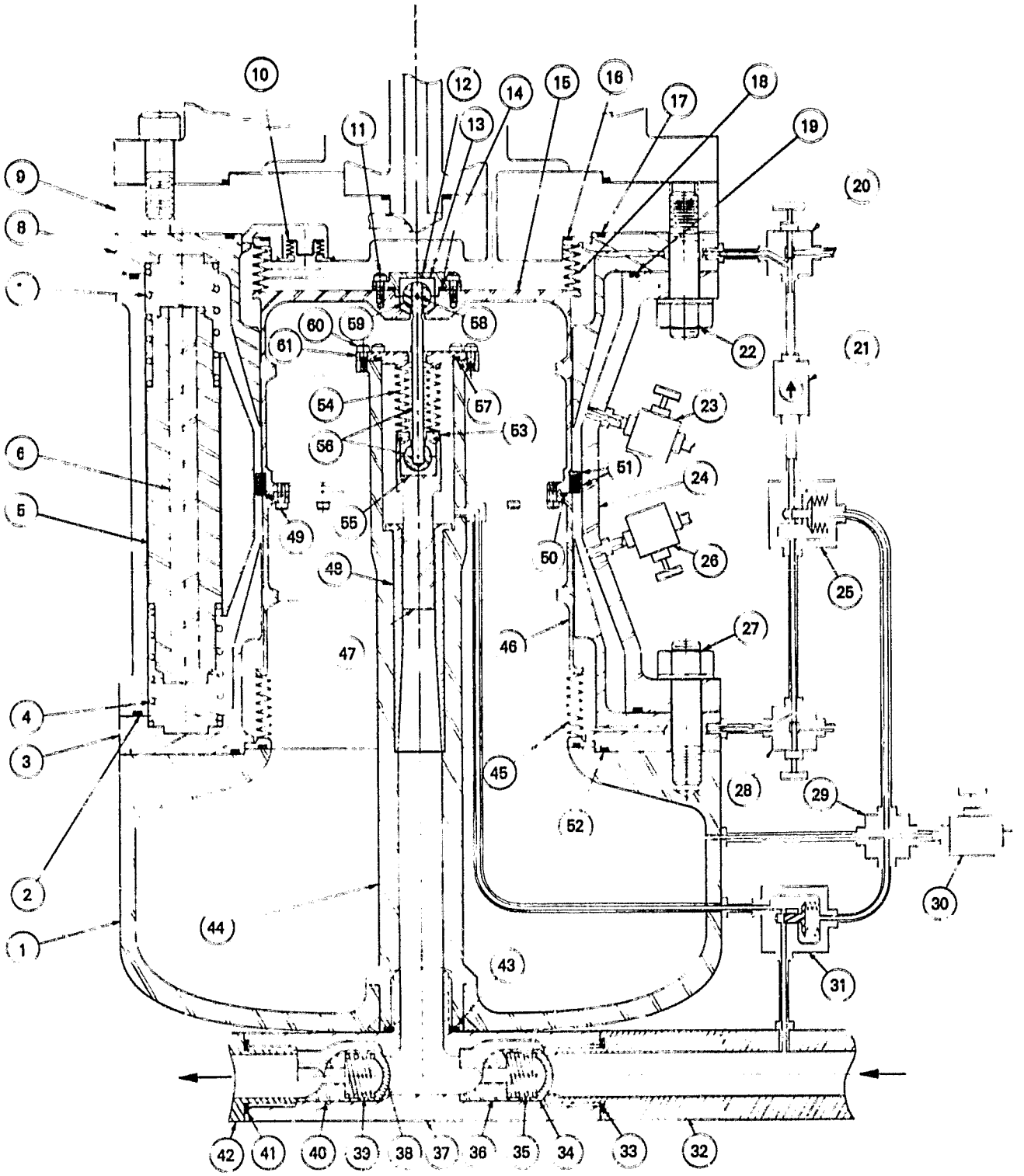

Figure 32. Hydraulic Converter Layout with Component Identifiers.

Table 12

15 kW HYDRAULIC CONVERTER PARTS LIST

Item No.	Component	Material	Notes	Number Required	Total Weight (kg)
1	Buffer Housing	Cast Steel			24.7
2	O-Ring	Nitrile			---*
3	Lower Piston Cylinder	Cast Steel			14.0
4	Counterbalance Spring	Music Wire		2	0.11
5	Counterbalance Piston	Steel	Chrome Plated on OD	2	3.96
6	Lead Piston Slug	Lead		2	0.97
7	Counterbalance Spring	Music Wire		2	0.11
8	Upper Piston Cylinder	Cast Steel			14.0
9†	Engine Part				---
10	Compensator Bellows	St. Steel	347 St. Steel		---
11	Screw, Socket Head	Steel	4140 HT 180 KS1 UTS	6	---*
12	Socket Cover	Steel	4130		0.044
13a/b	Socket Liner	Nomex Comp.	Dixon/Teflon/Epoxy (2 parts)		---
14	O-Ring	Nitrile			---
15	Power Piston Head	St. Steel	15-5 PH		2.72
16	O-Ring	Nitrile			---
17	O-Ring	Nitrile			---
18	Power Bellows	St. Steel	AM-350, Nesting Ripple Welded		---
19	O-Ring	Nitrile			---
20	Manual Valve	St. Steel	Shut-off, 2000 PSI, Oil		0.127
21	Check Valve	St. Steel	Ball type, 2000 PSI, Oil		0.089
22	Screw, Soc. HD	Steel	4140 HT, 5/8", 180 KSI UTS	14	---
23	Manual Valve	St. Steel	Shut-off, 2000 PSI, Oil		0.127
24	Central Housing	Cast Steel	Chrome Plated Bores		34.1
25	Make-up Valve	St. Steel	Special, Bellows Operated		0.302
26	Manual Valve	St. Steel	Shut-Off, 2000 PSI, Oil		0.127
27	Screw, Socket Head	Steel	4140 HT, 5/8", 180 KSI UTS	14	---
28	Manual Valve	St. Steel	shut-Off, 2000 PSI, Oil		0.127
29	Cross Fitting	St. Steel	2000 PSI, Oil		0.127
30	Manual Valve	St. Steel	Shut-Off, 2000 PSI, Oil		0.127
31	Make-Up Valve	St. Steel	Special, Bellows Operated		0.302
32	Inlet Pipe	Steel	4130		1.95
33	O-Ring	Nitrile			---
34	Valve Disc	St. Steel	440 C. Chrome Plated		0.015
35	Valve Spring	Steel	Music Wire		---
36	Valve Insert	Steel	1020		0.059
37	Tee	St. Steel	15-5PH		2.39
38	Valve Disc	St. Steel	440C, Chrome Plated		0.015
39	Valve Spring	Steel	Music Wire		---
40	Valve Insert	Steel	1070		0.059
41	O-Ring	Nitrile			---

*Seals, bellows, etc., counted total weight at end of table.
**Screws, nuts, bolts counted total weight at end of table.
†Item 9 is part of the engine, therefore not counted toward weight or expense of the converter.

Table 12 (continued)

15 kW HYDRAULIC CONVERTER PARTS LIST

Item No.	Component	Material	Notes	Number Required	Total Weight (kg)
42	Outlet Pipe	Steel	4130		1.95
43	O-Ring	Nitrile			---
44	Intensifier Cylinder	Cast Steel			4.10
45	Buffer Bellows	St. Steel	AM-350, Nesting Ripple Weld		---
46	Power Piston Skirt	St. Steel	15-5PH		1.50
47	Intensifier Piston	St. Steel	15-5PH, Chrome Plated		0.210
48	Intensifier Piston Sleeve	St. Steel	15-5PH, Chrome Plated		0.254
49	Screw, Socket Head	Steel	4140, 180KSI UTS	8	---
50	O-Ring	Nitrile			---
51a/b	Piston Seal Rings	St. Steel	15-5PH, Chrome Plated	2/3	0.380
52	O-Ring	Nitrile			---
53	Intensifier Piston Cap	St. Steel	347		0.063
54	Push Rod Bellows	St. Steel	347, Welded Bellows		---
55a/b	Socket Liner	Nomex Comp.	Dixon Teflon/Epoxy (2 parts)		---
56	Push Rod/ball	Steel	4140, Chrome Plated, 180KSI UTS		0.070
57	O-Ring	Nitrile			---
58	Retainer Pin	Steel	Commercial Dowel Pin		---
59	Push Rod Ball	Steel	440 C, Chrome Plated		0.050
60	Screw, Socket Head	Steel	41140, 180KSI UTS		---
61	Drive Seal Cover	St. Steel	347		0.136
	Nuts, bolts and screws				4.11
	Seals, bellows etc.				0.91
	Grand Total				114.3

A detailed cost breakdown of hydraulic converter components is given in Table 13, where the item numbers correspond with those in Figure 32 and Table 12. The total cost is $1995 for the counterbalanced version. Total cost for the non-counterbalanced version is estimated at $1261. This figure was arrived at by eliminating those components which are only required to effect the counterbalancing and estimating that the reduced size and complexity of a reconfigured central housing, item 24, would reduce material cost by 20% and labor cost by 50%.

The commercially purchased support items needed to convert the pumped hydraulic output into 3-phase electrical power and effect system cooling are identified in Table 14. These items were selected primarily for providing reliable high quality performance rather than minimum price. For the hydraulic motor and induction generator, high efficiency was a primary selection criterion.

In some cases, manufacturers were reluctant to estimate quantity prices without firm delivery dates being specified. In that situation, the costs given are 50% of the list price for single units. In other cases, costs are 60% of the discounted price as originally planned. The high pressure accumulator represents a disproportionately high cost relative to other items, considering its simplicity. The reason for this is apparently the lack of a large market for these items. Production rates are thus too low to have generated low cost high volume production methods. With firm orders of 25,000 units per year, it is likely that new production techniques and retooling would be justified so costs could drop substantially. The fan radiator is also expensive, but this just reflects the fact that it is a high quality unit. It should also be noted that a motor driven fan is included.

The final cost summaries for eight system options are given in Table 15. The "electric power system" includes the hydraulic converter (Table 13) all necessary auxiliaries (Table 14) for the Stirling hydraulic system. For the linear alternator, it includes the basic alternator (Table 11) and an auxiliary pump and fan radiator. The radiator costs used were the same ones given in Table 14 for the hydraulic system. The corresponding costs for an auxiliary electric motor driven pump to produce Stirling engine coolant flow was estimated at $200 for a single 15 kW system and $450 for a larger central pump used to cool four systems. No external unit corresponding to the coolant pump is required for the hydraulic system since the pumped hydraulic fluid is also used as the coolant.

Both single unit 15 kW and four gauged units for 60 kW net are considered. The hydraulic system benefits more from the multiple units because of the economics of scale for the items in Table 14. The only economics of a 4-unit system for the linear alternator system result from the auxiliary pump and radiator cooling system.

The non-counterbalanced hydraulic system boasts the lowest net cost by a substantial margin. This is the version that should be compared with the linear alternator system since that is inherently unbalanced. The counterbalanced hydraulic system should simply be viewed as offering an extra cost option of eliminating vibration in the main power train.

It should also be reiterated that the low cost magnet option is not really viable in the existing configuration. As described earlier in this section, a complete linear alternator redesign would be required to actually utilize low cost magnets.

C - 2

There is a potential for further significant cost reductions for the hydraulic converter if it is used with a more typical Stirling engine as described in Section 3.3.3. The resulting decrease in stroke volume by nearly an order of magnitude would reduce the buffer volume requirements by a similar amount making a much smaller and ligher (and therefore lower cost) system practical. Power piston diameter would also very likely be reduced, contributing to a smaller package. Configurational changes in the Stirling engine to incorporate an advanced concept heater head, and elimination of the displacer gas bearing by utilizing flexural support with no rubbing surfaces in the gas region, also have the potential for effecting major cost savings in the Stirling engine.

Table 13

15 kW HYDRAULIC CONVERTER COST BREAKDOWN

Item No.	Material	Labor	Overhead		Total Mfg.
1	65	65	98		228
2	2.00	-	-		2.00
3	56	56	84		196
4	10.00	-	-	(2)	20
5	9.00 ea	11.00 ea	16.50 ea	(2)	73
6	(Included with Item 5 above)				
7	10.00	-	-	(2)	20
8	56	56	84		196
9†					
10	17.50	-	-		17.50
11	1.20	-	-	(6)	7.20
12	0.50	1.00	1.50		3.00
13	0.20	0.50	0.80		1.50
14	2.00	-	-		2.00
15	36	36	54		126
16	2.00	-	-		2.00
17	2.00	-	-		2.00
18	110	-	-		110
	2.00	-	-		2.00
20	1.40	3.60	5.40		10.40
21	1.00	3.00	4.50		8.50
22	2.89	-	-	(14)	39.20
23	1.40	3.60	5.40		10.40
24	90	90	135		315
25	21.00	8.50	12.80		42.30
26	1.40	3.60	54.0		10.40
27	2.80	-	-	(14)	39.20
28	1.40	3.60	5.4		10.40
29	1.40	3.60	5.4		10.40
30	1.40	3.60	5.4		10.40

†Item 9 is part of the engine, therefore not counted toward weight or expense of the converter.

Table 13 (continued)

15 kW HYDRAULIC CONVERTER COST BREAKDOWN

Item No.	Material	Labor	Overhead	Total Mfg.
31	21.00	8.50	12.80	42.30
32	6.50	8.00	12.00	26.50
33	2.00	-	-	2.00
34	0.50	2.00	3.00	5.50
35	10.00	-	-	10
36	1.00	2.00	3.00	6.00
37	6.00	6.00	9.00	21.00
38	0.50	2.00	3.00	5.50
39	10.00	-	-	10.00
40	1.00	2.00	3.00	6.00
41	2.00	-	-	2.00
42	6.50	8.00	12.00	26.50
43	2.00	-	-	2.00
44	11	11	16.50	38.50
45	110	-	-	110
46	20	20	30	70
47	1.00	1.00	1.50	3.50
48	1.00	1.20	1.80	4.00
49	1.60	-	-	(8) 12.80
50	2.00	-	-	2.00
51	30.00	-	-	30.00
52	2.00	-	-	2.00
53	1.00	1.50	2.30	4.80
54	17.50	-	-	17.50
55	0.20	0.50	0.80	1.50
56	0.30	0.60	0.90	1.80
57	2.00	-	-	2.00
58	0.10	-	-	0.10
59	0.50	1.00	1.50	3.00
60	0.20	-	-	(10) 2.00
61	1.50	3.10	4.70	9.30
Total for Counterbalanced Converter				$1,994.90
Total Cost without Counterbalance Feature				$1,261.00

Table 14

HYDRAULIC SYSTEM PURCHASED COMPONENTS

Component	15 kW System Model	15 kW System Cost	60 kW System Model	60 kW System Cost
Hydraulic Motor	Volvo F11-10	323	Volvo F11-58	539
High Pressure Accumulator	Greer 50A-2-1/2A	644	Greer 50A-5A	872
Low Pressure Reservoir	--	60	--	80
Filter	--	60	--	100
Fan Radiator	Young OCS-175	358	Young OCS-300	510
Induction Generator	G.E.	437	G.E.	1628
Total Purchase Parts		1881		3729

Table 15

SYSTEM COST COMPARISONS IN DOLLARS

Power System	Electric Power System		+	Stirling Engine	Total	Total/kW
Hydraulic Motor System a. Counberbalanced:	15 kW	3,876	+	3,364	7,240	483
	60 kW	11,709	+	13,456	25,165	419
B. Unbalanced:	15 kW	3,142	+	3,364	6,506	434
	60 kW	8,773	+	13,456	22,229	370
Linear Alternator System SaCo Magnets:	15 kW	5,382	+	3,364	8,746	583
	60 kW	20,252	+	13,456	33,708	562
Low Cost Magnets:	15 kW	4,532	+	3,364	7,896	526
	60 kW	16,856	+	13,456	30,312	505

4.0 RESULTS AND CONCLUSIONS

The primary objective of this study was to develop a conceptual design for a hydraulic converter capable of interfacing with a previously designed free-piston Stirling engine. The hydraulic converter produces hydraulic flow at pressures suitable for operating a commercial hydraulic motor coupled to a commercial rotary alternator to produce 15 kW of electric power output. A further objective was to assess the production costs of the hydraulic converter, the Stirling engine and two versions of a linear alternator previously designed to interface with the same free-piston Stirling engine.

The concept used for the hydraulic converter design was based directly on a free-piston Stirling hydraulic system designed to power an artificial heart. This 5-watt output system is in an advanced stage of hardware development after 14 years of continuous funding by the National Heart, Lung and Blood Institute. It is designed to be fully implantable in the human body with a maintenance free life of 10 years.

Scale up of this technology to the 15 kW level resulted in a severe fluid flow loss in the main power train. A unique approach was developed to eliminate this flow loss while retaining the many advantages of the basic concept. An option for fully counterbalancing the inertial loads in the main power train was developed and incorporated in the reference design. All converter losses were thoroughly evaluated and documented. The final converter design was determined to be 93.5% efficient with counterbalancing and 97.0% without.

The specified Stirling engine design used as an interface exhibited an exceptionally large stroke volume for the given power output. This is advantageous for the linear alternator for which it was originally designed. It imposes severe penalties on the hydraulic converter however. The fully counterbalanced reference design hydraulic converter would exhibit an efficiency of 99.6% if coupled to a free-piston engine with characteristics typical of high technology Stirling engine.

Dynamic simulation studies showed that the specified engine design would not self start and was thus subject to stall under some conditions. It should be possible to reduce or eliminate the stall problem and reduce other dynamic sensitivities with a suitable engine redesign. Improvement of the hydraulic converter interface characteristics should also be an objective of such redesign. This action would also improve engine power density significantly and would improve efficiency more modestly.

Costs for the hydraulic output system were determined to be somewhat lower than those for the linear alternator system. The recommended engine redesign would further reduce costs of the hydraulic converter and would probably reduce engine costs as well.

In summary, the Stirling hydraulic system offers much potential for superior performance and extremely low maintenance at reasonable cost in comparison with other Stirling engine systems. A proof-of-principle demonstration system may well pay big future dividends if anticipated performance levels can be achieved. A first step would be an engine conceptual design to more optimally interface with the hydraulic converter and minor converter redesign to take advantage of the new engine characteristics. If this study is satisfactory the next stage should be detailed design, fabrication and testing of a demonstration system.

REFERENCES

1. Thornton, J. P., et al.: Final Report: A Comparative Ranking of 0.1-10 MWe Solar Thermal Electric Power Systems. Report No. SERI/TR-351-461, August 1980.

2. Assessment of the State of Technology of Automotive Stirling Engines. NASA CR-159631, September 1979.

3. Johnston, R. P., et al.: Implanted Energy Conversion System. NHLBI Annual Report No. NO1-HV-92908-1, July 1980.

4. Dochat, G. R.: Design of a 15 kW Free-Piston Stirling Engine-Linear Alternator for Dispersed Solar Electric Power Systems. NASA CR-159587, August 1979.

5. McPherson, A. T. and A. Klemin, A.: Engineering Uses of Rubber. Reinhold, 1956.

6. Trainer, T. M., et al.: Final Report - Development of Analytical Techniques for Bellows and Diaphragm Design. AFRPL-TR-71-115, Part I, September 1971.

7. Carmichael, C, Ed.: Kent's Mechanical Engineers' Handbook, Design and Production Volume, Section 24. Wiley, 1950.

8. Otis, David R.: Thermal Losses in Gas-Charged Hydraulic Accumulators. 8th IECEC Proceedings, p. 198, 1973.

9. Breckenridge, R. W. Jr.: Heuchling, T. P., Moore, R. W. Jr. Rotary-Reciprocating Refrigeration Systems Studies, Part I, Analysis. Arthur D. Little, Inc., Technical Report AFFDL-TR-71-115, Part I, September 1971.

10. A Stirling Engine Workshop, Lecture Notes Set I, p. 14. Sunpower Inc., October 1980.

11. White, M. A., et al.: A Stirling Engine Piezoelectric (STEPZ) Power Source. The 25th Power Sources Symposium, May 1972.

12. White, M. A.: Proof-of-Principle Investigation of 300 W(e) Stirling Engine Piezoelectric (STEPZ) Generator, Final Technical Report. Report No. MDC G4420, Contract No. DAAK02-71-C-0405, September 1973.

13. Martini, W. R.,et al.: The Thermocompressor and Related Machines and Their Application to Artificial Heart Power. 4th IECEC Proceedings, 1969.

14. Kays, W. M. and London, A. L.: Compact Heat Exchangers. McGraw-Hill, 1964.

15. Walker, G.: Stirling Engines, Section 5. University of Calgary, September 1978.

16. Paul, A. N.: An Introduction to Cost Estimating. Manufacturing Cost Estimating, Society of Manufacturing Engineers, Dearborn, MI, 1980. pp. 3-8.

17. Abdelnour, Z, et al.: Testing of the Permanent Magnet Material Mn-Al-C for Potential Use in Propulsion Motors for Electric Vehicles. NASA CR-165291, March 1981.

Appendix A

METAL DIAPHRAGM ANALYSIS

INTRODUCTION

The feasibility of using a diaphragm as the separation membrane between the engine working gas and the hydraulic converter fluid has been investigated. The advantages of such an approach are (1) lower cost and (2) reduced engine dead volume. Various materials, and unidirectional versus bidirectional stroking from the relaxed position, were considered. Continuous operation for 50,000 hours at 60 loading cycles per second was taken as the component life requirement.

Material options fall into two basic categories--elastomerics and metallics. Elastomerics present an advantage in cost and size, but this is countered functionally by difficulty in maintaining the gas charge due to permeation through the membrane. An active makeup system would be required which would likely negate the initial cost advantage. A further and overriding difficulty is the lack of established fatigue data for such materials, making diaphragm life unpredictable without a costly and time-consuming test program. For these reasons, the elastomeric option was discarded.

SUMMARY

The results of the analysis show that a corrugated metal diaphragm with 35.56 cm (14.0 in.) active diameter and a sheet thickness of 0.005 in. would operate at an alternating stress level of 172.5 MPa (25,000 psi) for a total stroke volume of 852.12 cc (52.0 in.^{3}). The optimum corrugation double-depth, 2d, is 2.03 cm (.080 in.). For AM-350 material, the fatigue stress margin of safety is 50% (MS = 0.50) for a design life of 50,000 hours at 60 Hz. Were the lower strength 347 stainless steel used, the required active diameter would be 41.66 cm (16.4 in.) with an alternating stress level of 86.25 MPa (12,500 psi). To assure ease of fabrication (forming) a sheet thickness of .025 cm (0.010 in.) was also considered. For AM-350, the required active diameter would then be 38.1 cm (15.0 in.) and the corrugation double-depth 0.25 cm (0.100 in.). A design sketch illustrating a hardware installation concept for the 38.1-cm (15.0-in.) diameter diaphragm is given in Figure A-1.

DISCUSSION AND ANALYSIS

The metal diaphragms investigated are corrugated to increase radial compliance of the membrane, thus allowing the required stroke volume with a miminum diameter at stress levels consistent with the life requirement. Circumferential membrane stresses generally establish diaphragm size and configuration, but edge bending stresses (radial) may also be critical. Tilting of the edge reduces these stresses to acceptable values. A .524-rad (30-degree) tilted edge has been found to reduce edge stresses to sufficiently small values that they no

longer prevail. For this reason the .524-rad (30-degree) tilt edge is taken as a standard edge configuration.

To identify the range of interest, a scoping analysis was done using first-order hand calculation methods. A more refined analysis was then made using the Battelle-developed NONLIN computer program to verify the first-order analysis and to include radial bending and edge stresses.

Nonlinearity of deflection relative to applied pressure is significant in diaphragm selection for the following reason. As the displaced volume of a diaphragm is progressively increased the relationship between the pressure and deflection (or displaced volume) becomes increasingly nonlinear. In the region of small deflections and high linearity the peak circumferential stresses occur at the crests of the corrugation, with a rather symmetrical stress distribution. As the diaphragm is further deflected, and the relationship becomes more nonlinear, the elements of the corrugation shift radially resulting in stresses elsewhere exceeding those at the crests. The analysis predicts stresses only at the crest. To assure that these are not significantly exceeded, experience has shown that nonlinearity (defined below) should not exceed 0.5. This additional criterion is therefore included in the design requirements. To minimize diameter it is necessary to operate the diaphragm as far into the nonlinear range as can be done safely.

For metal diaphragms, two stress levels corresponding to the fatigue allowables at 1×10^{10} cycles (50,000 hours at 60 Hz) for the two likely candidate materials were taken as basic criteria. For 347 Stainless Steel (18-8 austenitic), a fatigue allowable of 86.25 MPa (12,500 psi) fully reversed alternating stress is used. For the higher-strength AM-350, heat-treated to the SCT-800 condition, a fully reversed allowable of 172.5 MPa (25,000 psi) is used. The allowables were arrived at as follows.

For AM-350, data provided by Allegheny Ludlum for 0.040-in.-thick sheet shows a nominal fatigue allowable σ_f = 593.4 MPa (86,000 psi) at 1×10^7 cycles. Conservatively projecting this to 1×10^{10} cycles gives σ_e = 572.7 (83,000 psi). As the tests were for longitudinal grain direction, the value is reduced by the ratio of transverse to longitudinal ultimate stress, 192,000/197,000. Other modifying factors applied are

$$k_1 = (1 - 3\sigma) = 0.76$$

where 1 = standard deviation of the endurance limit dispersion = 0.08 (typically).

k_2 = .70 for surface condition

k_3 = .87 for uncertainty in stress prediction

where

design endurance limit = $k_1 k_2 k_3$ (fatigue specimen test).

Retaining a 50% margin of safety gives,

$$\text{design endurance limit} = \frac{(.76)(.70)(.87)\ 80{,}900}{1.5} = 172 \text{ MPa (25,000 psi)}$$

For 347 Stainless Steel the established endurance limit is 40,000 psi. Applying the same factors gives

$$\text{design endurance limit} = \frac{(.76)(.70)(.87)\ 40{,}000}{1.5} = 85.1 \text{ MPa } (12{,}340 \text{ psi})$$

A further consideration regards elastic instability of the diaphragm which strokes in both directions at it passes through the nominal central position.

If the diaphragm is not flat in the relaxed position, indeterminant stresses would result from instability during over-center operation.

In the welded design presented, straightening of the diaphragm after welding is fairly straightforward and inexpensive. For this reason the unidirectional diaphragm (deflected in one direction from the relaxed position) is discarded in favor of the smaller-diameter bidirectional option. The unidirectional approach would be in contention were it difficult or expensive to straighten after welding. A comparison point for the unidirectional diaphragm was derived, however, and is presented.

In the following pages the analysis performed is reported. Diaphragm geometric nomenclature and configuration are as shown in Figure A-2. In subsequent plots, parameter notation is

P = pressure differential across diaphragm.

$(\sigma_b)_r$ = bending stress-radial direction.

σ_t = circumferential membrane stress (tangential stress) at crest of corrugation.

f = centerline deflection.

Δ = nonlinearity factor where $dp/df = k(1 + \Delta)$.

V_s = stroke volume.

Figures A-3 through A-8 reflect the results of the first-order scoping analysis. Figure A-3 is a plot of maximum circumferential membrane stress σ_t, pressure differential P across the diaphragm, and nonlinearity Δ of pressure relative to deflection. A diaphragm diameter of 35.56 cm (14.0 in.) with a total stroke volume of 852.12 cc (52.0 $in.^3$) is assumed and values are plotted as functions of corrugation depth to sheet thickness ratio (d/h) for sheet thicknesses of 4.2, 7.0, and 10.0 mils. The value of this plot is in identifying trends. It is seen that stress increases fairly linearly with corrugation depth to thickness ratio and with sheet thickness. Pressure differential is minimum for d/h in the region of 5.0-7.0, depending on sheet thickness. Nonlinearity, Δ, is very sensitive to d/h in the lower region, and also to sheet thickness. As nonlinearity should be held to a maximum of 0.5, the effect of configuration on this function is seen to be critical. The .018-cm- (0.007-in.) and .025-cm- (0.010-in.) thick materials cannot satisfy both the nonlinearity and stress limitations at this diaphragm diameter, and in fact require larger diameters to be practical.

Figure A-4 shows stress level as a function of corrugation depth for the likely range of diaphragm diameters. Figures A-5, A-6, and A-7 present corrugation depth, depth to material thickness ratio, pressure differential, and nonlinearity as functions of diaphragm radius for 0.13-, 0.19-, and 0.25-mm (5.0-, 7.5- and 10.0-mil) sheet thicknesses respectively for the AM-350 design stress level of 172 MPa (25,000 psi). The nonlinearity limitation of 0.5 is indicated. A similar plot for a sheet thickness of 0.25 mm (10.0 mils) at the lower stress level of 86 MPa (12.5 ksi) for 347 SS is given in Figure A-8. Figure A-9 shows diaphragm radius versus sheet thickness for a stress level of 172 MPa (25,000 psi) with the 0.5 nonlinearity restriction imposed. A single point at sheet thickness of 0.25 mm (10.0 mils) is presented for the 172-MPa (12,500-psi) stress level.

Results of the scoping analysis indicate that the area of interest lies between a 17.8- and 20.3-cm (7.0- and 8.0-in.) radius and corrugation double-depths of 2.0 to 2.5 mm (.080 to .100 in.). Runs were made on the computer for diaphragm radii varying from 17.8 to 22.9 cm (7.0 to 9.0 in.) for sheet thicknesses of 0.13 and 0.25 mm (.005 and .010 in.) Figures A-10, A-11, and A-12 show the trend of radial bending stress $(\sigma_b)_r$, circumferential membrane stress σ_t, pressure differential, and nonlinearity as functions of diaphragm radius for different corrugation double-depths and for a sheet thickness of 0.13 mm (.005 in.). It is seen that the smallest diaphragm which satisfies the stress and nonlinearity requirements for the higher-strength AM-350 material has a radius of 17.8 cm (7.0 in.) at a corrugation double-depth of 2.0 mm (.080 in.) (Figure A-8c). For the lower-strength 347 Stainless Steel, the smallest diaphragm would have a radius of 20.8 cm (8.2 in.) with a corrugation double-depth of 1.8 mm (.070 in.) (Figure A-11). Pressure differential across the diaphragms would be 1586 and 483 Pa (0.23 and 0.07 psi) respectively, well within tolerable limits. Figure A-13 is a plot of the same parameters as functions of corrugation double-depth and d/h for the 17.8-cm (7.0-in.) radius diaphragm. It is seen that minimum pressure occurs at a corrugation double-depth of 1.8 mm (0.070 in.) (d/h = 7.0) with crest circumferential membrane and radial bending stresses dropping rapidly with decreasing corrugation double-depth. However, the nonlinearity limitation ($\Delta = 0.5$) is exceeded below d/h = 8.0. From these plots is is concluded that for a sheet thickness of 0.13 mm (.005 in. a suitable diaphragm radius would be 17.8 cm (7.C in.) with a corrugation double-depth of 2.0 mm (0.080 in.)

Because of concern about the ability to form the diaphragm of 0.13-mm-(.005-in.-) thick sheet, sheet thicknesses of 0.25 mm (0.010-in.0 were investigated. Figures A-14, A-15, and A-16 are plots of a maximum crest circumferential stress, maximum radial bending stress, pressure differential and nonlinearity versus diaphragm radius. It is seen that the minimum radius diaphragm for AM-350 is 19.0 cm (7.5 in.) (Figure A-14) at a corrugation double-depth of 2.5 mm (0.100 in.) (d/h = 5.0). Circumferential stress is used as the criterion since radial bending stress can be reduced somewhat by increasing corrugation pitch, if required. For 347 Stainless Steel, the minimum radius is 22.9 cm (9.0 in.) Figure A-17 shows stress, pressure, and nonlinearity for a 19.0-cm (7.5-in.) radius AM-350 diaphragm with a material thickness of 0.25 mm (0.010 in.) as functions of corrugation double-depth and d/h. Both the nonlinearity and stress limitations occur at a corrugation double-depth of 2.5 mm (0.100 in.) (d/h = 5.0). Pressure differential at the design displaced volume is 3655 Pa (0.53 psi), which is tolerable.

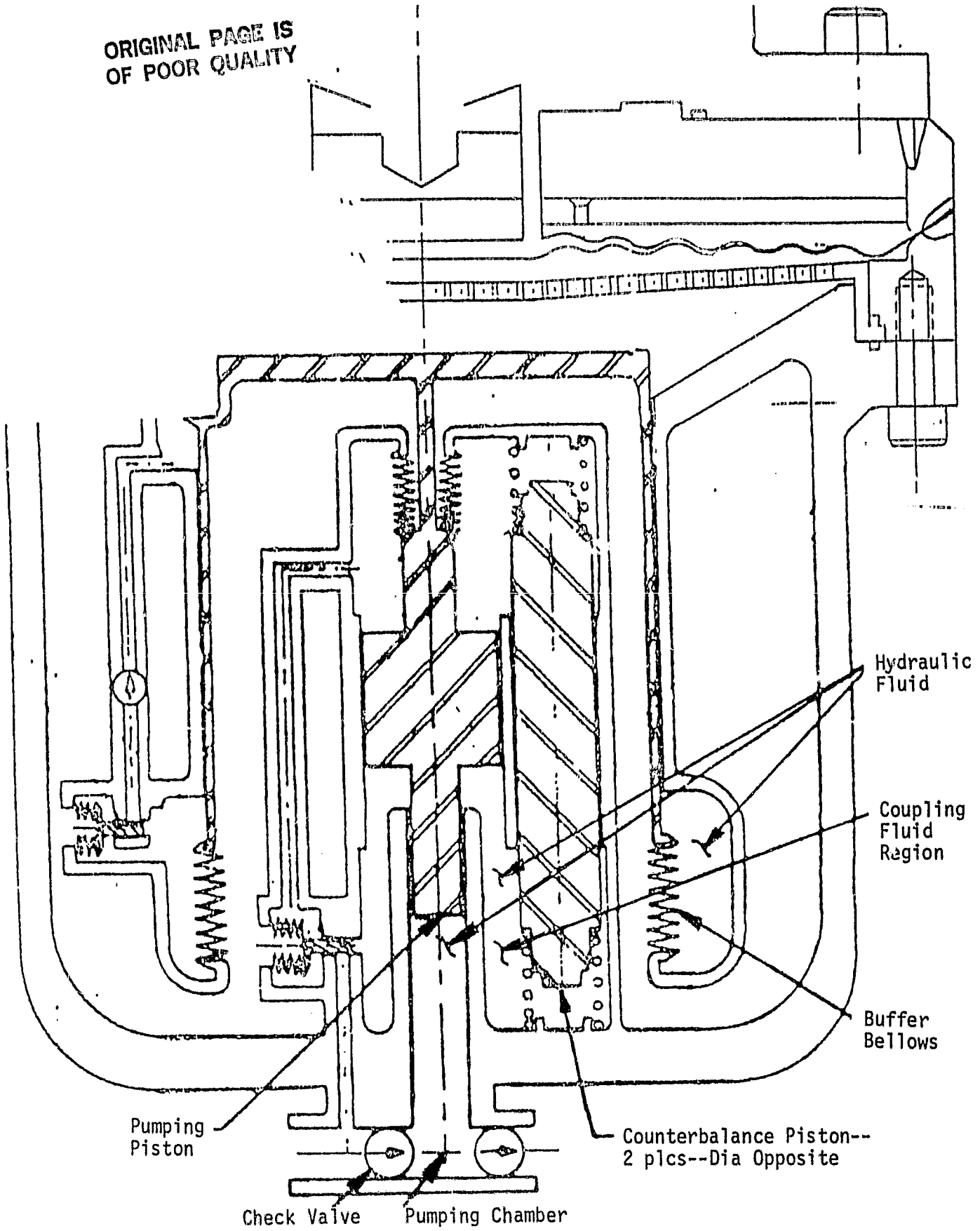

Figure A-1. Hydraulic Converter with Metal Diaphragm

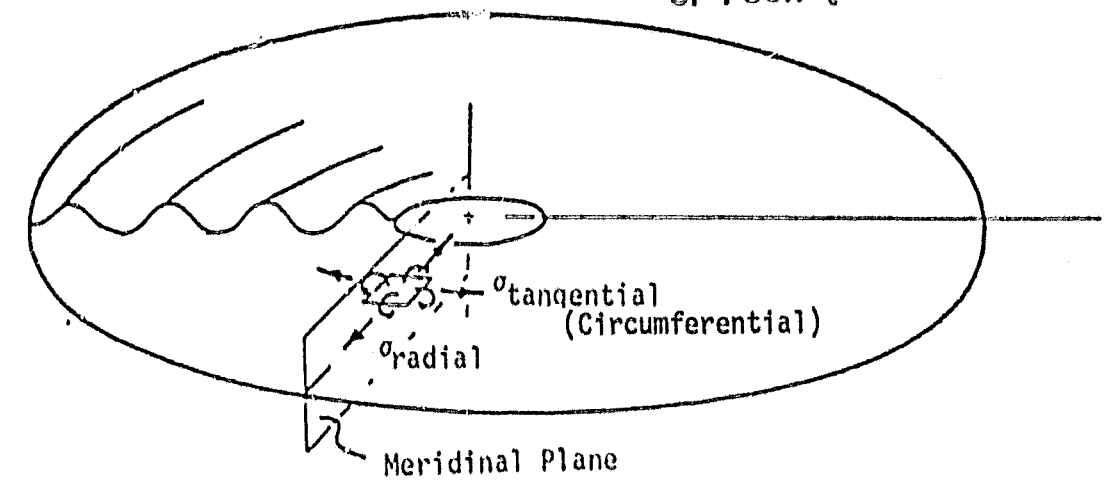

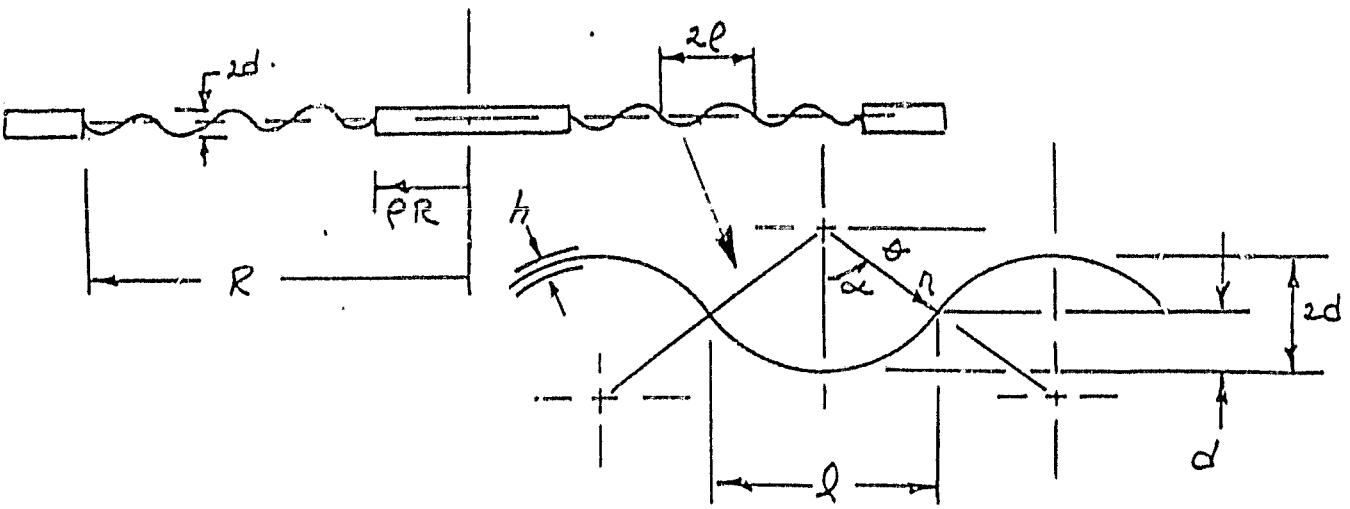

Arc-Shaped Convolution

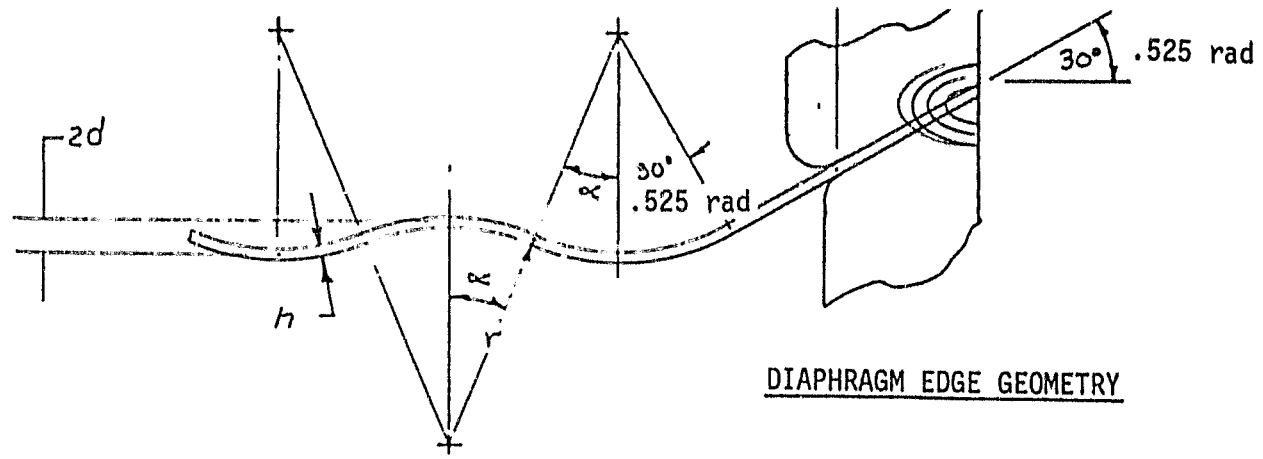

DIAPHRAGM EDGE GEOMETRY

Figure A-2. Diaphragm Geometry

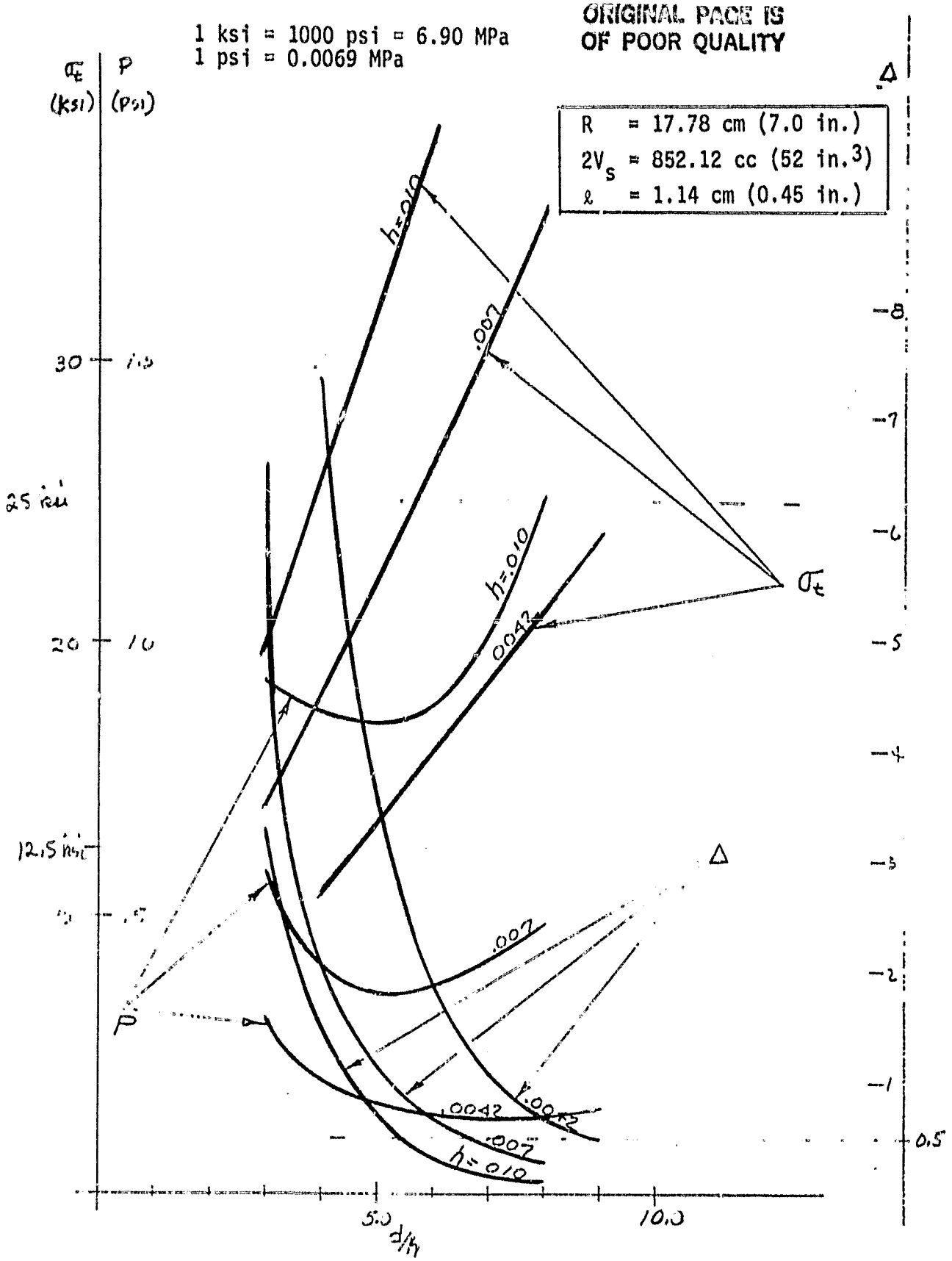

Figure A-3. Tangential Stress, Pressure Differential, and Nonlinearity vs Convolution Depth to Sheet Thickness Ratio

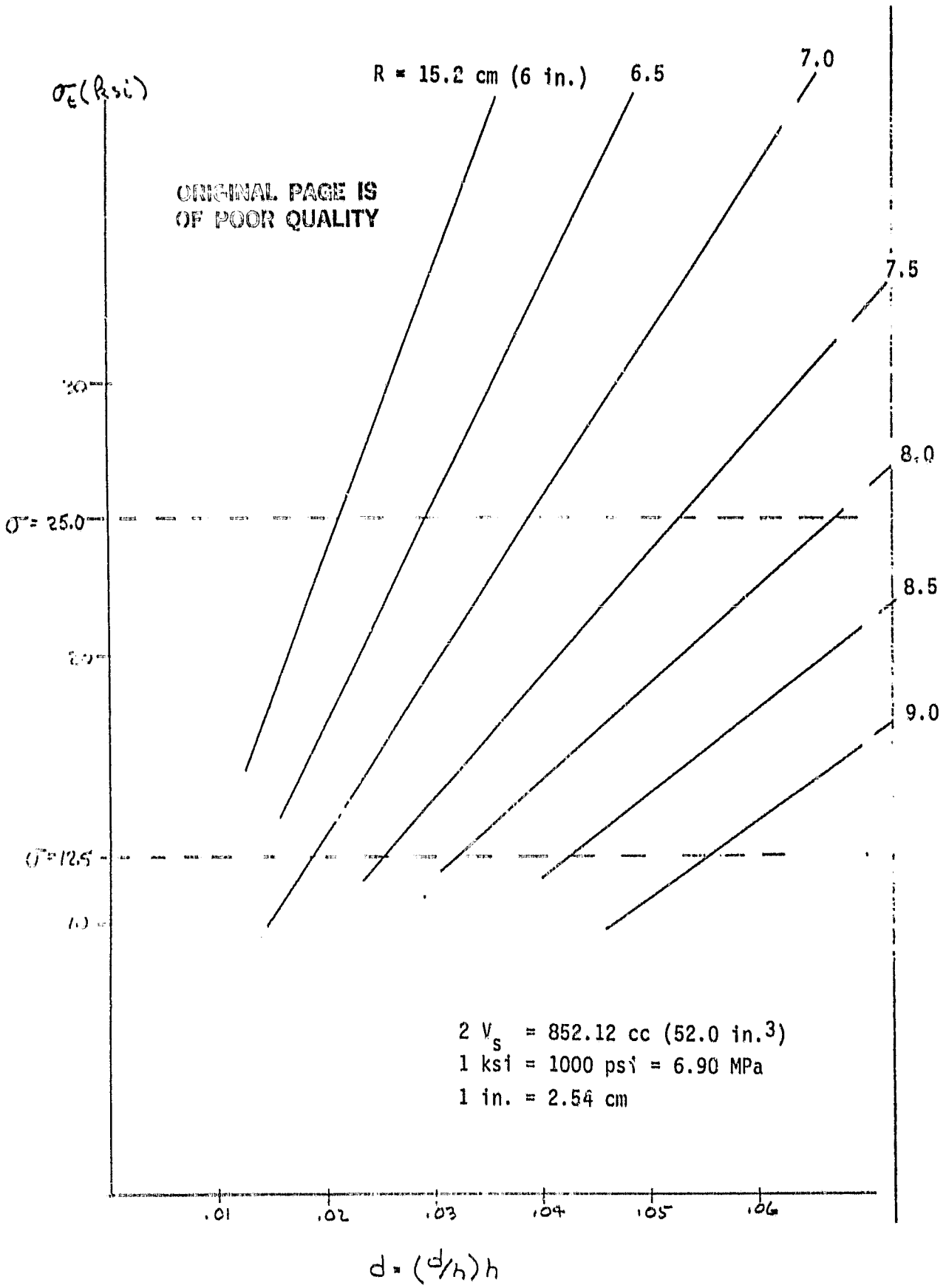

Figure A-4. Tangential Stress vs Convolution Depth to Sheet Thickness Ratio for Diaphragm Radii Shown

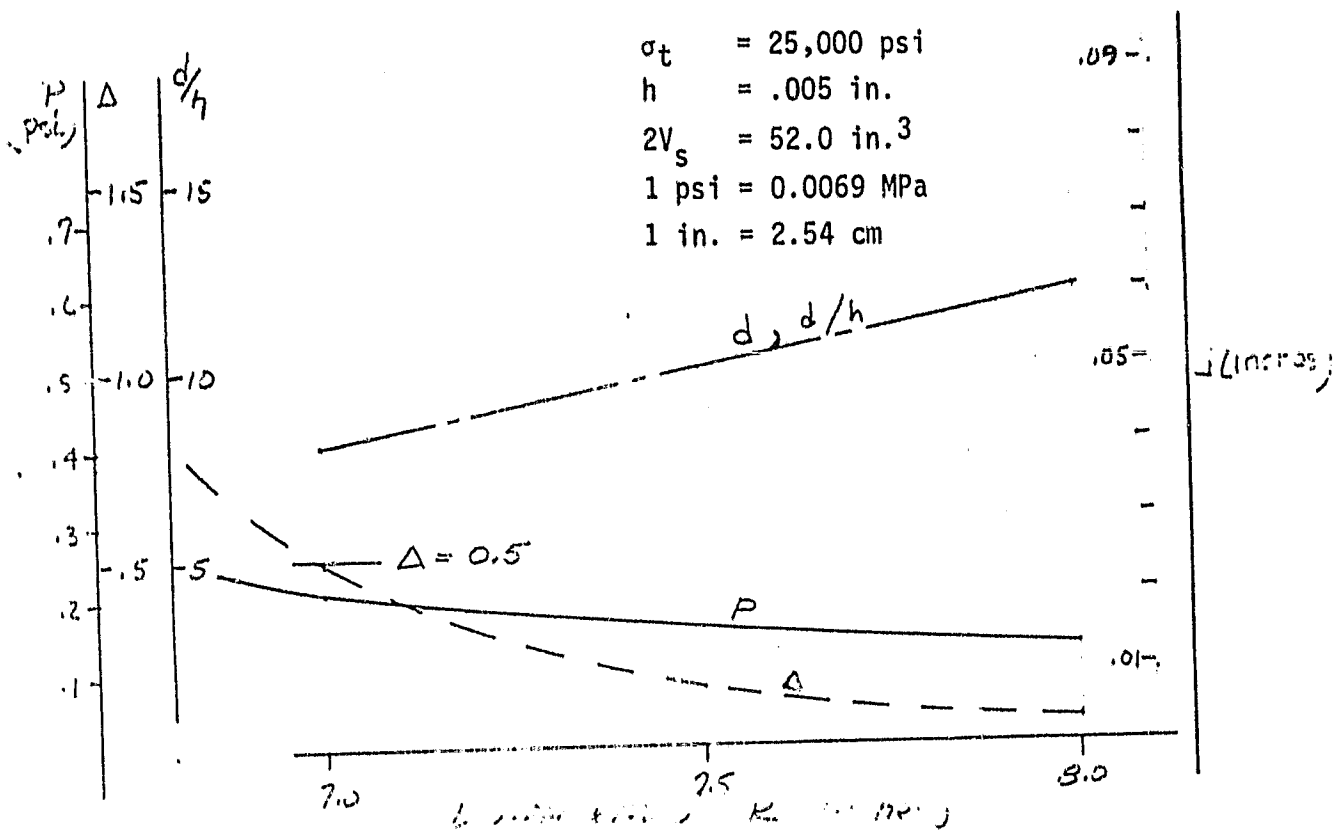

Figure A-5. Pressure Differential, Nonlinearity, Convolution Depth, and Convolution Depth to Sheet Thickness Ratio vs Diaphragm Radius

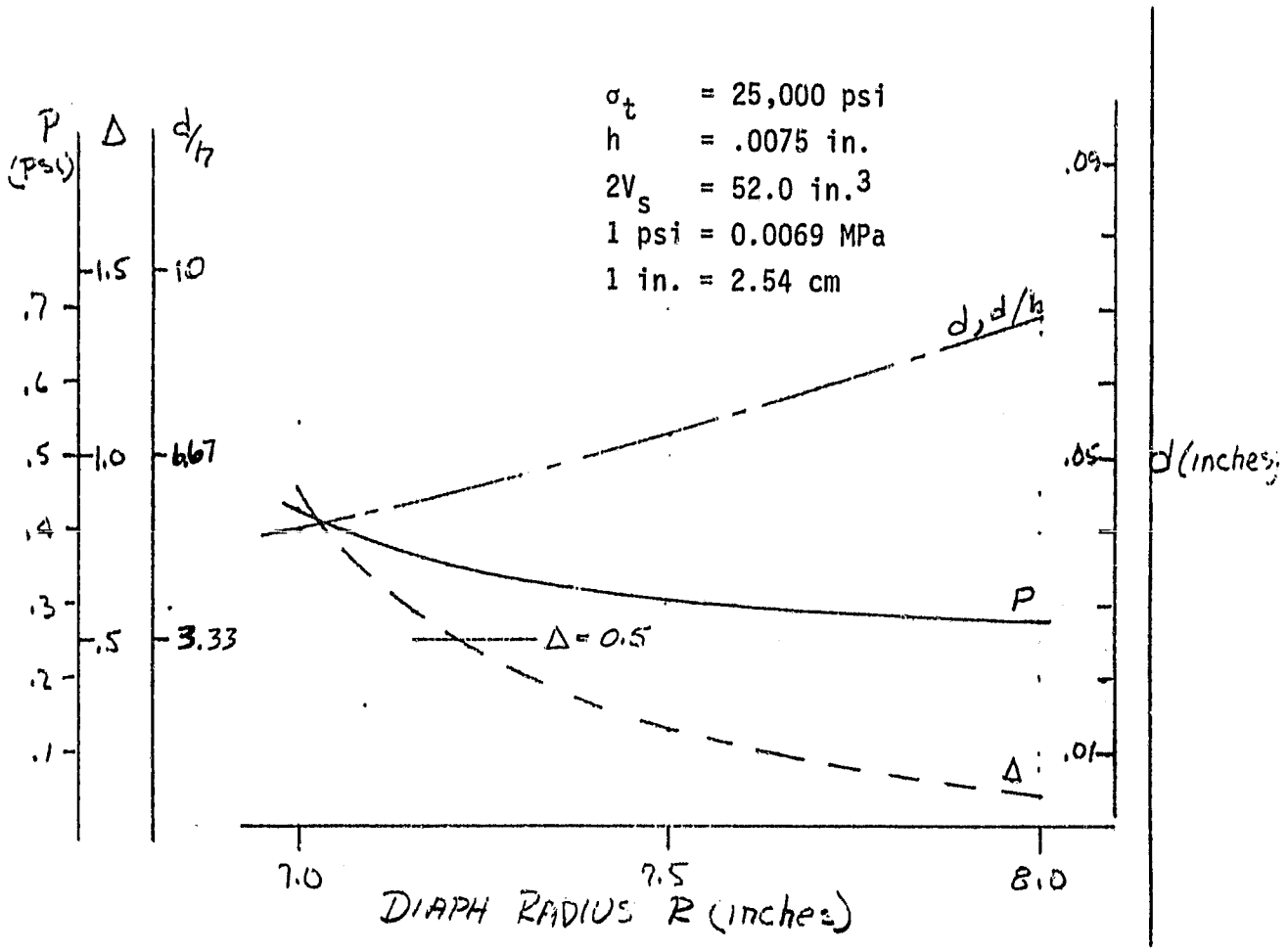

Figure A-6. Pressure Differential, Nonlinearity, Convolution Depth, and Convolution Depth to Sheet Thickness Ratio vs Diaphragm Radius

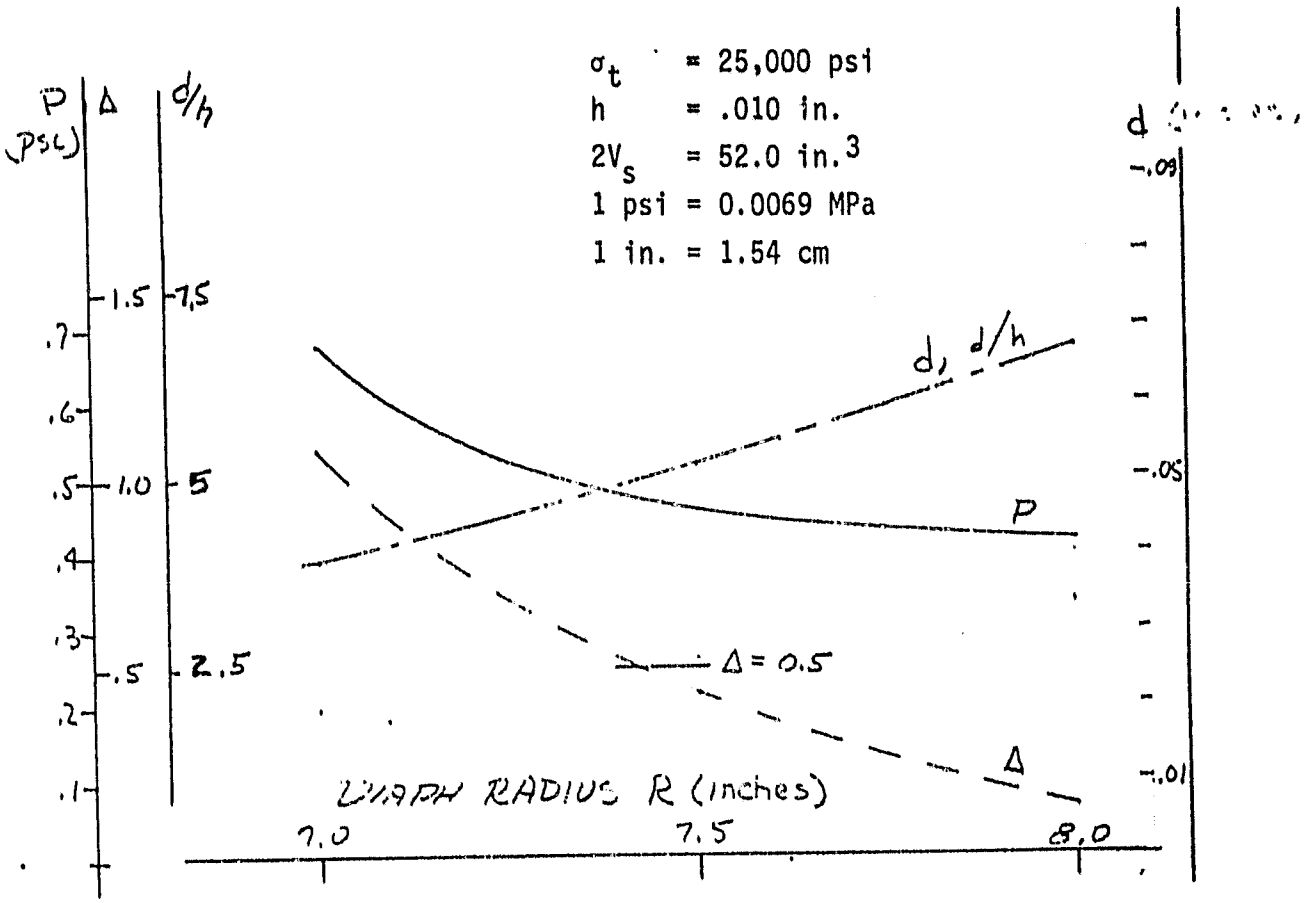

Figure A-7. Pressure Differential, Nonlinearity, Convolution Depth, and Convolution Depth to Sheet Thickness Ratio vs Diaphragm Radius

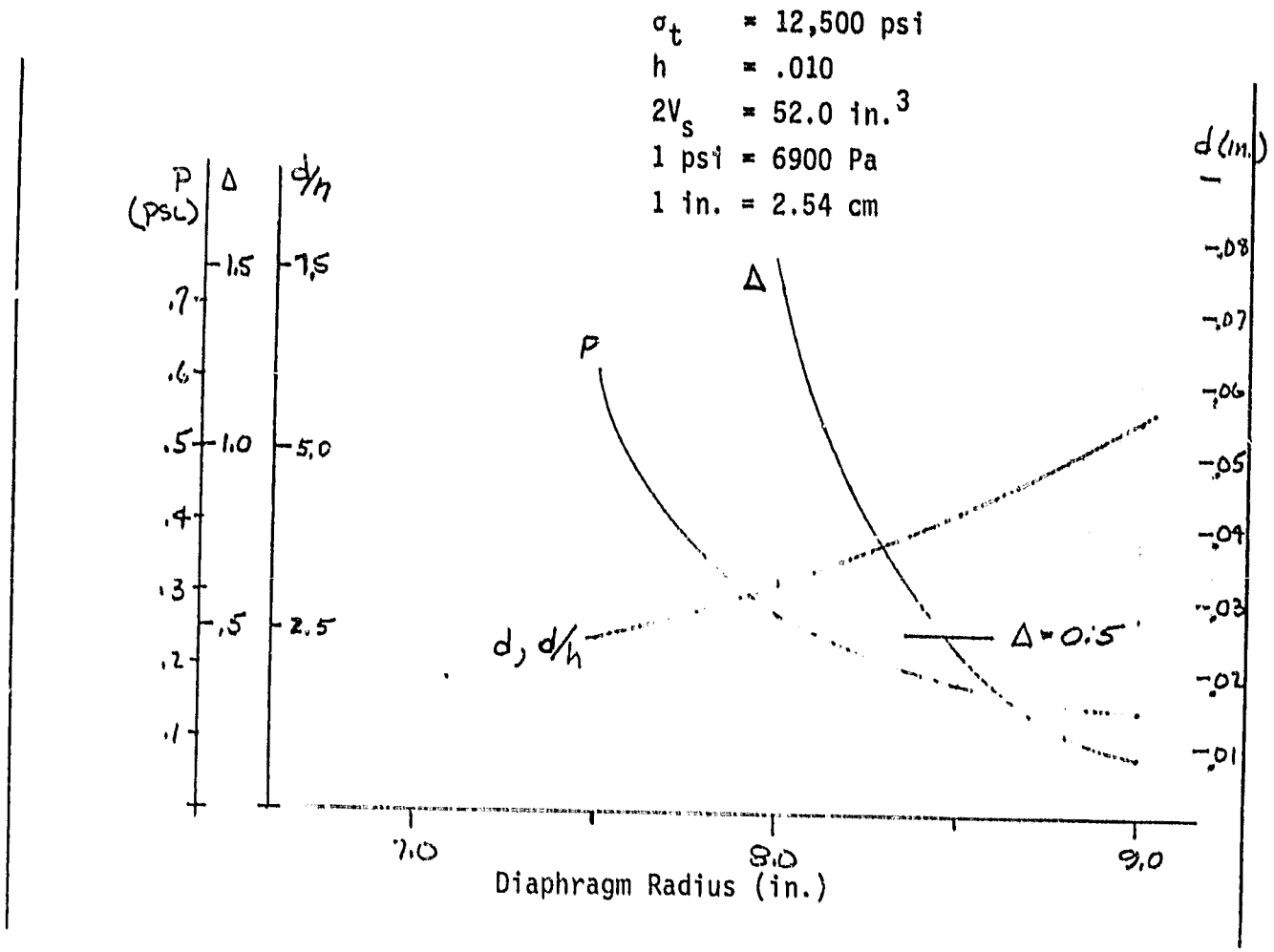

Figure A-8. Pressure Differential, Nonlinearity, Convolution Depth, and Convolution Depth to Sheet Thickness Ratio vs Diaphragm Radius

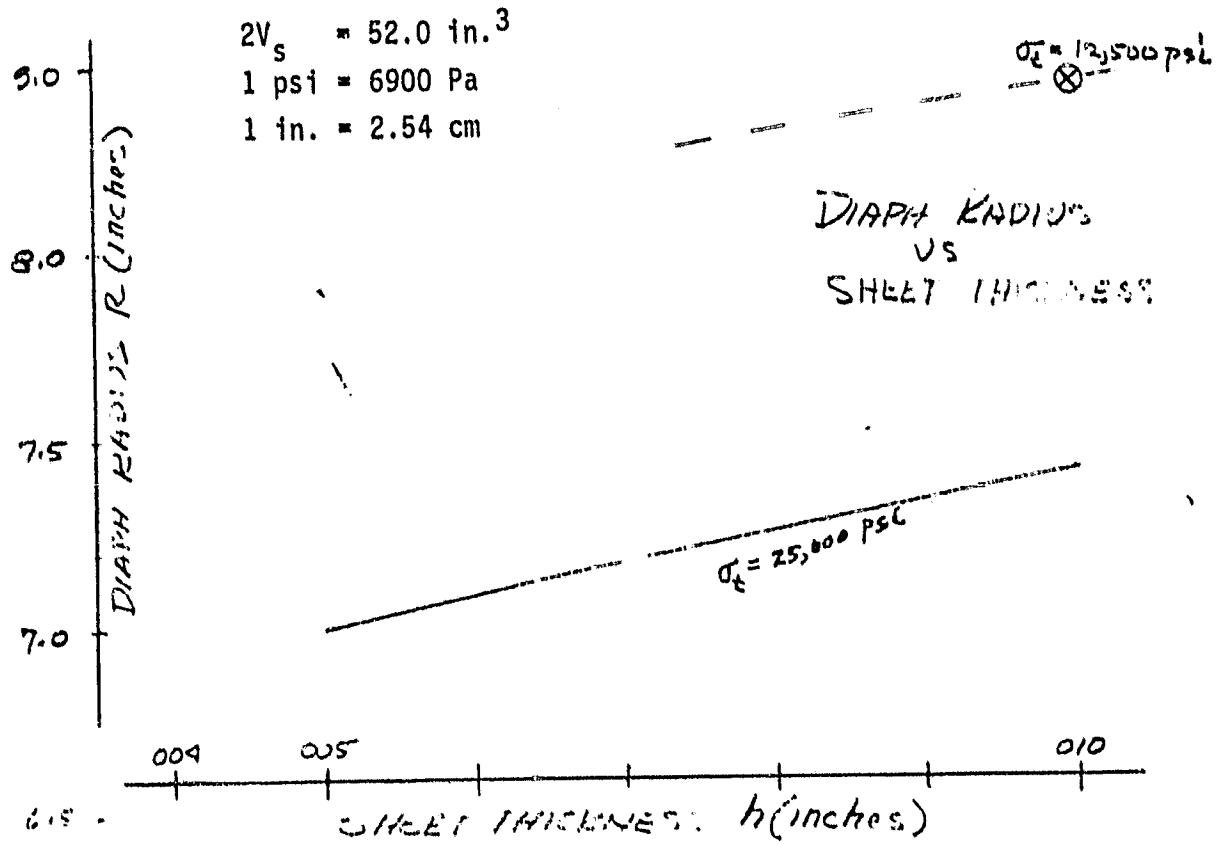

Figure A-9. Diaphragm Radius, vs Sheet Thickness for Tangential Stress Levels of 12,500 psi and 25,000 psi

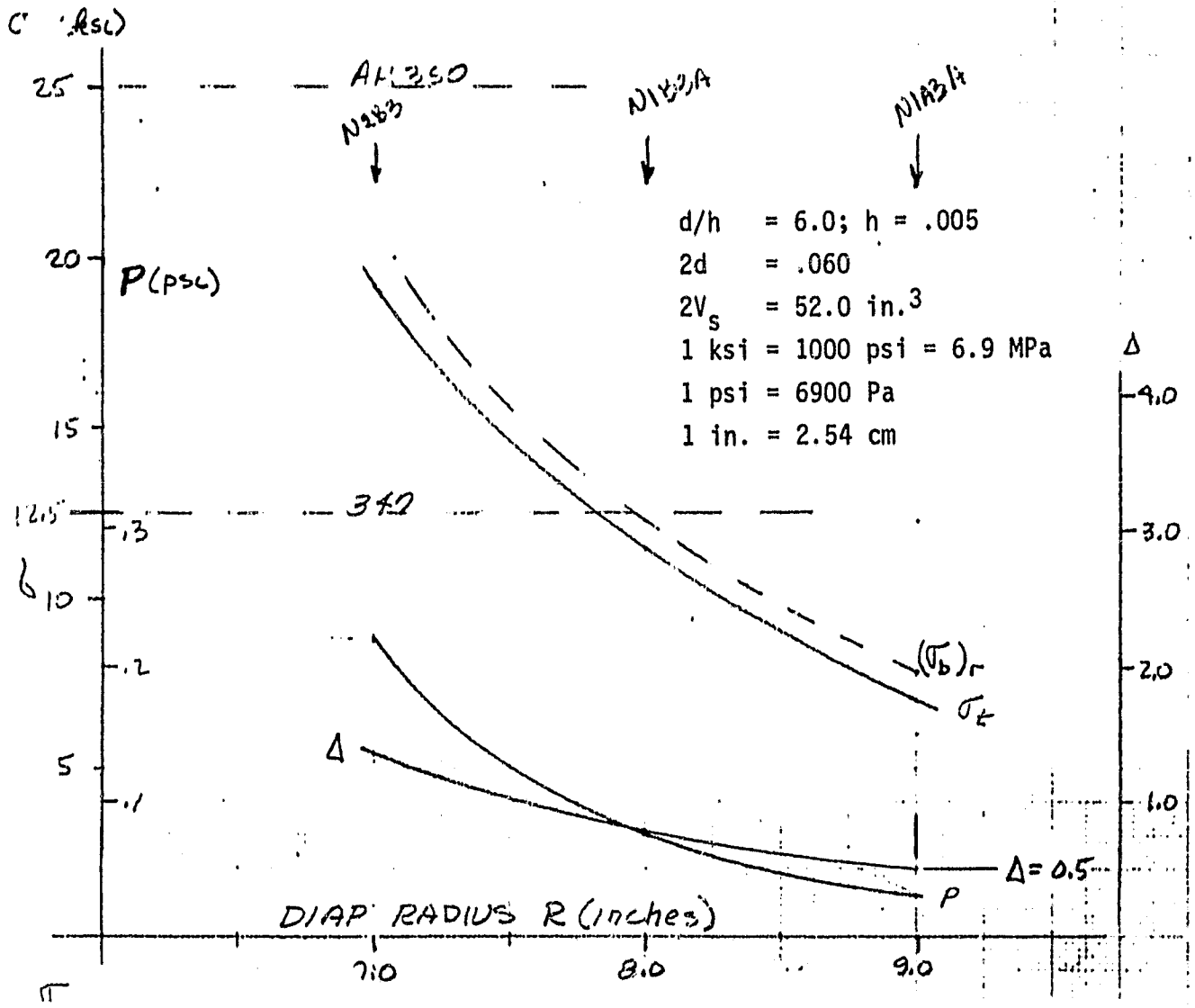

Figure A-10. Stress, Pressure Differential, and Nonlinearity vs Diaphragm Radius

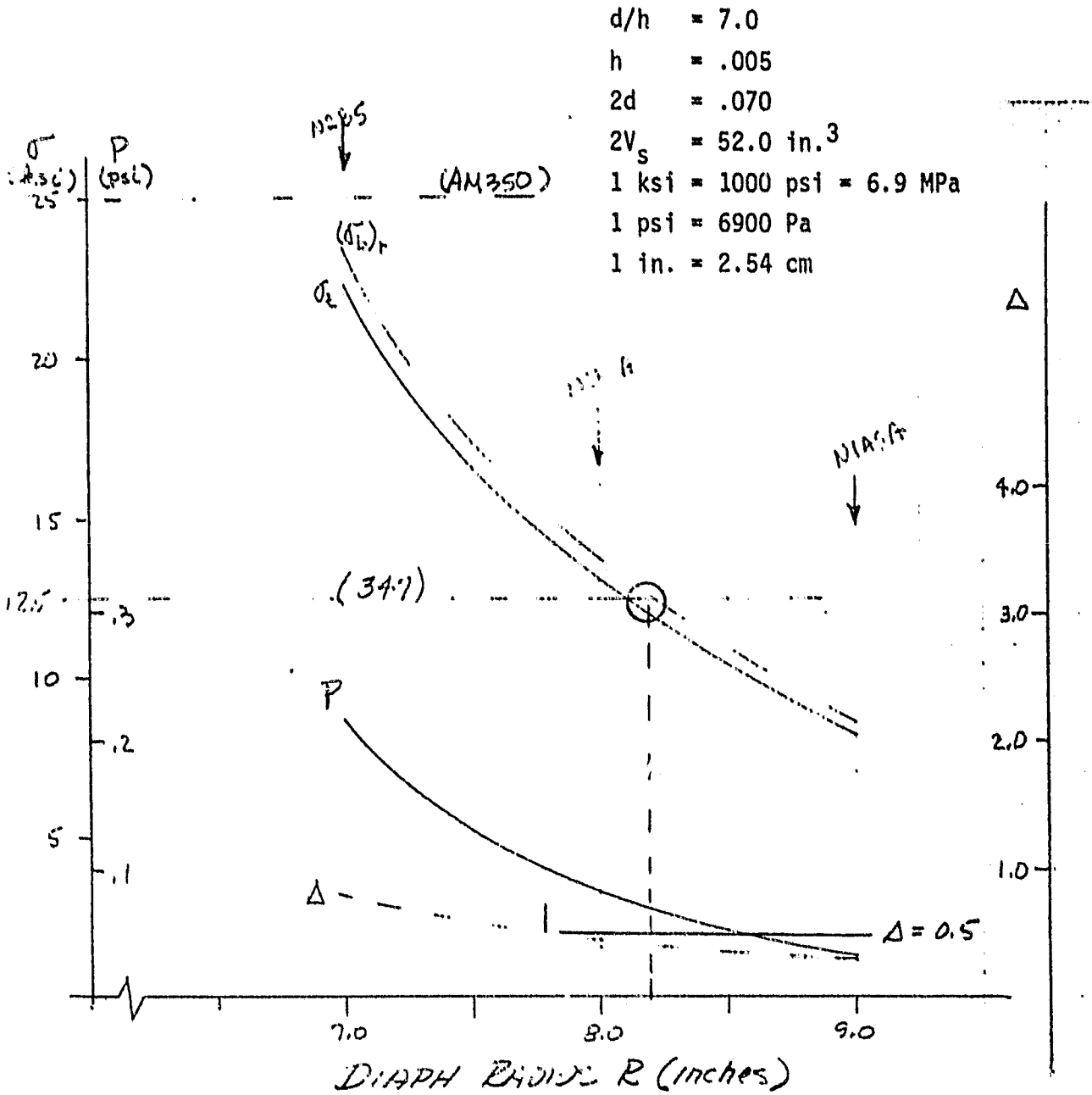

Figure A-11. Stress, Pressure Differential, and Nonlinearity vs Diaphragm Radius

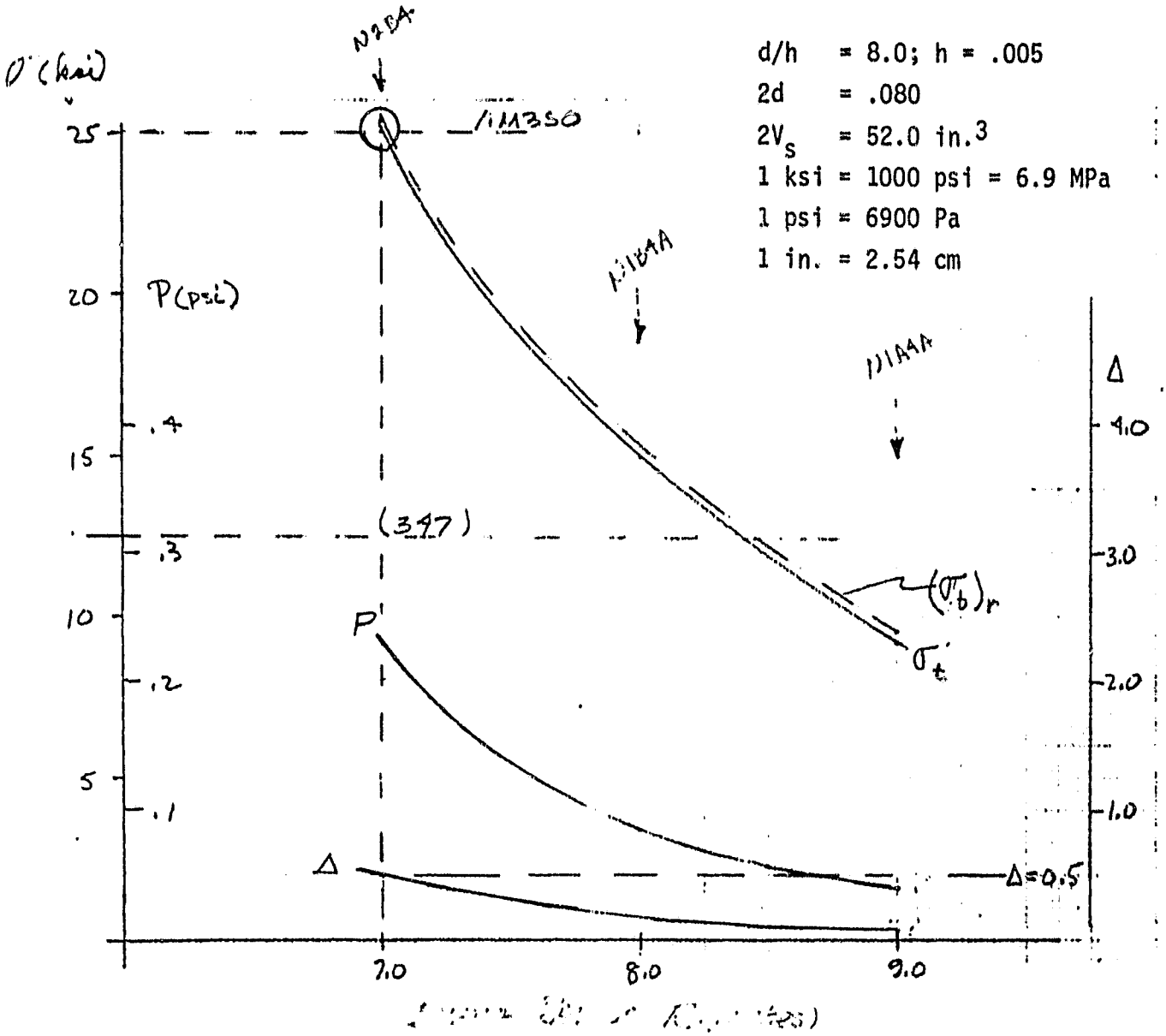

Figure A-12. Stress, Pressure Differential, and Nonlinearity vs Diaphragm Radius

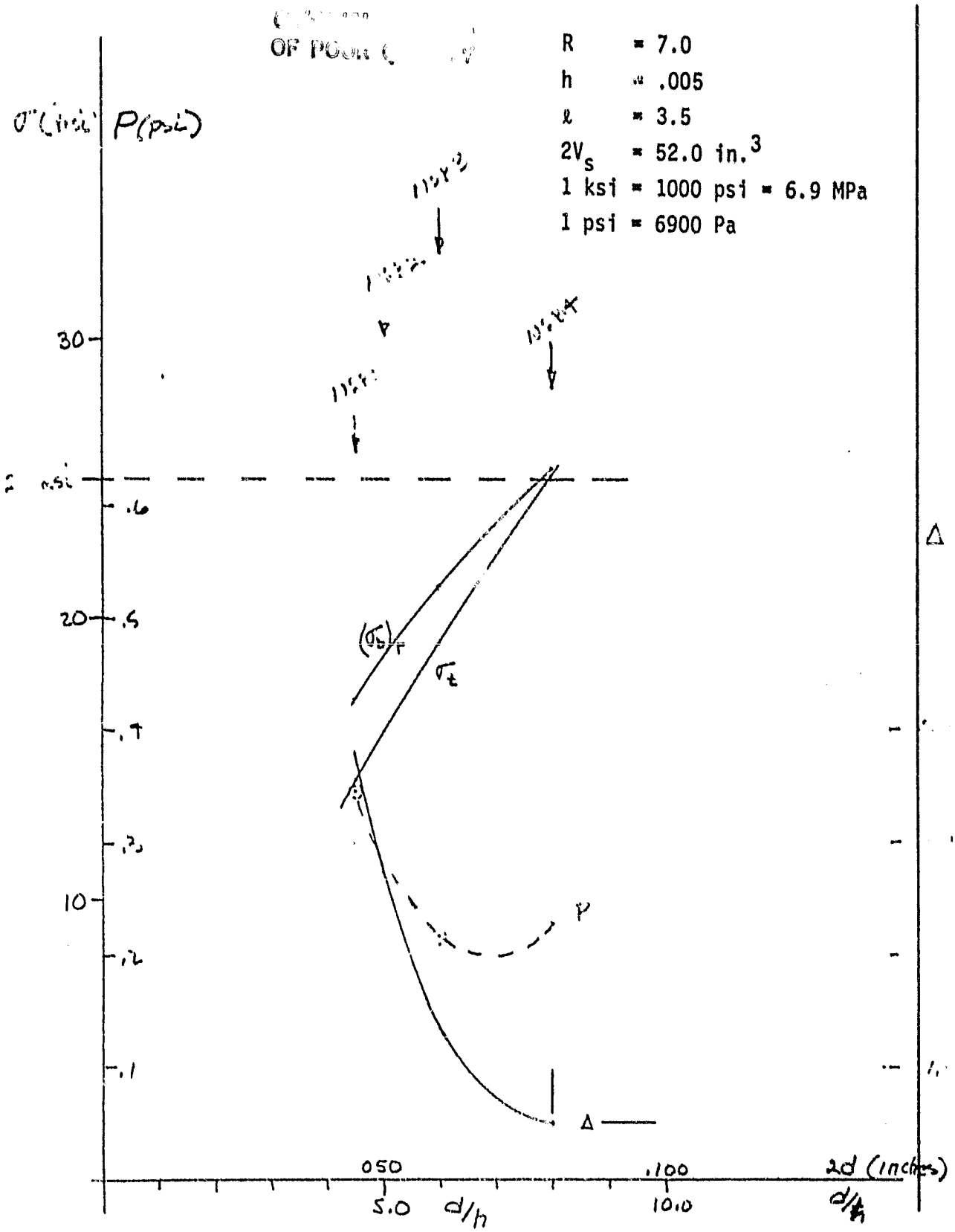

Figure A-13. Stress, Pressure Differential, and Nonlinearity vs Convolution Depth to Sheet Thickness Ratio and Convolution Depth

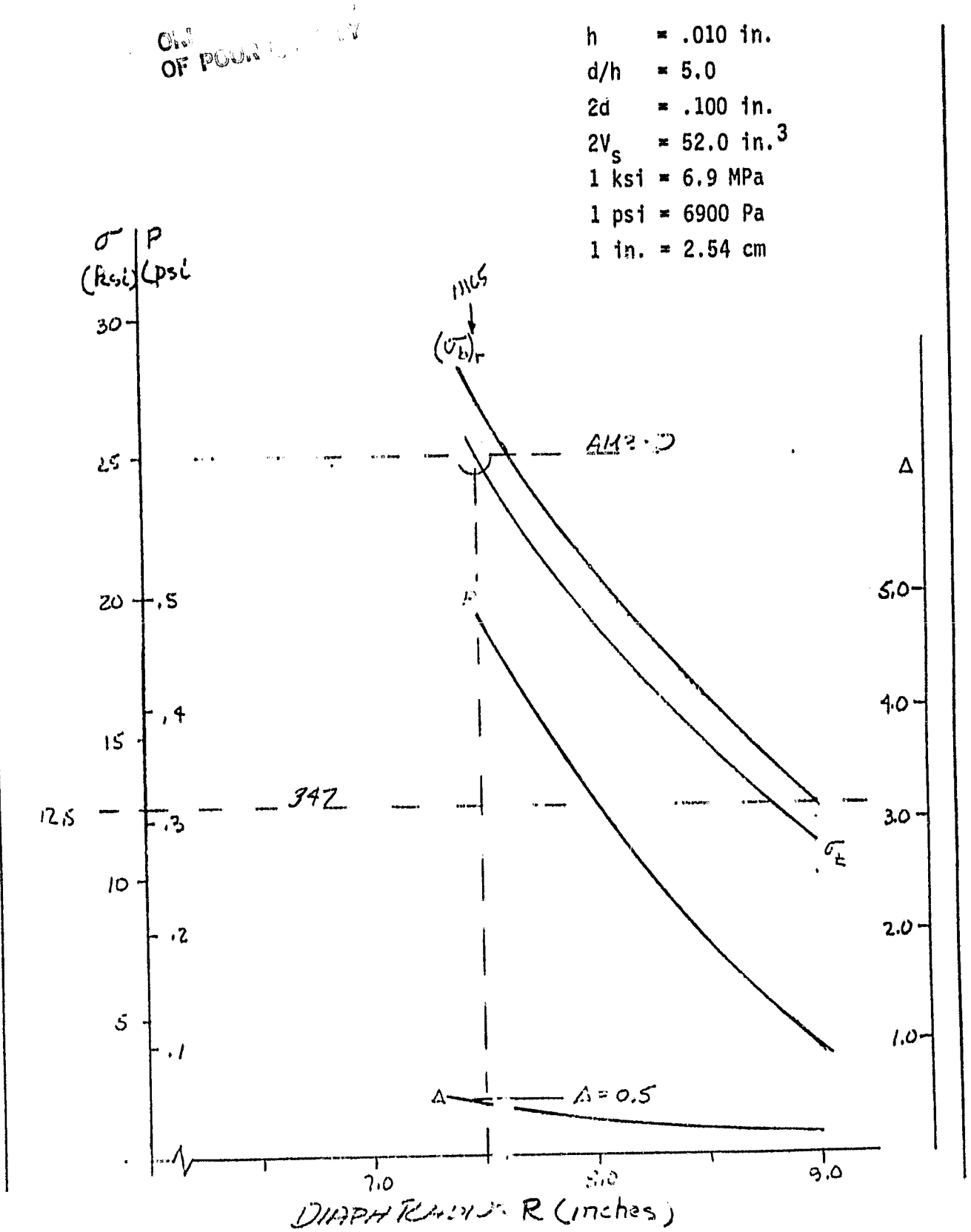

Figure A-14. Stress, Pressure Differential, and Nonlinearity vs Diaphragm Radius

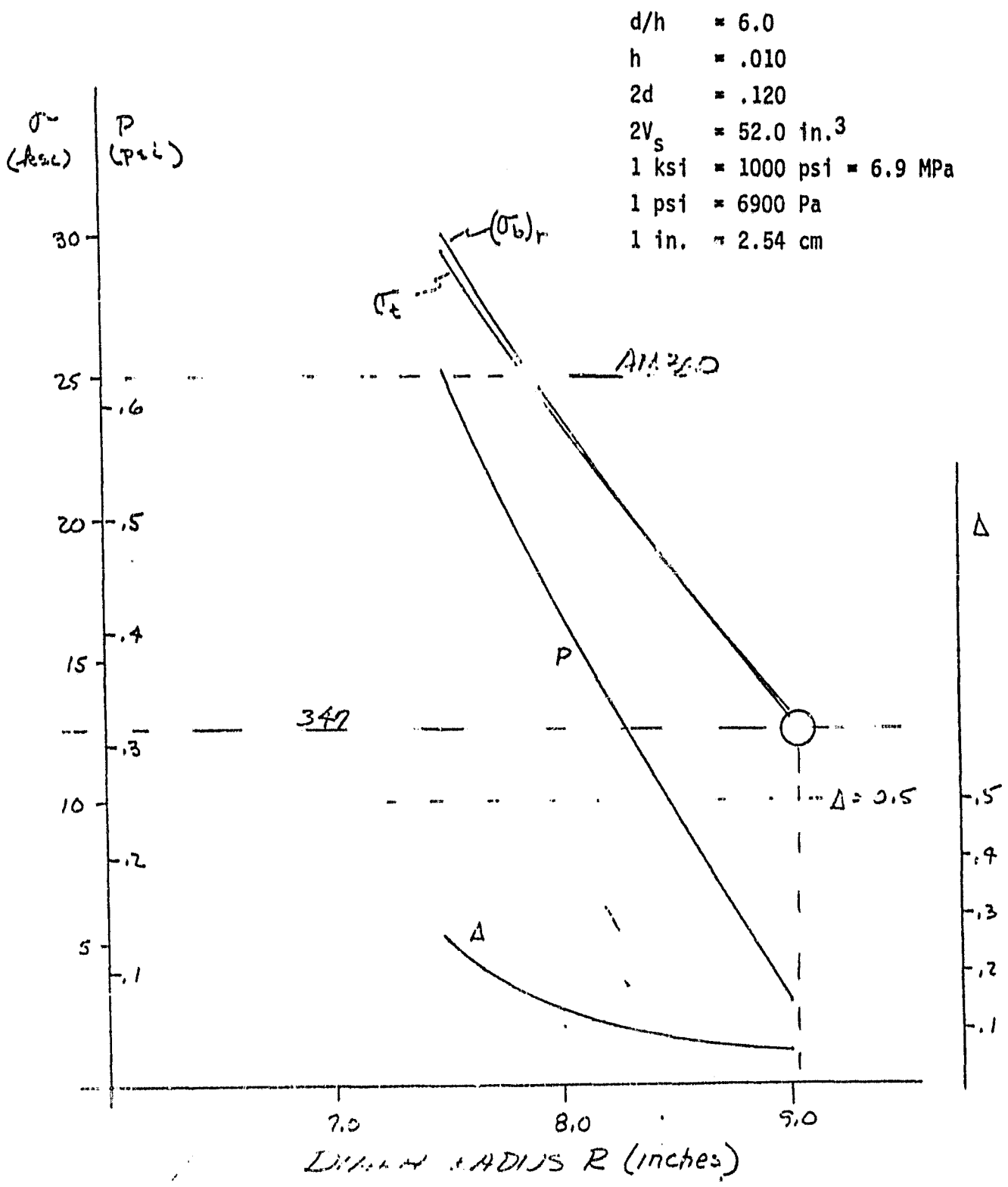

Figure A-15. Stress, Pressure Differential, and Nonlinearity vs Diaphragm Radius

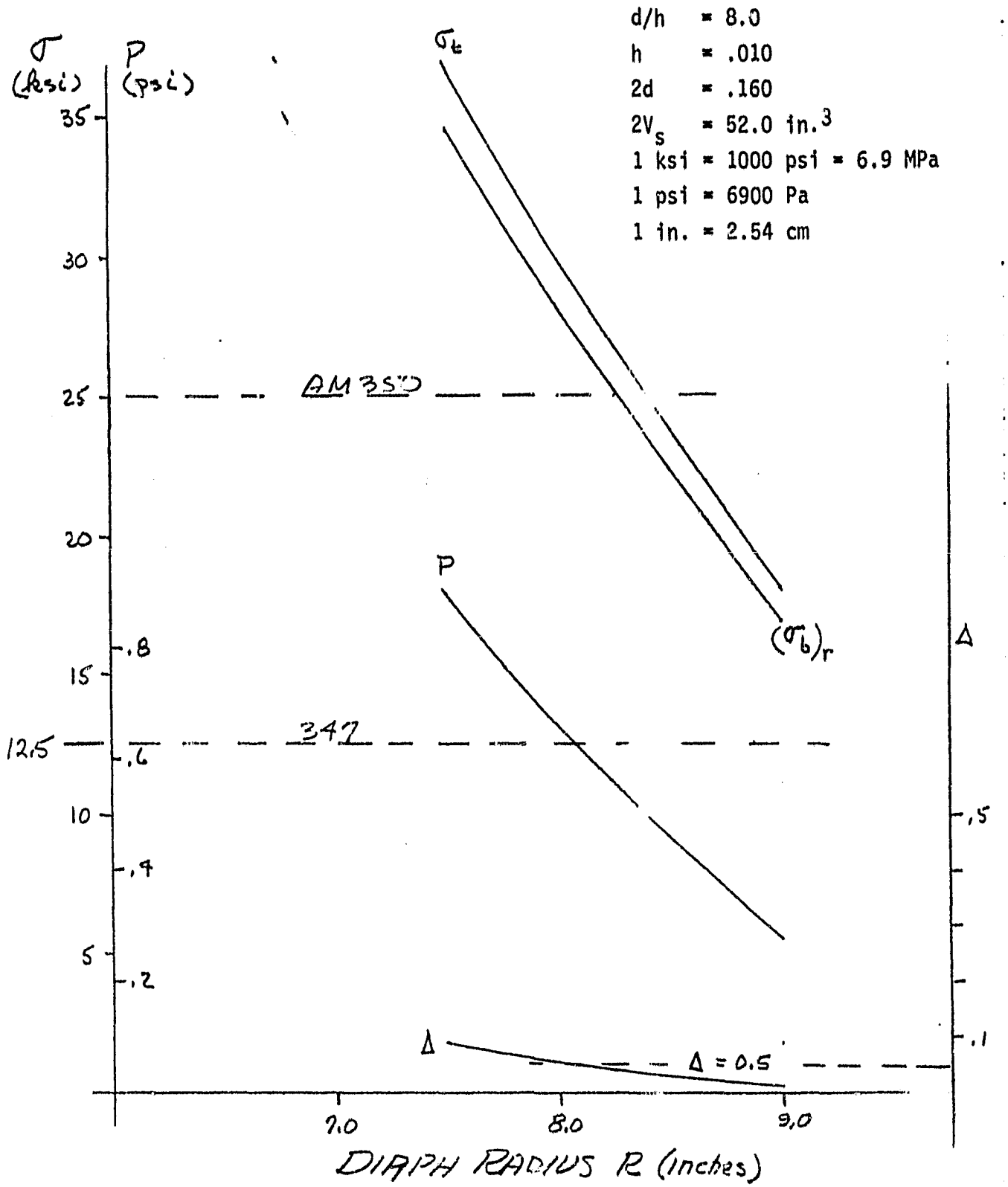

Figure A-16. Stress, Pressure Differential, and Nonlinearity vs Diaphragm Radius

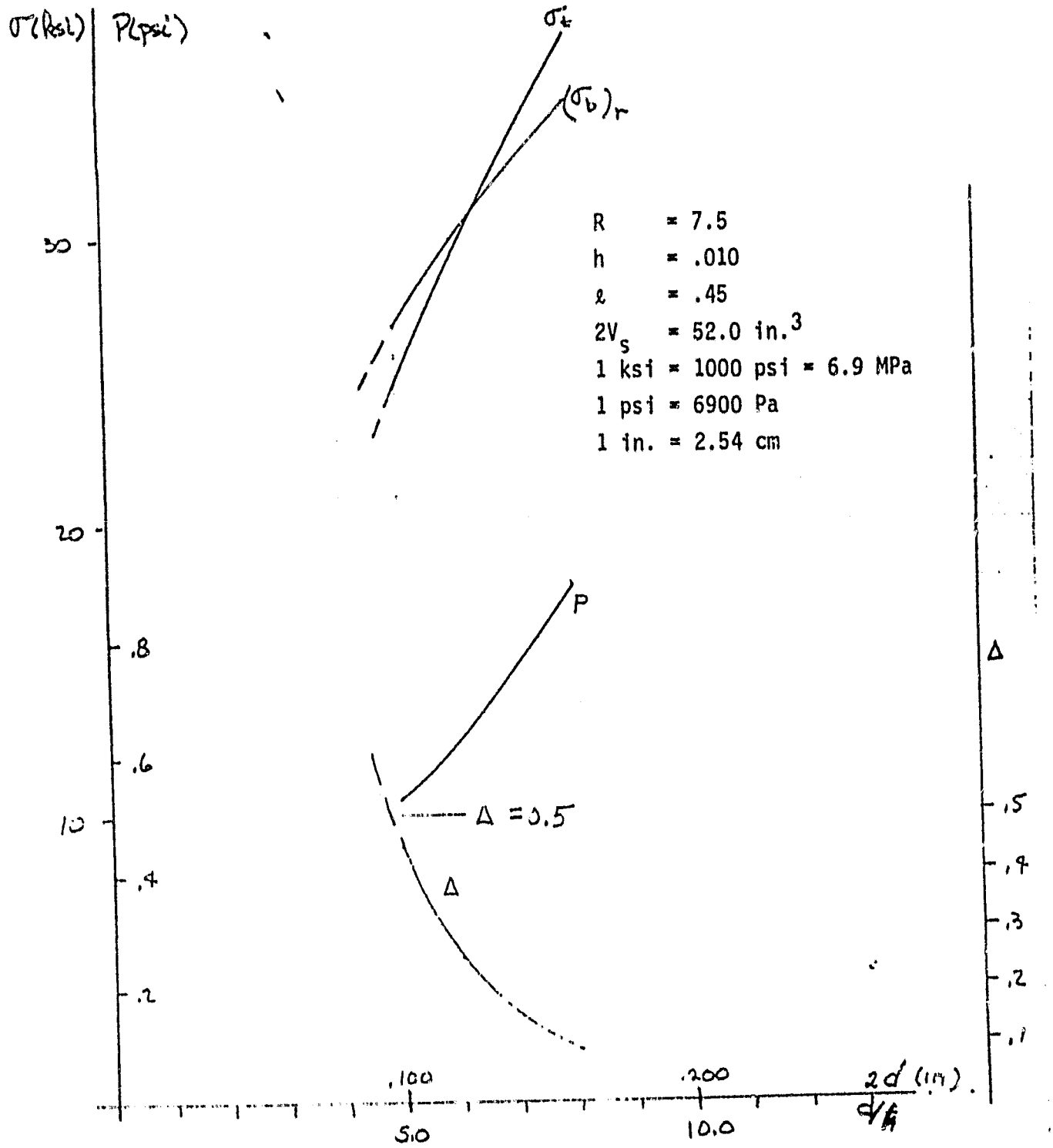

Figure A-17. Stress, Pressure Differential, and Nonlinearity vs Convolution Depth to Sheet Thickness Ratio and Convolution Depth

Appendix B

INPUTS FROM MARTINI ENGINEERING

MARTINI ENGINEERING

2303 Harris, Richland, Washington 99352
Telephone (509) 375-0115

30 March 1981

Mr. M.A. White
Joint Center for Graduate Study
100 Sprout Road
Richland, Washington 99352

Dear Maury,

I've essentially finished the assignment to provide engineering analysis for and adapt my isothermal second-order analysis of a Stirling engine to the free-piston machine that you are studying as part of your contract with NASA-Lewis. I have also been asked to gather some information on pumping rings to see if they might be applicable to the hydraulic converter that you are designing.

Since the work is essentially done, I'm enclosing an invoice in triplicate as requested by a copy of the field order which is also enclosed. If the reports enclosed herewith meet with your approval, please send the invoices to your purchasing department for payment.

Enclosed is a report entitled "Analysis of Pumping Rings" by Dennis C. Kuzma. I obtained this by a letter request to Earl Heffner of the General Motors Corporation. It appears from a study of this report that a calculation of a particular annular flow channel could be derived from a specialized computer program based upon the equations given in this report. It appears that a pumping ring works because of the taper on the ring and the elasticity of it. As the shaft moves in one direction, oil creates a pressure underneath the ring and expands the ring and allows the oil to enter the high pressure space even against a very large pressure difference. When the shaft moves in the opposite direction, the wedge pumping pressure disappears and the ring collapses onto the shaft and does not allow the oil to leak back again. This report gives a number of very clear graphs which show the effect of the different parameters upon the pumping rate for this ring. Since it is my understanding that the desire in your particular case is to not have pumping, one should make the two surfaces as stiff as possible and as accurately cylindrical as possible and have as large as possible oil film between the two surfaces. The pumping rings given in this analysis and the report enclosed were made with a slight interference fit. Certainly having a good slip fit would allow back leakage which almost was not allowed in this analysis to limit the pressure difference between one side and the other.

Enclosed is a sample of the input and output characteristics of the computer program which has been modified to take the case that is of interest on the subject contract. Before modification this computer program was shown to have an error of $\pm 10\%$ when compared with the General Motors 4L23 data (1-5).

On beyond the program which is already documented, the following modifications have been made in order to treat the free-piston Stirling engine which is the subject of this program. The modifications are as follows:

1. The change was made from a two piston machine to a piston-displacer machine.

2. A heater annulus and a internal flow tube replace the tubular heat exchangers normally used.

3. The equations for the foam metal regenerator material used in the General Motors engines are replaced with equations modified for changing porosity and low density knitted wire regenerator material. The equations used are an adaption of the cross rod, randomly stacked correlation given in Reference 6. An equation was derived from the graphical data to take into account porosity as well as Reynolds number.

4. Equations to determine the engine volumes from the geometry of the cranking machanism used previously were replaced with programming to accept an array of information which gives the time, position of the displacer from the midpoint position and position of the power piston from the midpoint position for a number of times during one complete cycle. These data are stored as a file on the computer and several data packages can be stored and called in at will. They come from an analog simulation of the engine. The last data point must be interpolated from the data points given so that the position of the power piston for data point 1 and the position of the power piston for the last data point are the same. This would mean that the time for this last data point is not an even number of milliseconds like the others would be.

5. The previous program determined mass fraction of the gas at the interface between the regenerator and the heater and at the interface between the regenerator and the cooler for each point during the cycle. Since this original program used the crank operated machine, it was known in advance where the maximum and minimum mass fractions would be and a program was developed to determine the average mass flow which is assumed to be steady for a period of time, stop altogether, and then be steady for a period of time in the opposite direction. Flow frictions and heat losses were calculated based upon the approximation of two steady flows and two periods of rest per cycle instead of many different flows for each time step during the cycle. This method of analysis has been refined so that the steady flow can be calculated no matter how the engine positions are presented to the program providing there is just one cycle present. Instead of just two mass fraction arrays being calculated as previously, a mass fraction is calculated for the middle of the hot flow tube, the middle of the heater, the middle of the regenerator, and the middle of the cooler. These mass fraction arrays are used to calculate the average flow and the fraction of the time this average flow occurs for these four places which are then used to calculate the flow friction and the heat transfer as appropriate.

6. This program was developed in BASIC on the TRS-80 instead of in FORTRAN on the Altos computer because the job of modification and debugging of the program was much more efficiently done in BASIC than in FORTRAN and the time spent with production runs was relatively negligible.

7. The pressure-volume curve at the beginning and end of the analysis and the effective hot space and cold space temperatures for each iteration are plotted on the computer screen to give the operator an idea of what is

happening. This program would be ideal for design of such a Stirling engine provided additional programming were added to determine the position of the displacer and power piston as a function of time.

This program is entirely independent of similar programs that you have been using to calculate this same engine. Differences will show up. I will be happy to help you examine these differences and review in detail the equations that went into calculating these different parts. However, I do not wish to publish the complete computer program.

An array of engine positions which are published in your proposal was used as a test case for the development of the computer program. This array is filed in the computer as File A and is shown in Table 1. The part of the table used is determined from the elapsed times given. Notice that for data point 18, the elapsed time is odd, being almost the same as data point 17. This was chosen so that the power piston position at data point 1 is exactly the same as the power piston position in data point 18. This means that the displacer piston position at data point 1 should be the same as the displacer piston position in data point 18. This is not exactly true but it is close.

Table 1

ENGINE POSITIONS AND TIMES FOR FILE A ARE

DATA PT	ELAPSD T SECONDS	DISPL. POS. CM	P P POS. CM
I	ET(I)	X1(I)	X2(I)
1	969	-2.2672	.21749
2	97	-2.2287	- 44362
3	971	-2.6882	-1.0252
4	972	-3.7062	-1.4461
5	973	-3.2765	-1.5826
6	974	-2.4285	-1.4466
7	975	-1.2246	-1.0803
8	976	.1821	- 52199
9	977	1.6409	.1166
10	979	2.8893	.76722
11	979	3.6426	1.3216
12	98	3.8952	1.6924
13	981	3.9092	1.8177
14	982	1.3156	1.7079
15	983	.13889	1.298
16	984	-1.025	.90922
17	985	-2.2452	.29342
18	985115	-2.24882	.21749

Table 2 gives the operating conditions and the dimensions that must be specified to the computer before it can calculate the results. Part of these are the engine positions given in Table 1 and the rest are built into the computer program as the default operating conditions and dimensions which were determined from a reading of the MTI report given with the proposal and from a conference with Pete Riggle who has been analyzing this engine as well. Table 3 gives these current operating conditions and current dimensions

Table 2

```
*******NOMENCLATURE KEY**********

OPERATING CONDITIONS
  DU,DV=TEMPERATURE CHANGE CONVERGENCE CRITERIA, K
  ET( )=ELLAPSED TIME, SECONDS
  GG=1 FOR H2--2 FOR HE--3 FOR AIR
  PS=CHARGE GAS PRESSURE, PSIA
  TM=INSIDE HEATER THIMBLE WALL TEMP. K
  TX=INSIDE COOLER TUBE METAL TEMP . K
  X1( )=POSITION OF DISPLACER FROM MIDPOINT TOWARD COLD SIDE, CM
  X2( )=POSITION OF POWER PISTON FROM MIDPOINT AWAY FROM COLD SIDE, CM
DIMENSIONS
  BF=CORRECTION FACTOR
  CI=ID OF COOLER TUBES, INCHES
  CX=COLD DEAD VOLUME, CU. CM
  DC=ENGINE POWER PISTON DIAMETER, INCHES
  DD=DISPLACER AND HEATER ANNULUS DIAMETER, INCHES
  DH=DIAMETER OF HOT GAS PASSAGE, INCHES
  DP=DISPLACER DRIVE ROD DIAMETER, INCHES
  DW=DIAMETER OF WIRE IN REGENERATOR, INCHES
  FA=FACE AREA FOR REGENERATOR, CM2
  FF=FRACTION OF REGENERATOR FILLED WITH SOLID
  GJ=HEATER ANNULUS GAP, INCHES
  GI=GAP AROUND DISPLACER, INCHES
  LB=LENGTH OF DISPLACER, INCHES
  LC=LENGTH OF COOLER TUBES, INCHES
  LH=LENGTH OF HEATER ANNULUS, INCHES
  LP=LENGTH OF HOT GAS PASSAGE, INCHES
  LR=LENGTH OF REGENERATOR, INCHES
  MC=HEAT CAPACITY OF MATRIX, J/G K
  NC=NUMBER OF COOLER TUBES PER CYLINDER
  V1=VELOCITY HEADS IN HEATER
  V2=VELOCITY HEADS IN COOLER
  V3=VELOCITY HEADS IN HOT GAS PASSAGE
  VH=HOT CLEARANCE VOLUME, CM3
  WD=WIRE DENSITY IN REGENERATOR, G/CM3
  X0=HALF MAXIMUM DISPLACER STROKE, INCHES
  X2=HALF MAXIMUM POWER PISTON STROKE, INCHES
  ZH=SPECIFIED STATIC CONDUCTANCE, WATTS/K
```

using the nomenclature defined on Table 2. Next Table 3 gives the power and the heat requirements itemized with the losses that are calculated. Note that for this base case the chief flow loss is through the hot gas flow passage inside the annular heat exchanger and the next most important loss is the loss through the heater annulus. The other flow losses through the regenerator and cooler are relatively unimportant. On the heat requirement side, the basic heat is added to by two important losses, the reheat loss and the pumping loss. I checked over both of these losses in the formulation and I find that they are correct. We discussed why the pumping loss or some people call it appendix loss is so large. The pumping loss depends to 2.6 power upon the gap thickness around the displacer which is now set at .05". As far as I know we have no information about what this radial clearance is. If this radial clearance were less, the pumping loss would be much less and the shuttle loss

Table 3

CURRENT OPERATING CONDITIONS ARE:

DU= 64	DV= 64	OG= 2	PS= 844	TM= 1089	TX= 320.5	
CURRENT DIMENSIONS ARE						
BF= 8	CX= 56	DC= 7	DD= 4	DH= 1.3	DR= 1.115	DW= 3E-03	FA= 111.95
FF= 08	GJ= 12	GI= .05	CI= .138	LB= 12.6	LC= 4	LH= 14.82	LP= 8
LP= 5	MC= 1.05	NC= 200	V1= 1.5	V2= 1.5	V3= 1.5	VH= 9	WD= 7.5
X0= 1.5	X3= .669	ZH= 1.317					

CALCULATED BY HYS2/BAS FOR TRS-80 FROM MARTINI ENGINEERING COPYRIGHTED 1981

POWER, WATTS		HEAT REQUIREMENT, WATTS	
BASIC	21480.1	BASIC	37599.6
HOT G. PASS. F. L.	2719.23	REHEAT	7226.76
HEATER F. L.	1991.29	SHUTTLE	437.578
REGEN. F. L.	495.726	PUMPING	7184.84
COOLER F. L.	214.065	TEMP. SWING	68.8296
NET	16059.7	CONDUCTION	701.842
		FLOW FRIC. CREDIT	-2229.15
		HEAT TO ENGINE	48252

INDICATED EFF. %= 33.2824

HOT METAL TEMP. K= 1089 COLD METAL TEMP., K= 320.5

EFFECT HOT SP. TEMP. K = 933.74 EFFEC. COLD SP. TEMP. K. = 399.632

==========

THE FINAL CALCULATED WORK DIAGRAM DATA ARE

TIME SECONDS	HOT VOL. CMC3	COLD VOL. CMC3	TOT VOL. CMC3	PRESSURE MPA
.969	666.19	1189.89	3293.83	5.90641
.97	596.254	1090.15	3124.26	6.24517
.971	559.101	977.628	2974.49	6.62148
.972	557.622	876.96	2872.25	6.9517
.973	592.478	810.932	2841.17	7.12107
.974	661.228	781.291	2880.28	7.12167
.975	758.022	782.966	2978.74	6.97949
.976	872.959	812.097	3122.81	6.71588
.977	991.148	865.128	3294.03	6.40311
.978	1092.26	933.221	3463.44	6.09471
.979	1152.42	1014.64	3605.82	5.82445
.98	1156.89	1102.77	3698.41	5.6146
.981	1102.01	1185.24	3725.01	5.48814
.982	1005.21	1247.16	3690.23	5.44483
.983	889.642	1276.9	3604.3	5.48683
.984	775.015	1261.27	3474.04	5.62851
.985	676.089	1199.61	3313.45	5.8721
.985115	667.688	1188.5	3293.95	5.90824

would be greater since this depends upon the first power of this radial clearance. I'm not going to guarantee that the program that I have developed for this engine is completely free of error, but I do say that it works satisfactorily and gives reasonable results and has been very carefully checked over. Any time you are ready to submit the input data which you'd like to use, I will run it through the computer and supply the output data. This will be very quickly and easily done now that the computer program is finished.

Sincerely,

W. R. Martini

WRM/df

References

1. W.R. Martini, "Validation of Published Stirling Engine Design Methods Using Engine Characteristics from the Literature," 1980 IECEC Record, pp. 2245-2250.
2. W.R. Martini, "Documentation and Validation for the Martini Engineering Isothermal Second-Order Design Program for Stirling Engines," Martini Engineering, Feb. 1981. $20.
3. W.R. Martini, B.A. Ross, "An Isothermal Second-Order Stirling Engine Calculation Method," 1979 IECEC Record, pp. 1091-1097.
4. W.R. Martini, "A Simple Method of Calculating Stirling Engines for Engine Design Optimization,"1978 IECEC Record, pp. 1753-1763.
5. W.R. Martini, "Stirling Engine Design Manual," DOE/NASA/3252-78/1, April 1978. Also corrected version from Martini Engineering $35.
6. W. Kays and A.L. London, "Compact Heat Exchangers," McGraw-Hill, 1964, p. 230.

Enclosures

1. "Analysis of Pumping Rings," by Dennis C. Kuzma
2. A copy of field order 767880.
3. Invoice in triplicate for $3,000.

Appendix C

NOMENCLATURE

A_R	Regenerator matrix heat transfer area.	cm^2
A_s	Internal surface area of a gas spring.	cm^3
B	Beale Number	Joule bar^{-1} cm^{-3}
B1	Force coefficient of displacer velocity	dyne sec cm^{-1}
B2	Force coefficient of displacer velocity squared.	dyne sec^2 cm^{-2}
B2V	Displacer drag coefficient induced by square-law speed control valve	dynes cm^{-2} sec^2
BVL	Viscous load coefficient for a linear generator. The ratio of armature drag to armature linear velocity.	dyne sec cm^{-1}
C_p	Specific heat at constant pressure	Joules gm^{-1} K^{-1}
D	Primary seal diameter.	dimensionless
d	Total displacer dwell per cycle.	sec
F	Gas spring hysteresis loss enhancement factor.	dimensionless
f	Operating frequency.	Hz
f_{fan}	Fanning friction factor.	dimensionless
f_s	Bellows surge frequency.	Hz
G	Mass velocity through a woven wire screen computed as though the flow area were the void volume fraction times the frontal area.	g cm^{-2} sec^{-1}
H	Radial seal clearance.	cm
h	Film coefficient of a woven wire screen.	W cm^{-2} K-1
K_g	Thermal conductivity of gas in a gas spring.	W/(cm K)
L_{max}	Maximum length of a rubber part cycled in tension.	cm

L_{min}	Minimum length of a rubber part cycled in tension.	cm
ΔL	L_{max} minus L_{min}	cm
L_o	Relaxed length of a rubber part cycled in tension.	cm
M_s	Hot space swept mass.	g
N	Number of active convolutions in a bellows.	dimensionless
N_R	Reynolds' number	dimensionless
$\bar{P}_E$	Engine charge pressure.	mPa
P	Engine charge pressure.	bar
$\hat{P}_L$	Seal power loss.	watts
P_o	Mean pressure of gas in a gas spring.	K
P_s	Bellows static pressure difference capability.	MPa
P_1	Pressure at low-pressure end of a seal.	MPa
P_2	Pressure at high-pressure end of a seal.	MPa
ΔP	Pressure drop across seal	MPa
Q_m	Regenerator main reheat loss.	W
r_H	Hydraulic radius of a woven wire screen.	cm
T	Cycle period.	sec
t	Bellows or diaphragm material thickness.	mm
ΔT_m	Hot to cold metal temperature difference.	K
T_o	Mean temperature of gas in a gas spring.	K
V	Seal relative velocity.	
VBC	Displacer bounce chamber volume.	cm^3
V_o	Mean gas volume of a gas spring.	cm^2
ΔV_{po}	Power piston swept volume.	cm^3
ΔV	Gas spring half stroke volume change.	cm^3
Z	$\gamma - 1$	
α	Pressure correlation coefficient for viscosity.	MPA^{-1}

β	Fraction of the cycle during which the displacer is in motion.	dimensionless
μ	Viscosity.	g cm sec^{-1}
μ_a	Effective average viscosity of oil in a seal.	g sec cm^{-1}
μ_o	Oil viscosity at ambient pressure.	g sec cm^{-1}
η	Efficiency of a power processing stage. The ratio of output power to input power.	dimensionless
γ	Ratio of specific heats for gas in a gas spring.	dimensionless
ω	Angular frequency.	radians/sec